T.C.
NECMETTİN ERBAKAN UNIVERSITY
INSTITUTE OF SCIENCE

DEVELOPMENT OF PROTEIN DEGRADERS AND PROBES TARGETING DRUG RESISTANT CANCER CELLS

Emin ŞAHİN

MASTER'S THESIS

Department of Molecular Biology and Genetics

July -2025

KONYA

THESIS APPROVAL AND ACCEPTANCE

The thesis entitled “Development of Protein Degraders and Probes Targeting Drug Resistant Cancer Cells” prepared by Emin ŞAHİN, has been accepted as a MASTER'S THESIS by the following jury on 03/07/2025 unanimously in the Department of Molecular Biology and Genetics of the Institute of Science at Necmettin Erbakan University.

Jury Members	**Signature**
Chair Assist. Prof. Tuğba Nur Aslan	……..
Advisor Assoc. Prof. Dr. Sündüs Erbaş ÇAKMAK	……..
Member Assist. Prof. Fatma Seçer Çelik	……..

Approved by the Institute of Science Administrative Board on …./…/20.. with the decision number ……..

Prof. Dr. Havvanur UÇBEYİAY
Institute Director

This thesis study was supported by TUBITAK 1001 with project number 221Z058. Research involving novel PROTAC development is supported by Necmettin Erbakan University Scientific Research Project (Grant No: 23GÜAMER03001).

TEZ BİLDİRİMİ

Bu tezdeki bütün bilgilerin etik davranış ve akademik kurallar çerçevesinde elde edildiğini ve tez yazım kurallarına uygun olarak hazırlanan bu çalışmada bana ait olmayan her türlü ifade ve bilginin kaynağına eksiksiz atıf yapıldığını bildiririm.

DECLARATION PAGE

I hereby declare that all information in this document has been obtained and presented in accordance with academic rules and ethical conduct. I also declare that, as required by these rules and conduct, I have fully cited and referenced all material and results that are not original to this work.

Emin ŞAHİN
Tarih: 03.07.2025

ÖZET

YÜKSEK LİSANS TEZİ

İLAÇ DIRENÇLİ KANSER HÜCRELERİNİ HEDEFLEYEN PROTEİN PARÇALAYICILARIN VE PROBLARIN GELİŞTİRİLMESİ

Emin ŞAHİN

Necmettin Erbakan Üniversitesi Fen Bilimleri Enstitüsü
Moleküler Biyoloji ve Genetik Anabilim Dalı

Danışman: Doç. Dr. Sündüs Erbaş Çakmak

2025, 89 Sayfa

Jüri
Doç. Dr. Sündüs Erbaş Çakmak
Dr. Öğr. Üyesi Tuğba Nur Aslan
Dr. Öğr. Üyesi Fatma Seçer Çelik

İlaç direnci, ilacın etkinliğinin vücut tarafından azaltıldığı veya ilacın tolere edildiği, aynı ilacın artan miktarının kullanılmasını veya ilacın değiştirilmesini gerektiren bir durum olarak tanımlanabilir. İlaç dirençli kanseri hedef alan ve dirençli hücreleri ayırt edebilen terapötik veya tanısal yaklaşımlar büyük önem taşımaktadır. Bu tezde, bu zorluk hücresel parametrelere yanıt veren, bilgi işleme kapasitesi olan, orantılı floresan sensörlerinin geliştirilmesiyle aşılmak istenmiştir. Bu amaç doğrultusunda, sadece karboksilesteraz veya hem karboksilesteraz hem de nitroredüktaz enzimlerine duyarlı olan piridinyum BODIPY tabanlı enzim probları tasarlanmıştır. Sensörlerin enzimler tarafından dönüştürüldüğünde önemli boyutta bir anti-Stokes kayması gösterdiği ve farklı hücresel durumlarda (hipoksik kanser mikro çevresi, sorafenib direnci gibi) belirgin floresan çıktı gösterebildiği anlaşılmıştır.

Bu tez ayrıca daha önce hedeflenmemiş proteinlere karşı yeni hedefli protein yıkım kimerasının (PROTAC) geliştirilmesine dayalı araştırmayı da içerir. Aldehit dehidrogenaz 1 (ALDH1), karboksilesteraz (CE) ve ABC Taşıyıcı protein gibi daha önce bu yöntemle hedeflenmemiş proteinler için yeni PROTAC yapıları geliştirilmiştir. Hedeflenen proteinlerin, ilaçların kimyasal dönüşümüne (karboksilesterazlar, ALDH1, nitroredüktaz), ilacın hücre dışına atımına (ABC Taşıyıcı) veya tedaviden sonra kanser kök hücreleri aracılı kanser nüksetmesinin bir sonucu olarak etkisiz tedaviye yol açarak ilaç metabolizasyonunda ve/veya direncinde rol oynadığı bilinmektedir. PROTAC yapıları tez çalışması kapsamında sentezlenmiş ve hücre kültürü çalışmalarından ilk veriler toplanmıştır.

Anahtar Kelimeler: Hedefli Protein Parçalanması, İlaç Direnci, ALDH1, Karboksilesteraz, ABC Taşıyıcı Protein, Floresan Enzim Sensörü

ABSTRACT

MS THESIS

DEVELOPMENT OF PROTEIN DEGRADERS AND PROBES TARGETING DRUG RESISTANT CANCER CELLS

Emin ŞAHİN

INSTITUTE OF SCIENCE
NECMETTİN ERBAKAN UNIVERITY
THE DEGREE OF MASTER SCINCE IN MOLECULAR BIOLOGY AND GENETICS

Advisor: Assoc.Prof. Dr. Sündüs Erbaş ÇAKMAK

2025, 89 Pages

July

Assoc. Prof. Dr. Sündüs Erbaş ÇAKMAK
Assist. Prof. Tuğba Nur Aslan
Assist. Prof. Fatma Seçer Çelik

Drug resistance can be defined as a phenomenon in which drug efficacy is decreased or the drug is tolerated by the patient which requires either the use of increasing amount of the same drug or change of the drug. Therapeutic or diagnostic approaches targeting and discriminating against drug resistant cancer are of great importance. In this thesis, this challenge is addressed by the development of information processing, ratiometric fluorescent sensors responsive to cellular environmental parameters. Pyridinium BODIPY-based enzyme probes that are sensitive to only carboxylesterase or both carboxylesterase and nitroreductase enzymes were designed. Sensors are shown to display significant anti-Stokes shift upon conversion by the enzymes and can display distinct fluorescent output under different cellular states (i.e. hypoxic cancer microenvironment, sorafenib resistant state).

This thesis also involves the research based on the development of novel targeted protein degradation chimera (PROTAC) against previously untargeted proteins Aldehyde dehydrogenase 1 (ALDH1), carboxylesterase (CE) and ABC Transporter Targeted proteins all of which are known to be involved in drug metabolization and/or resistance through either leading to chemical conversion of the drugs (carboxylesterases, ALDH1, nitroreductase), drug efflux (ABC Transporter) or inefficient treatment as a result of cancer stem cells mediated relapse of cancer after treatment. Efficient synthesis of the PROTACs is achieved as a part of the thesis and the initial data from the cell culture studies were collected.

Keywords: Targeted Protein Degradation, Drug Resistance, ALDH1, Carboxylesterase, ABC Transporter Protein, Fluorescent Enzyme Sensor

ACKNOWLEDGMENT

I would like to thank TÜBİTAK for the financial support provided to me through the 2210-A Domestic Graduate Scholarship Program of the TÜBİTAK Scientist Support Programs Directorate (BİDEB).

Thesis research involving fluorescent sensors is supported by TÜBİTAK 1001 Project, Grant no: 221Z058. Research involving novel PROTAC development is supported by Necmettin Erbakan University Scientific Research Project (Grant No: 23GÜAMER03001).

I also thank Dr. Safaa Altves for her experimental support. I would like to express my appreciation to SEC Research team.

Emin ŞAHİN

July, 2025

CONTENTS

SYMBOLS AND ABBREVIATIONS

Symbols:

mL: mililiter

μL: microliter

nm: nanometer

μM: Micromolar

mM: Milimolar

MHz: Mega Hertz

Abbreviations:

BODIPY: Boron-Dipyrromethene

DAPI: 4',6-Diamidino-2-Phenylindole

DMEM: Dulbecco's Modified Eagle Medium

DMSO: Dimethyl Sulfoxide

ECL: Enhanced Chemiluminescence

FBS: Fetal Bovine Serum

GAPDH: Glyceraldehyde-3-Phosphate Dehydrogenase

Hep3B: Hepatocellular 3B (Human Liver Carcinoma Cell Line)

HG-DMEM: High Glucose Dulbecco's Modified Eagle Medium

MTT: 3-(4,5-Dimethylthiazol-2-yl)-2,5-Diphenyltetrazolium Bromide

PeT: Photoinduced Electron Transfer

SDS-PAGE: Sodium Dodecyl Sulfate-Polyacrylamide Gel Electrophoresis

QTOF-LC/MS: Quadrupole Time-Of-Flight Liquid chromatography–Mass Spectrometry

NADH: Nicotinamide adenine dinucleotide (NAD) + hydrogen(H)

PROTAC: Proteolysis Targeting Chimera

UPS: Ubiquitin Proteasome System

HOMO: Highest Occupied Molecular Orbital

LUMO: Lowest Unoccupied Molecular Orbital

1.INTRODUCTION

Cancer is the second cause of the death after cardiovascular diseases. Since it is complex disease, its diagnosis and therapy are compelling for scientist. Even though there are some diagnostic tools such as Computerized tomography (CT) scan, magnetic resonance imaging (MRI), positron emission tomography (PET) scan, scientist have tried to find new diagnosis methods. Fluorescent Enzyme Probe can cheap and easy method to diagnosis the cancer cell from healthy cell in medical or scientific research. Enzyme sensitive fluorescent probes allow monitoring enzyme activity in the cell. Thanks to that, status of cell or cancer can be investigated.

Even if commercial anticancer drug has significant cytotoxic effect on the cancer cells their efficacy has low in some cancer type due to drug resistance. Scientist have tried to overcome drug resistance with different strategies. Although genetic engineering method allows the reliable strategies, it is not cheapest. Given to fate of anticancer drugs, traditional chemical inhibitors are not enough to this issue. It is necessary that cheap and reliable strategies overcome drug resistance in cancer. Proteolysis Targeting Chimera (PROTAC) allowing specific protein degradation has been become popular recently. It can be used to overcome cancer drug resistance.

2. LITERATURE REVIEW

2.1. Fluorescent Enzyme Probes for Cancer Imaging

Imaging enzymes related to cancer development, progression and drug resistance is vital to early diagnosis and treatment of this disease. Fluorescence imaging techniques have attracted interest in recent years for visualizing proteins, ions, organelles, amino acids and ions due to their robust spatiotemporal resolution. Although fluorescent proteins (FPs) fused with Protein of Interest (POI) are preferred because of their advantages such as direct monitoring of POI expression, easy expression controlled via genetic engineering, yet introducing the FPs into target protein can interfere with the target protein function. In addition, technique is relatively expensive and requires longer steps. Considering this, small molecule-based fluorescent probes can be best alternative since they can be easily applied, sensitive, non-invasive and cheaper (Kowada et al., 2015). Since these probes have relatively small sizes and most have versatile functionalization capacity, numerous molecule-based fluorescent probes have been designed so far. These probes having different photophysical properties, either display change in fluorescence intensity in the presence of analyte or a change in fluorescence wavelength. Chemical and physical properties of the probe can be tuned to use different fluorescence sensing mechanisms such Photoinduced Electron Transfer (PeT), Excited-state Intramolecular Proton Transfer (ESIPT), Aggregation-Induced Emission (AIE), Fluorescence Resonance Energy Transfer (FRET) or Intramolecular Charge Transfer (ICT). Since each of these mechanisms has some strengths and weaknesses, working principle of each mechanism should be considered carefully to develop a new fluorescent probe.

2.2. Photoinduced Electron Transfer

Enzyme responsive probes using PeT mechanism mainly consist of a fluorophore and enzyme sensitive unit which are not conjugated together. In most cases, fluorophore is reduced by the enzyme responsive module through electron transfer in the excited state leading to fluorescence quenching (Figure 2.1)(Daly et al., 2015). By enzyme activity, the Highest Occupied Molecular Orbital (HOMO) of the electron donor part (enzyme responsive part) is stabilized, blocking the electron transfer to fluorophore. In the case of reverse PeT excited electron of the fluorophore module is transferred to Lowest Unoccupied Molecular Orbital (LUMO) of the relatively electron poor enzyme responsive auxiliary group leading to

fluorescence quenching. In this case, enzymatic conversion destabilizes the LUMO and blocks the electron transfer from the fluorophore.

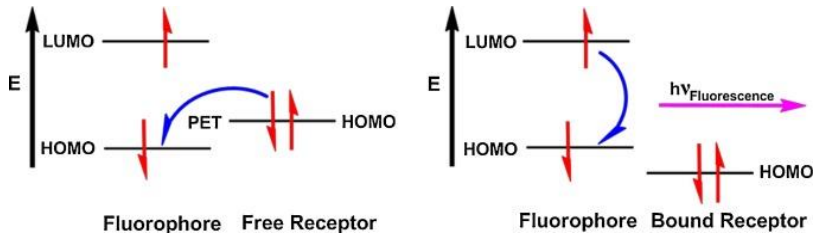

Figure 2.1. Mechanism of PeT (M. Li et al., 2018)

The enzyme sensitive donor part transfers an electron to the excited fluorophore and quenches the emission. However, because of the enzyme activity, HOMO energy level of the donor is stabilized and electron transfer into acceptor part is blocked. Fluorophore emission is reinstated.

Although PeT-based molecular sensors are widely used, these probes have many disadvantages, some of which are listed below:

- Each probe should be designed individually for the target enzyme since enzyme-responsive module is specific for each enzyme. Therefore, this module might have different redox potential. HOMO and/or LUMO levels of fluorophore and auxiliary modules should be carefully analyzed. This requirement limits the generalizability of the sensors and limits their application to certain enzymes only.
- Since energy levels of the orbitals are sensitive to environmental conditions, probe is affected by solvent or localization of it in the cell. Unpredictable outputs likely to bias analysis of the probe emission.
- Enzyme activity should have significant effect on the energy levels of the probe parts. Many enzymes cannot show this change on its substrate, i.e. if the enzymatic conversion does not lead to a change in the electron rich-poor properties of the modules, then the PeT may not change too. This situation restricts the application of PeT based probes.
- PeT probes essentially allow monitoring the emission intensity. Emission intensity can be changed according to probe photostability, location, probe amount in the cell. Since PeT based probe lacks internal reference, it possibly gives unreliable outputs.

Considering the above-mentioned disadvantages such as lack of internal calibration, environment sensitivity and difficulty of the design, PeT mechanism is not the most suitable method for biological sensing applications.

2.3. Excited-State Intramolecular Proton Transfer

The fluorescence of probes using ESIPT is based on the intramolecular proton transfer between proton donor, such hydroxyl or amine group, and proton acceptor, such as carbonyl oxygen or imine nitrogen in the excited molecule (Sedgwick et al., 2018). Proton transfer between these groups change structure and leads to remarkable shift in absorbance and emission spectrum, so called Stroke Shift (Figure 2.2)(Sedgwick et al., 2018; Klinhom et al., 2019).

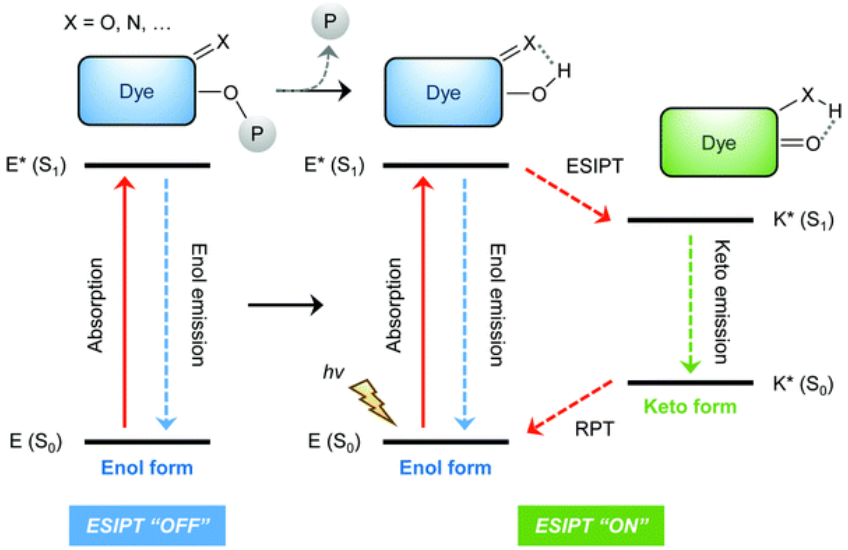

Figure 2.2. ESIPT based probes depend on proton transfer within the molecule in the excited state(Sedgwick et al., 2018)

In this probe design, hydrogen bond donor is blocked with enzyme sensitive specific chemical group, only enol emission can be observed. Enzyme activity liberates hydrogen donor group, enables proton transfer and keto emission can be observed. However, such a probe design is very complicated. Also, ESIPT based probes are generally sensitive to environmental conditions such as pH and solvent which leads nonspecific emission change (Y. H. Wang & Wan, 2013). Moreover, ESIPT based probes usually display weak emission which leads to low signal to noise ratio (Sedgwick et al., 2018).

2.4. Aggregation-Induced Emission

AIE probes are based on increased emission due to aggregation. The restriction of intramolecular motion, rotation and vibration is the most supported idea by intensive experimental and theoretical studies, among the hypothesis suggested to explain AIE working principle. These probes tend to self-aggregation upon the enzyme activity. Stacking of the fluorophores may lead to fluorescence quenching or restricted rotation of the aggregates may enhance fluorescence signal (Figure 2.3). Since probe aggregation can lead cellular damage and reduce clearance of the probe from the body, it can be said that these probes are less biocompatible and not suitable for biological application (Gao & Tang, 2017).

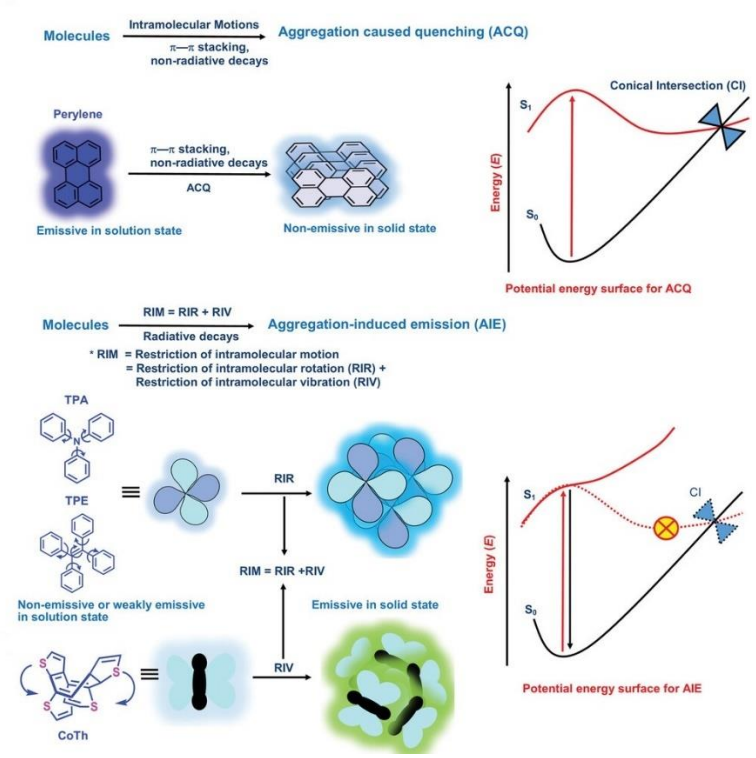

Figure 2.3. Change in the fluorescence of the probes upon the formation of aggregates(Kachwal & Tan, 2023)

2.5. Fluorescence Resonance Energy Transfer

Fluorescence resonance energy transfer mechanism based on energy transfer between two fluorophores or between fluorophore/quencher pair within the probe structure. When probe is excited by light, firstly donor part absorbed energy and then transfer this energy to acceptor part leading to emission at longer wavelength (Udhayakumari, 2024).

Effect of the proximity on the emission intensity is the major determinant of FRET-based probes spectral. Overlap between donor emission and acceptor absorbance is required to emission (Figure 2.4).

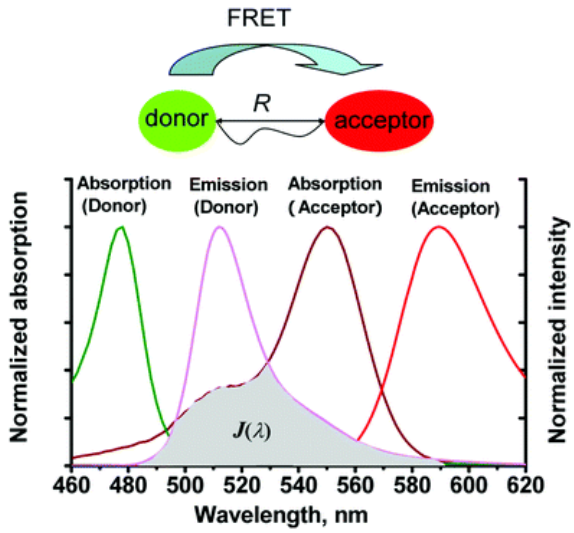

Figure 1.4. FRET mechanism (L. Wu et al., 2020)

2.6. Intramolecular Charge Transfer

ICT probes are based on push and pull electron system within the molecule. Distribution of electrons among electron rich and electron withdrawing groups in the molecule is altered upon enzyme catalyzed chemical conversion. This charge transfer changes the emission of the probe leading to either blue-shift towards low energy spectral region (hypsochromic shift) or to red-shift (bathochromic) as a result (Figure 2.5) (Udhayakumari, 2024).

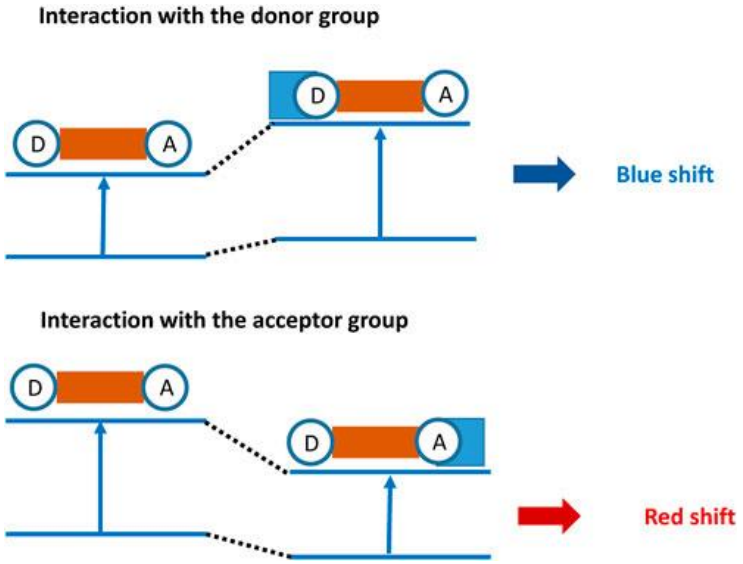

Figure 2.5. Enzyme dependent change in intramolecular charge transfer leads to a decrease or an increase in the HOMO-LUMO gap of the fluorophore and a resulting shift in emission wavelength.(Y. Wu et al., 2023)

In ICT mechanism change in emission intensity as well as emission wavelength is usually observed. Ratiometric change in emission at the initial maximum emission wavelengths and the final one, or ratiometric change with respect to unchanged isosbestic point can be monitored. While shift in emission wavelength occurs, intensity at isosbestic point does not change and this point can be considered as a reference point for internal calibration of the fluorescence. Misinterpretations due to probe quenching, degradation or uneven accumulation in certain organelle of the cell can easily be prevented by taking advantage of isosbestic point and emission wavelength shift.

2.7. Fluorophores Widely Used as Fluorescent Sensors

Fluorescent probes can be designed using commonly used fluorophores such as coumarin, fluorescein, BODIPY, rhodamine, and cyanine (Figure 2.6). Each of these molecules has different chemical structures, photostability and photophysical properties. Near IR light can penetrate through the tissue better than others. To enable visible, near-IR or IR emissions highly conjugated structures are usually preferred. Various modifications on the core structure to extend the conjugation further or to adjust electronic properties allows fine-tuning of the photophysical character of the probe.

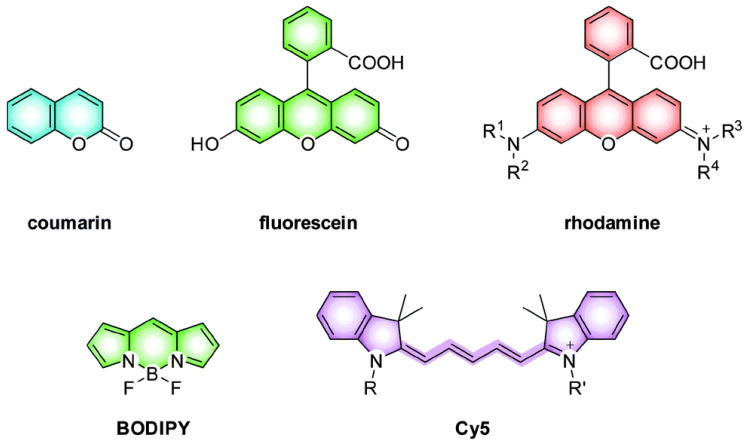

Figure 2.6. Chemical core structures of common probes (Kowada et al., 2015)

Major limitations of some common fluorophores are listed below:

- negatively charged fluorophores such fluorescein has limited cell-membrane permeability problem and usually requires esterification to overcome this limitation.
- While cationic dyes such rhodamine shows higher penetration capacity, tends to localize in the mitochondria or adsorb nonspecifically to proteins or lipids
- Although near-IR emission of cyanine makes this dye suitable for tissue or organism imaging, it has lower photostability.
- Coumarin dyes has limited modification capability and the absorption at the highly penetrable Near-IR spectrum is limited.
- BODIPY dyes are usually photostable and can be functionalized at multiple positions but the Stoke shift is usually small.

Since BODIPY has high photostability, sharp absorption and emission spectra, high extinction coefficient, high fluorescence quantum yield, uncharged, it is preferred in various biological applications as probes. Some of these dyes are commercially available and used for biological labelling (Kowada et al., 2015). Also, BODIPY structure can be easily modified that enable tuning of the photophysical/photochemical properties and can be made sensitive to a target enzyme (Loudet & Burgess, 2007). Most of the BODIPY core structure emits light at around 520 nm. Derivatization of this compound to produce mono-, di-, tri- or tetra-styryl forms by means of Knoevenagel condensation reaction can stepwise increase the emission wavelength above 700 nm (Kachwal & Tan, 2023). Extending the conjugation by pyridine carboxaldehyde yields distyryl-BODIPY derivatives which can emit light above 600 nm which is very suitable for sensor applications since penetration of light through tissues is higher beyond this wavelength (Deniz et al., 2008; Erbas-Cakmak et al., 2015).

2.8. Fluorescent Probes for Esterase Enzymes

Esterase is an enzyme family that catalyze the hydrolysis of wide range of ester molecules which are found on lipids, proteins or signal transduction pathway elements (Gil-Rivas et al., 2023). Since esterases are responsible for detoxification of ester contain molecules, they usually facilitate the excretion of such drugs from the body or alter their activities. Activity of these esterases may lead to resistance against ester containing drugs, such as analgesic, antibiotic and anti-cancer (Potter & Wadkins, 2006). Since probe molecules can easily be functionalized with ester moiety on carboxylate groups, several esterase probes were designed which display change in photophysical properties upon hydrolytic esterase activity selected esterase probe examples from literature are shown in Figure 2.7.

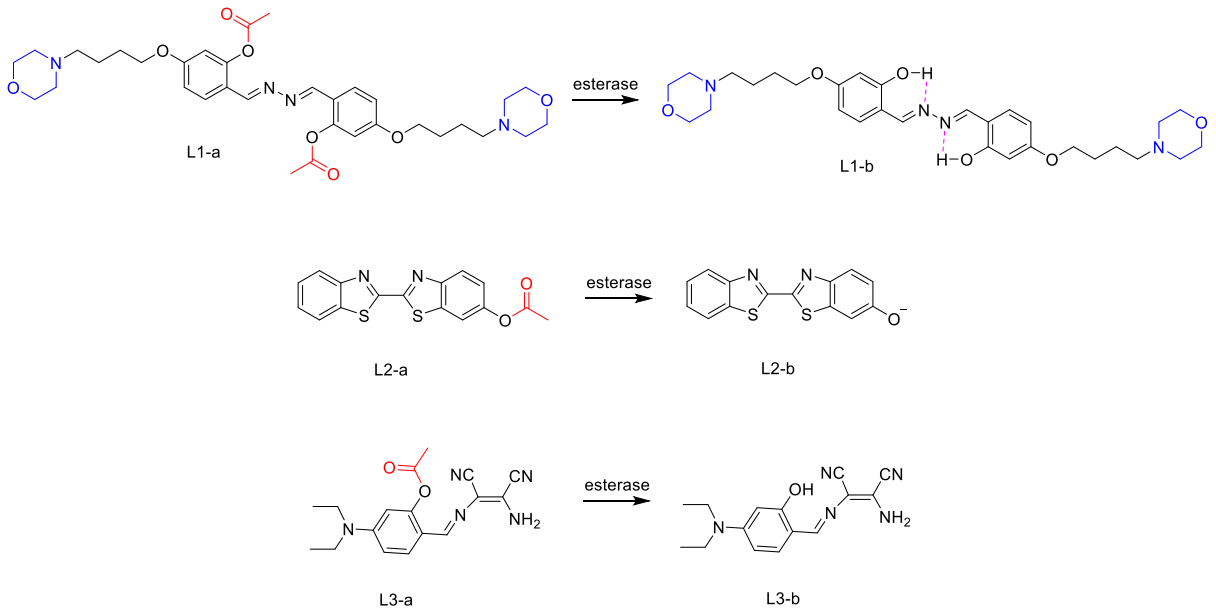

Figure 2.7. Selected examples of turn-on fluorescent esterase probes in literature. Esterase enzymes catalyze the hydrolysis of ester group (red) on the probe.

Lysosomes targeted esterase probe L1 designed by Gao team is shown to emit at 532 nm upon esterase activity (Figure 2.7.) (Guo et. Al. 2014). It is shown that emission intensity of this probe uses AIE and ESIPT mechanism. Upon acetyl removal intramolecular charge transfer is enabled. Emission enhancement is shown in a time dependent manner in MCF-7 cell line. Mao team developed esterase responsive turn-on probe L2 to evaluate health status of cells and/or discriminate living cell from dead cell using MDA-MB-231 cell line (Mao et. al, 2020). In this study, probe emission at 569 nm increases with the esterase activity upon excitation with 370 nm light. Another AIE and ESIPT based esterase probe was proposed by Peng group. The

probe emits at 580 nm when excited at 365 nm in the presence of esterase (Peng et al., 2017). Also, MCF-7 cell studies show that this probe localizes in mitochondria because of the interaction between negative charge of mitochondrial membrane and ammonium cation on the molecule.

Even though there are many esterase-responsive fluorescent probes in literature, only a few of them allow the ratiometric sensing. Guo group reported an ER-targeted esterase probe which emits light at 435 nm in the absence of esterase enzyme (Figure 2.8)(Guo et al., 2023).

Acetyl group is removed by esterase activity changing the molecule into acceptor-p-donor form hence shifting this fluorescence signal to 560 nm. 52-fold change in the ratio of fluorescence intensities at these wavelengths is observed (I_{560}/I_{435}).

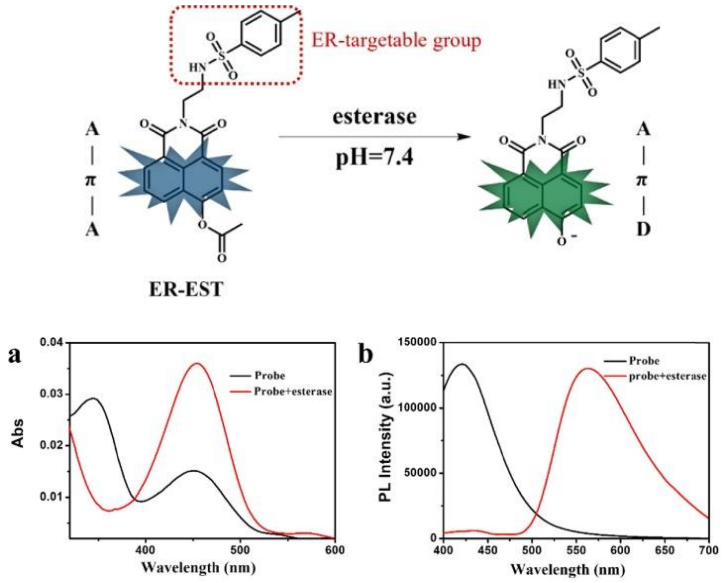

Figure 2.8. ER targeted esterase probe with a large bathochromic shift in emission upon cleavage of ester by the esterase enzyme (Guo et al., 2023).

Another ratiometric esterase fluorescent sensor with a strong intermolecular charge transfer character is reported by Yadav group which localizes in mitochondria through its cationic structure. At around pH 8, esterase activity in live, metabolically active cells convert the probe into deacetylated form having a red emission (Yadav et al., 2023). On the other hand, dead cells without enzymatic activity display a green emission enabling ratiometric discrimination of live cells from the dead (Figure 2.9).

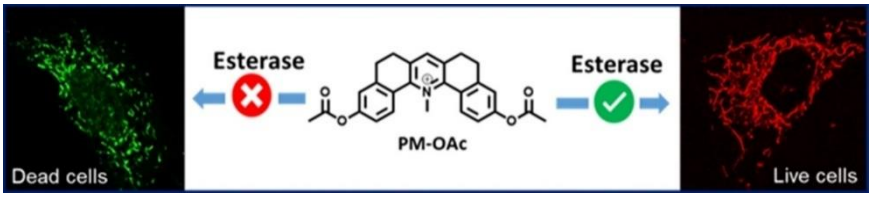

Figure 2.9. Esterase responsive ratiometric fluorescent sensor which can discriminate live cells from the dead ones(Yadav et al., 2023)

BODIPY compounds display distinct photophysical properties depending on the position and nature of modification. Direct modification on the meso position is widely used for sensing applications. Kim et. al. developed a ratiometric fluorescent probe having an ester group at this position (Kim et al., 2015). The molecule emits at 597 nm which shifts to 550 nm upon acetyl removal by the esterase enzyme activity (Figure 2.10). Response of this probe was analyzed in esterase expressing HEP2G and esterase negative PHCASM cells.

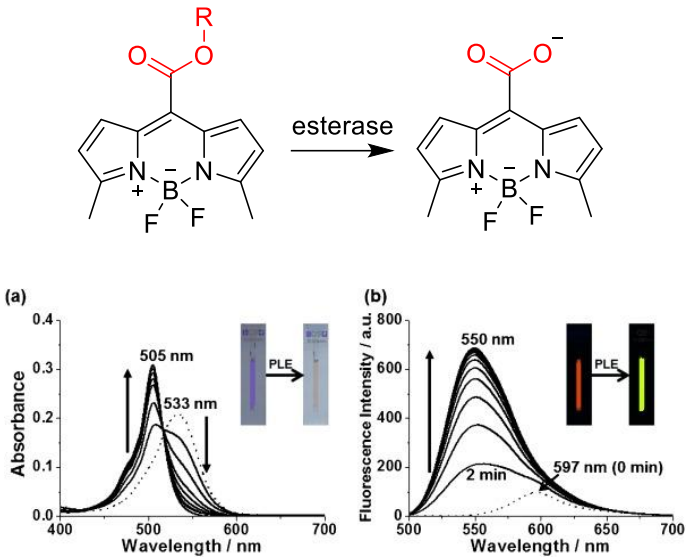

Figure 2.10. BODIPY-based ratiometric esterase sensor (Kim et al., 2015)

Although there are many esterase probes in literature, there are limited number of Near-IR absorbing (absorbing in the therapeutic window) ratiometric probes with large spectral shift induced by enzyme activity.

2.9. Dual Enzyme Sensitive Fluorescent Probe

Among many diseases, cancer is a complex disease in which many cellular pathways are affected, and the expression of several proteins are altered as a result abnormal metabolism. Adaptation to hypoxic conditions is one of the most obvious features of solid cancers. Since in hypoxic conditions, cells cannot be maintained with sufficient oxygen due to inadequacy of angiogenesis, cells reprogram their metabolism towards glycolysis. Nitroreductase enzyme catalyzing the reduction of nitro group to amine is one of the most known reductive enzymes targeted to monitor hypoxic microenvironment. So, nitroreductase is used as hypoxia marker for cancer cell (Qiao et al., 2021; Liu et al., 2018). Apart from hypoxia, several other tumor markers are used for cancer imaging i.e. low pH, elevated enzyme levels etc. (Wangngae et al., 2022; Zhou et al., 2024; X. Li et al., 2021).

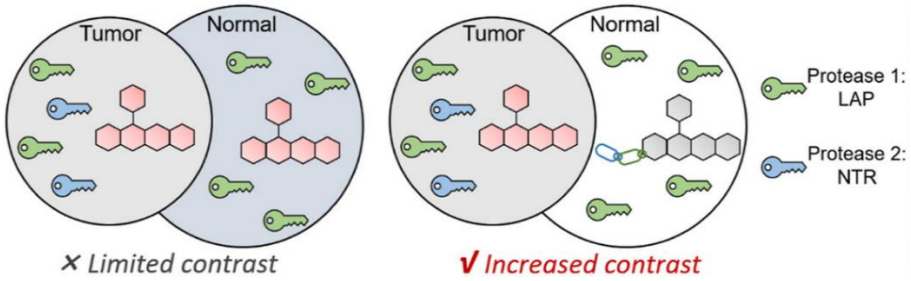

Figure 2.11. Schematic representation of dual enzyme sensitive fluoresce probe(Liu et al., 2025)

Since enzyme targeted by a sensor can also be present in normal cells, sensor should discriminate against cancer cell with high precision. Therefore, additional analyte responsiveness can better improve the contrast during imaging.

Although an increasing number of probes visualizing cancer cells are reported each day, there are still limited examples that accurately discriminate healthy cells from the cancer cells. Well-accepted cancer markers may already be present in certain healthy cells too; therefore, a false-positive result is likely to be obtained during imaging. Additionally, many cancer cells have their own specific markers, and it is not straightforward to design probe for each of them. Using a single probe molecular scaffold would save time and cost. Moreover, integration of more than one enzyme responsiveness enables more accurate sensing, prevent false positive results(Liu et al., 2025)

In the literature there are some multi-analyte sensing probes that sensitive to more than one enzyme or conditions, developed recently (Luo et al., 2025; Kong et al., 2019). Thesis

project addresses drug resistant cancer cells using esterase and nitroreductase multi-responsive fluorescent probe which is not addressed yet.

2.10. Drug Resistance

Drug resistance can be defined as a phenomenon in which drug efficacy is decreased or tolerated by the patient which requires either the use of increasing amount of the same drug or change of the drug. It can be studied as intrinsic or acquired resistance depending on the time when resistance is developed. Intrinsic resistance is innate factors that reduce the drug efficiency caused by the following:

- pre-existing mutations decrease the sensitivity of cancer cell to chemotherapy. For instance, in triple negative breast cancers drug sensitivity is low due to lack of common cancer drug targets such estrogen/progesterone receptors/HER2.
- Tumor heterogeneity, pre-existing insensitive subpopulations such as cancer stem cells reduces drug sensitivity since these cells lead to relapses after treatment.
- activation of defense mechanism protects the organism from environmental toxin and anticancer drug**.**
- factors involved in the ADME (absorption, distribution, metabolism, excretion), character of a drug pharmacokinetics affect the drug efficiency on the target side (Emran et al., 2022).

In addition to the intrinsic resistance of the cancer, many cancer types are susceptible to chemotherapy initially, but drug efficiency decreases gradually during treatment, which is a result of one or combinations of cases below:

- secondary proto-oncogene activation leads to survival of the tumor or sustain tumor development.
- mutations on the target or altered expression levels of the drug targets.
- changes in tumor microenvironment (Rueff & Rodrigues, 2016; X. Wang et al., 2019)

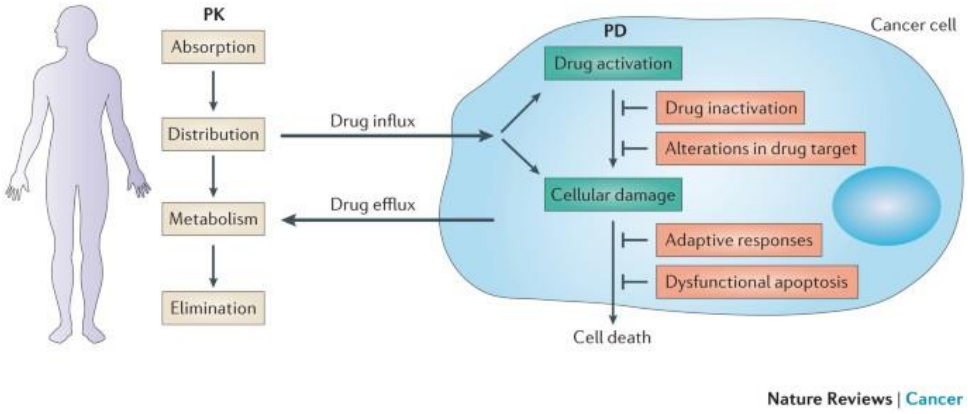

Figure 2.12. General principles of drug resistance, pharmacokinetics and molecular mechanism affecting the drug resistance.(Holohan et al., 2013)

Both intrinsic and acquired resistance can co-exist and prevent therapy by decreasing the drug efficiency. There are several mechanisms that are involved in the development of drug resistance through which cells can be tolerant against single or multiple drugs. In general, after drug administration, while some of it is absorbed and distributed throughout the body and delivered to the target site, some are metabolized especially by liver enzymes. Cells of the target tissue resist the drug penetration and develop some mechanism to efflux the drug out of the cell. In addition to that, cells can inactivate drug through chemical conversions/adducts or make alteration on the drug target to prevent initiation of cellular response. Even though, drug escape these steps and trigger the anticancer response, cell prevent cellular damage by developing adaptive response or avoid apoptosis (Figure 2.12) (Holohan et al., 2013).

2.11. Drug Efflux Pumps

Efflux pumps are evolutionary conserved transport proteins that regulate the interior environment of the cell by pumping out the toxins such antimicrobial agent, anticancer drug etc. (Nishino et al., 2021). ATP binding cassette (ABC) transporter superfamily is well-studied one in terms of cancer drug resistance. Its members are categorized in 7 subfamilies, encoded by 48 distinct ABC genes in the human genome. These transporters utilize the ATP energy to efflux various types of hydrophobic compounds from the cell (Figure 2.13) (Dean, 2005).

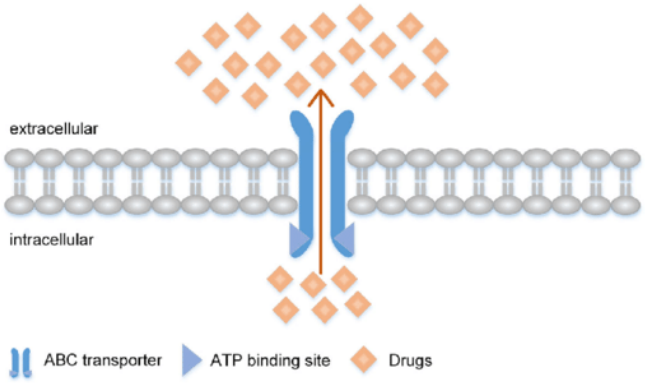

Figure 2.13. Schematic representation of ABC transporter working principle (S. Wu & Fu, 2018)

Multi-drug resistance protein 1 (MDR1; also known as P-glycoprotein and ABCB1) is most known and first identified ABC transporter. Even though, it is expressed in low amounts in most of the tissues, excretory epithelial cells express this protein in high amounts. Also, its overexpression is associated with chemoresistance in many types of cancer such as kidney, colon and liver cancers, some leukemias and lymphomas. While another type of ABC transporter MRP1 overexpression is observed in chemoresistance in prostate, lung and breast cancers; BCRP is related with chemoresistance in breast cancer and leukaemia. High efflux pumps activity in cancer cell leads to development of resistance against many anticancer agents such as sorafenib, paclitaxel, cisplatin, doxorubicin irinotecan, oxaliplatin (Thomas et al., 2003).

There are some strategies developed to overcome ABC transporter mediated-drug resistance. The major approaches are:

- Modifying the chemical structure of the anticancer drug to enable escape from drug efflux pump. However, this might decrease the efficiency of the agent on its target
- Use of chemical compounds that directly
    - prevent/disrupt the activity of ABC transporter in different ways (Nanayakkara et al., 2018)
    - prevent ATP binding to ABC transporter (Nanayakkara et al., 2018). This approach may increase the risk of the side effects
- Genetic engineering methods that prevent the expression of MDR by post-transcriptional gene silencing (Takara et al., 2006)

2.12. Drug Inactivation by Enzymes

Drug inactivation is another strategy of cancer cell to cope with the anticancer drug. Organisms protect themselves from toxins by degrading or modifying them using enzymes such hydrolases, reductases, dehalogenases, transferases, oxygenase, esterase. Through this way, cytotoxic effect is minimized or completely eliminated. Cancer patients overexpress such enzymes in either cancer tissue or another tissue such as liver leading to resistance against to cancer drug. The major outcome of the drug metabolization is the generation of more aqueous soluble drugs that is excreted easily (Zhao et al., 2021).

Among these enzymes, CYP3A4, oxidase cytochrome enzyme, metabolizes many cancer drug such as paclitaxel, doxorubicin, imatinib, sorafenib, Lenvatinib and leads to drug resistance (F. Wang et al., 2023). Aldehyde dehydrogenase (ALDH) is another enzyme family responsible for drug resistance directly or indirectly. Aldophosphamide kind of DNA alkylating agent is metabolized by the enzyme (Figure 2.14) (Ibrahim et al., 2018).

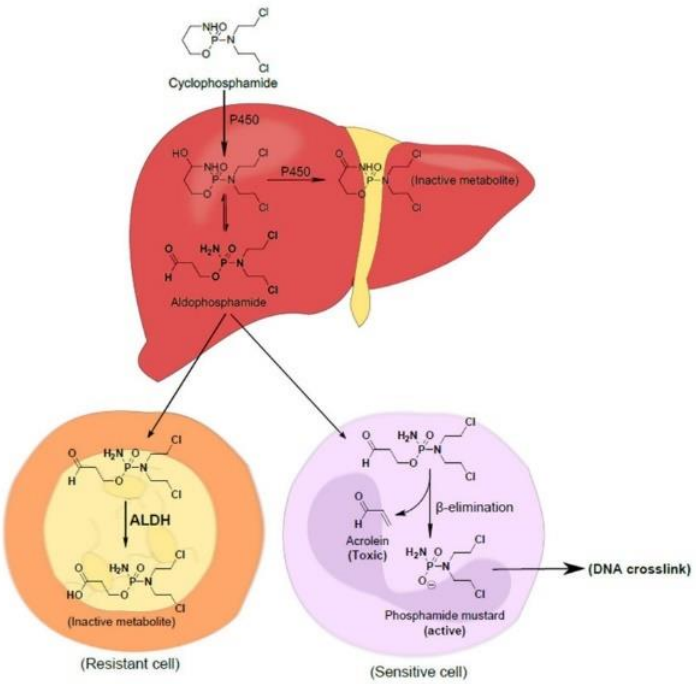

Figure 2.14. Cyclophosphamide activation and deactivation pathways by metabolizing enzymes(Ibrahim et al., 2018)

Even if there is not a clear evidence showing a correlation between esterase and drug resistance in cancer cells, esterase enzyme activity increases in most of cancer cells and its overexpression has vital role on migration, invasion, survival of tumor cells (Kong et al., 2019).

Usage of drug cocktail consists of more than one inhibitor against these enzymes during the chemotherapy can be a suitable option to overcome resistance, but side effects of these cocktails lead to severe results because some enzymes such as the cytochrome enzymes are vital for the organism. Therefore, a novel strategy needs to be developed to address this challenge.

2.13. Cancer Stem Cells

Cancer stem cells (CSCs) are a subpopulation of cancer tissue cells with ability of self-renewal, differentiation in addition to possession of normal cancer cell characteristics (Figure 2.15.). CSCs show tumorigenicity when they are transplanted into different host tissue. Some surface markers such CD44, CD24, CD123 are used to identified CSCs (Yu et al., 2012). Existence of stem cells, usually buried inside the solid tumor and they can easily escape from traditional therapy, forms the basis of cancer recurrence after therapy.

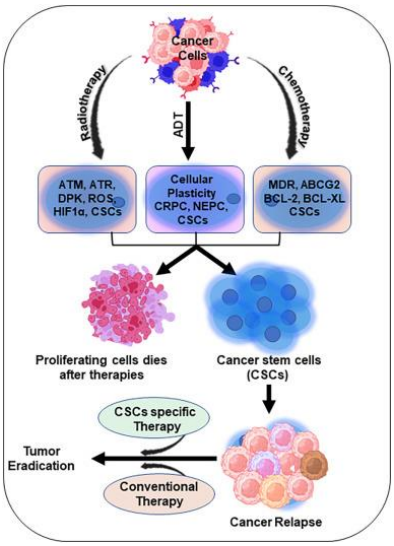

Figure 2.12. Cancer stem cell has self-renewal capacity leading to tumor recurrence after therapy(Verma et al., 2023)

Aldehyde dehydrogenase (ALDH) is a cytosolic enzyme widely used to identify CSCs in many cancers types such liver, breast, colon and ovarian. This enzyme contributes to drug resistance during the chemotherapy because it enables metabolization of the anticancer drug such cyclophosphamide. Enzyme also decreases the reactive oxygen species, hence protects the cancer cell from DNA damage (Muralikrishnan et al., 2020 ; Visvader & Lindeman, 2008).

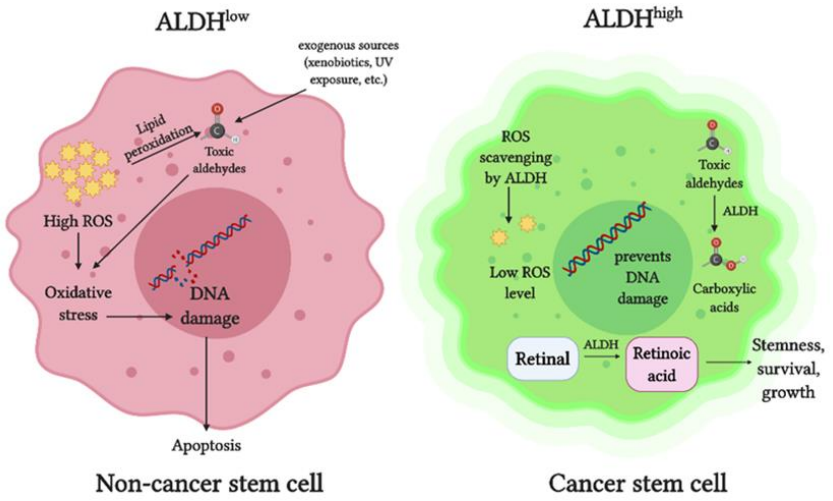

Figure 2.16. Role of ALDH in cancer stem cells (Muralikrishnan et al., 2020)

Moreover, ALDH indirectly affects the pro-oncogenic and pro-survival gene transcription. It converts retinol to retinoic acid. Retinoic acid enters the nucleus, binds to the retinoic acid receptor, a type of ligand-activated transcription factor. In this way transcription of several genes are initiated (Yue et al., 2022). These gene products might also contribute drug resistance (Figure 2.16.). ALDH1A1, a member of ALDH enzyme family, leads to cisplatin resistance by increasing drug efflux pumps expression via NEK-2(Figure 2.16.) (Uddin et al., 2020) .

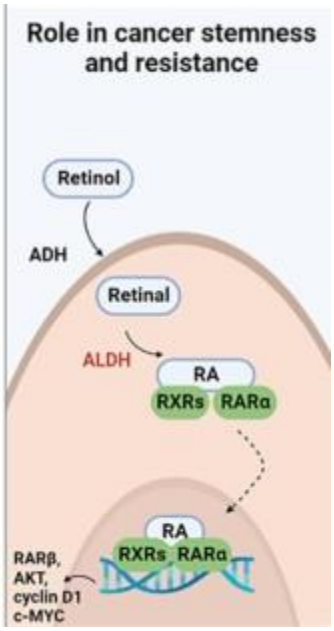

Figure 2.13. ALDH mediated retinol metabolism and its effect on the transcription of genes responsible for cell proliferation (Al-Shamma et al., 2023)

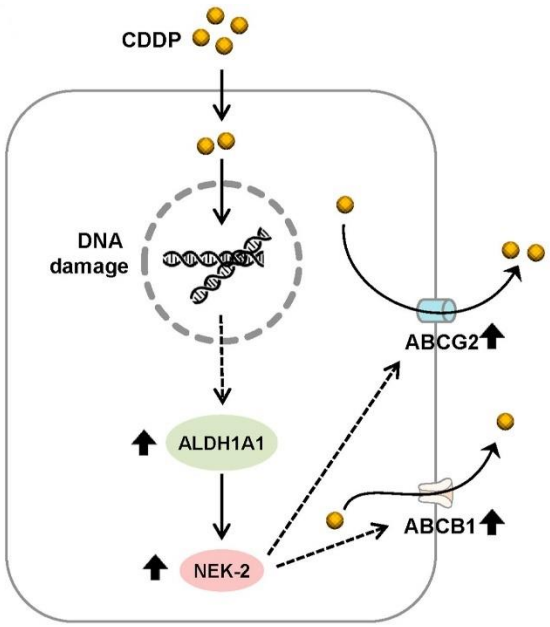

Figure 2.17. Overexpression of ABC transporters through ALDH1A1 activation mediated by NEK-2.

2.14. Targeted Protein Degradation and Overcoming Drug Resistance via PROTAC

Strategies to overcome cancer drug resistance have been explored by many research groups for many years. Scientists develop new inhibitors against to molecular targets associated with the drug resistance. Combinations of these inhibitors are applied in cancer therapy in recent years. This strategy might share the same fate because basic principle of these therapies is same that inhibit the target factor in the cancer cell which also might trigger the drug resistance. Other strategies can be generalized as genetic engineering applications such transcriptional gene silencing or mRNA vaccines. These are taught as sophisticated methods but these are expensive and their application requires well-trained employees.

Proteolysis Targeting Chimera (PROTAC) might be a new strategy against cancer drug resistance. PROTAC is the smart therapeutic agent that hijack the Ubiquitin Proteosome System (UPS). UPS is a native protein turn over mechanism that allows specific protein degradation in the eukaryotic cell by initial ubiquitin labelling and subsequent proteasomal degradation of the labelled protein (Figure 2.18).

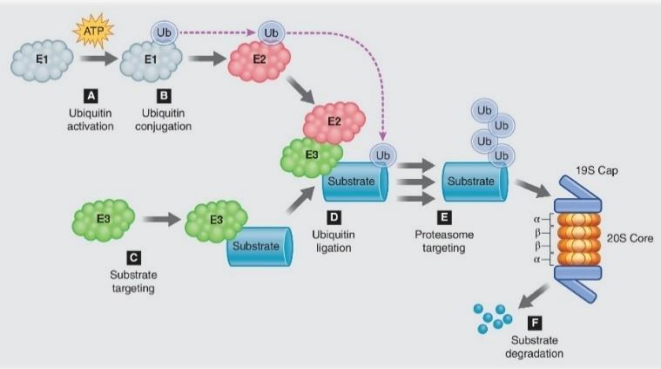

Figure 2.18. Schematic representation of ubiquitin proteosome system (Schneider et al., 2021)

PROTAC molecules are bifunctional molecules with two molecular heads binding to ubiquitin ligase and protein to be degraded. Through this way, target protein and E3 ligase get closer to each other enabling accelerated target protein ubiquitination. After ubiquitination, targeted protein is recognized by proteosome complex and degraded (Sun et al., 2019). This proximity-based approach allows rapid degradation of protein of interest by using the native proteolysis pathways of the cell (Figure 2.19).

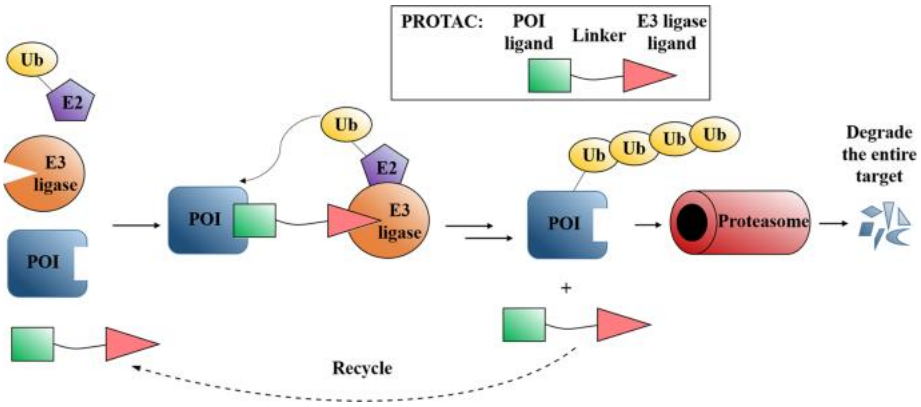

Figure 2.19. Schematic representation of PROTAC working principle(Sun et al., 2019)

PROTAC molecules are generally heterobifunctional compounds. It consists of 3 different modules:

- Protein of interest (POI) ligand: binds to target protein
- E3 ligase Ligand: binds to E3 ligase
- Linker: connects POI and E3 ligase ligand

Compared to traditional inhibitor approaches, there are several advantages of PROTACs as therapeutic tools. First of all, traditional inhibitors generally bind to the active side of the protein in this way catalytic activity is blocked. However, there are some proteins that share a similar catalytic pocket. Therefore, target specificity problem arises. Also, not all proteins are

druggable. PROTAC can target protein without binding to the catalytic side or well-defined activity modulating domain. Another advantage of PROTAC is recycling. After ubiquitination of target protein, PROTAC become free, and it can be re-used again and again. So, it can be effective in even very low concentrations unlike the traditional inhibitor. These above-mentioned advantages decrease the risk of resistance development against PROTACs (Zeng et al., 2021).

Liu group have suggested VHL-based CYP1B1 degraders that reverse the Taxol resistance in A549/Taxol cell at even nanomolar concertation(Figure 2.20) (Yao et al., 2024).

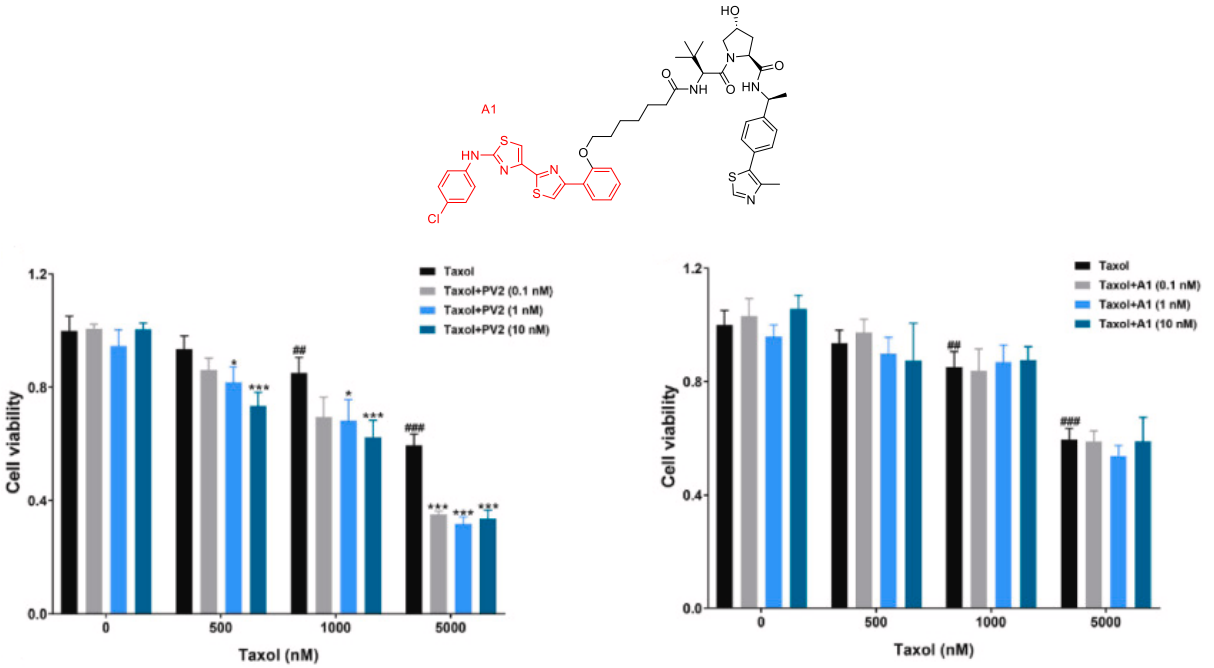

Figure 2.20. Compared with CYP1B1 inhibitor (A1, red), CYP1B1 degrader effectively increased the sensitivity of A549/Taxol cells to Taxol(Yao et al., 2024)

3. MATERIAL AND METHOD

Thesis project aims to develop ratiometric fluorescent probes for esterase and/or nitroreductase enzymes specifically to enable drug resistant cancer cell imaging. Additionally, within the scope of the theses, three different PROTAC molecules are developed with the aim of targeting HCE2, ALDH1A1 and MDR1 proteins.

3.1. Molecular Design of Fluorescent Probes

In the first part of the thesis, the aim is to develop diagnostic agents that discriminate drug resistance cancer cell from nonresistant cancer cell. To accomplish this aim, new fluorescent probes were designed for esterase, as well as nitroreductase (Scheme 3.1) Distrylpyridinium BODIPY core (black) emits above 600 nm (Verirsen v.d. 2025). Through quaternization of pyridine moiety, enzyme sensitive moieties can easily be incorporated to probe core. In the thesis project, the aim is to target human carboxyl esterase (HCE) and nitroreductase (NTR) enzymes. As their pseudo-substrates, nitro benzyl group (green) and ester group (red) are attached to the distrylpyridine BODIPY which leads to bathochromic spectral shift. Enzyme activities lead to a change in intra-molecular charge transfer character as the enzyme sensitive parts are released from BODIPY. This allows ratiometric emission change to evaluate distinct cell status.

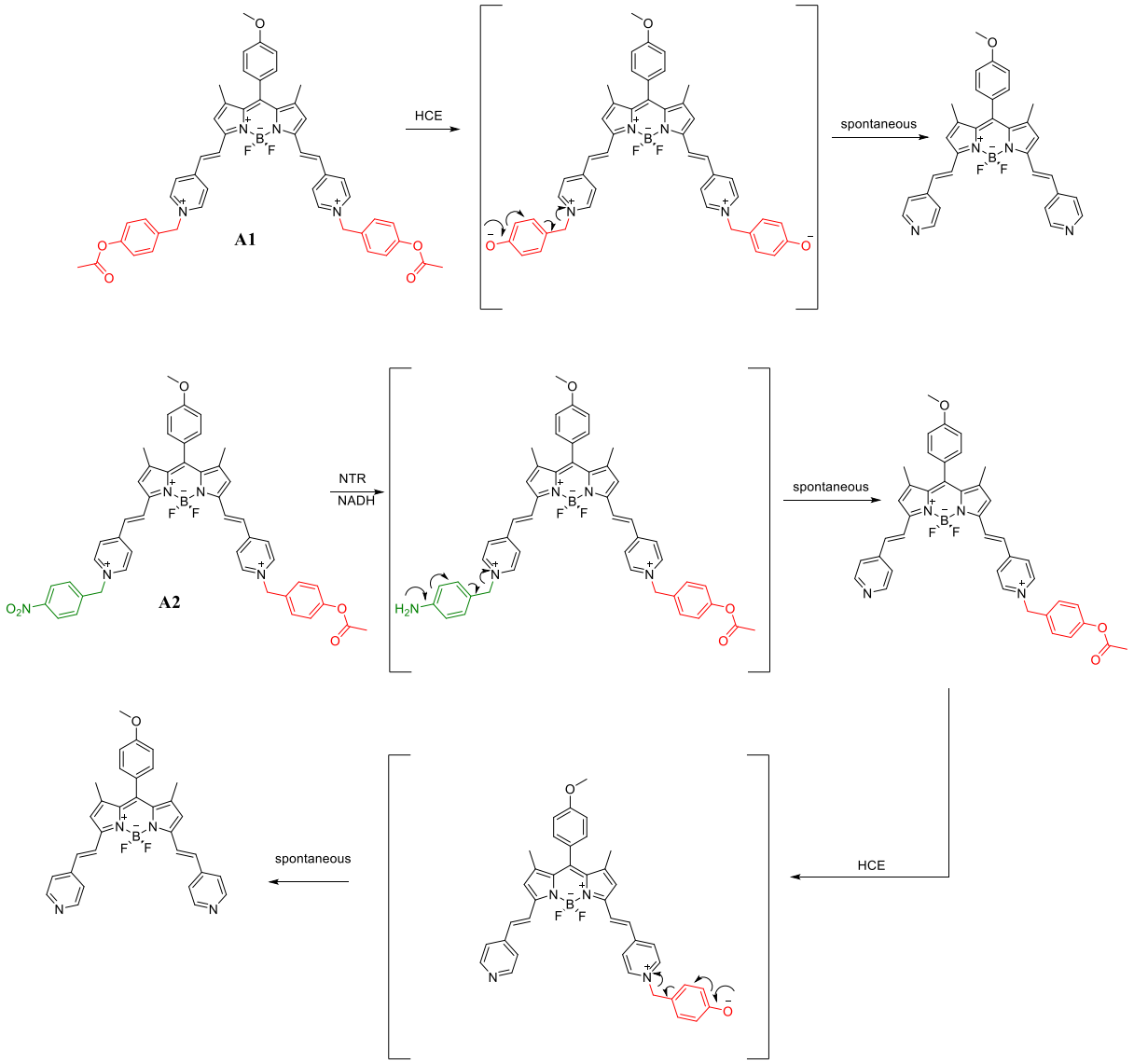

Scheme 3.1. Chemical structure and working mechanism of the probes A1 and A2. Enzyme mediated hydrolysis (by esterase, HCE) and reduction (by nitroreductase, NTR) leads to spontaneous elimination of enzyme-responsive modules.

3.1.2 Synthesis of the probes

Compound A1 and A2 were synthesized in five sequential steps as shown in Scheme 3.2. A common scaffold, compound 2, is used for the synthesis of both target probes. Purity of each compound are characterized by Nuclear Magnetic Resonance (NMR) and High-Resolution Mass Spectra. Details of the synthesis are given below.

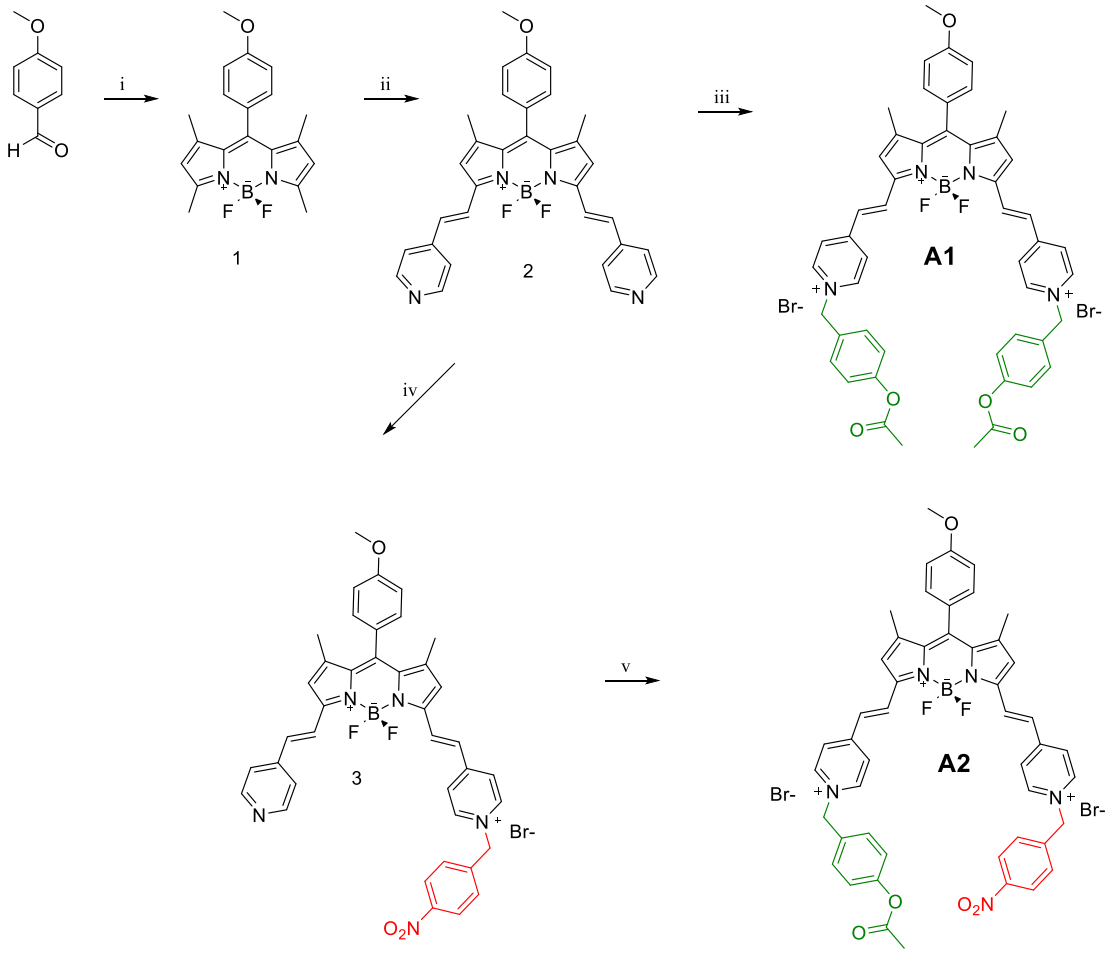

Scheme 3.2. Synthesis pathway of compound A1 and A2. Reaction conditions: i) a. 2,4- dimethyl pyrrole, TFA, DCM, N2, R.T.; b. p-chloranil, R.T.; c. Et3N, BF3.OEt2, R.T.; ii) 4- pyridinecarboxaldehyde, piperidine, AcOH, benzene, Dean-Stark, 90 °C; iii) 4-acetoxybenzyl bromide, DMF, RT; iv) 4-nitrobenzyl bromide, DMF, RT; v) 4-acetoxybenzyl bromide, DMF, RT

3.1.3. Synthesis of compound 1

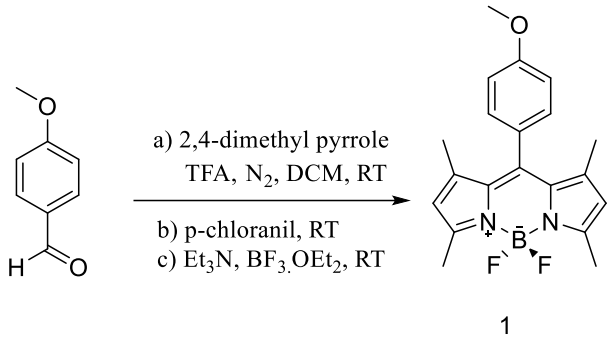

Scheme 3.3. Synthesis of Compound 1

100 mL of dichloromethane (DCM) in the flask was purged with N_2 for 15 minutes. 1.3gr (9.5 mmol) of p-anisaldehyde was added and nitrogen gas was purged for 5 minutes. Then, 2.2 mL (21 mmol) 2,4 dimethyl pyrrole and 5 drops of trifluoroacetic acid (TFA) were added. It was stirred in nitrogen gas for 16 hours at room temperature. After 16 hours, 2.41 g (9.80 mmol) p-chloranil was added. After 3 h stirring, 6 ml of triethyl amine and 6 ml of boron trifluoride etherate ($BF_3.OEt_2$) were added. It was stirred for 3 hours. Extraction was completed with water and DCM. The organic phase was collected and dried over sodium sulfate (Na_2SO_4), the solvent was evaporated under vacuum. It was purified by silica column chromatography using a mobile phase mixture of Hexane: EtOAc (20:1; v: v). 400 mg red solid product is obtained with 12% yield.

^{1}H NMR (400 MHz, $CDCl_3$) δ 7.17 (d, J = 8.6 Hz, 2H), 7.01 (d, J = 8.6 Hz, 2H), 5.97 (s, 2H), 3.87 (s, 3H), 2.55 (s, 6H), 1.43 (s, 6H).

^{13}C NMR (100 MHz, $CDCl_3$) δ 160.4, 155.5, 143.4, 142.1, 132.1, 129.4, 127.3, 121.3, 114.8, 55.5, 55.4, 14.8.

MS (ESI): m/z Theoretical value: 341.1637 $(M+H)^+$; Experimental value: 341.16168 (Δ: 5.92 ppm).

3.1.4. Synthesis of compound 2

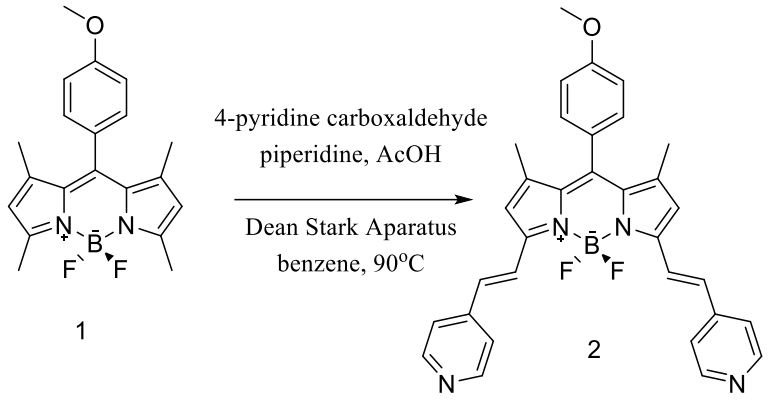

Scheme 3.4. Synthesis of Compound 2

420 mg (1.19 mmol) compound 1 was dissolved in 5 mL benzene. 400 µL 4-pyridine carboxaldehyde was added. 450 µL acetic acid and 400 µL piperidine were added. It was refluxed using Dean-Stark apparatus at 90ºC. When the reaction color was turned into purple-blue, reaction progress was monitored by thin layer chromatography (Acetone: Hexane; 1:2; v: v) It was be cooled and extraction was completed with water and DCM. The organic phase was dried over sodium sulfate (Na_2SO_4), the solvent was evaporated under vacuum. It was purified by silica column chromatography using a mobile phase mixture of Acetone: Hexane (1:3; v: v). 10 mg violet-blue solid was obtained with 3.9% yield.

^{1}H NMR (400 MHz, $CDCl_3$) δ 8.57 (d, J = 6.2 Hz, 4H), 7.82 (d, J = 16.3 Hz, 2H), 7.40 (d, J = 6.3 Hz, 4H), 7.16 (d, J = 8.7 Hz, 2H), 7.09 (d, J = 16.4 Hz, 2H), 6.99 (d, J = 8.7 Hz, 2H), 6.62 (s, 2H), 3.83 (s, 3H), 1.46 (s, 6H).

^{13}C NMR (100 MHz, $CDCl_3$) δ 160.7, 151.8, 150.2, 144.1, 141.6, 134.8, 133.3, 130.8, 129.5, 126.7, 123.7, 121.6, 118.8, 115.0, 55.6, 15.2.

MS (ESI): m/z Theoretical value: 533.2324 $(M+H)^+$; Experimental value: 533.22847 (Δ: 7.37 ppm).

3.1.5. Synthesis of compound A1

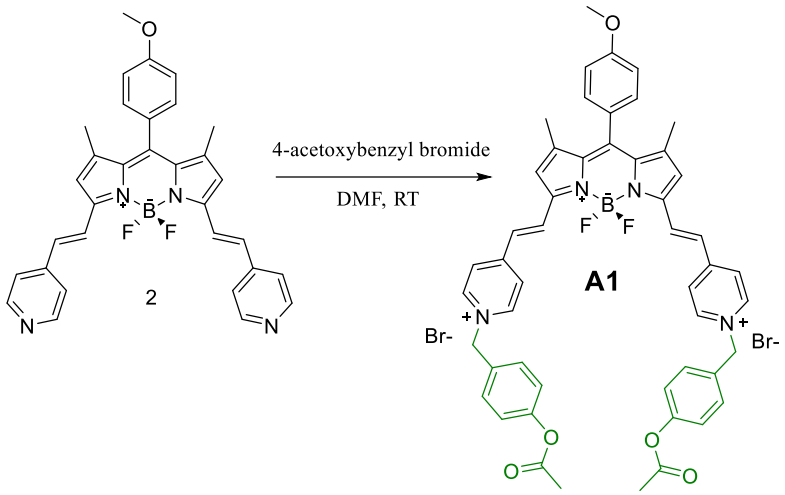

Scheme 3.5. Synthesis of Compound A1

30 mg (0.056mmol) compound 3 was dissolved in 5 mL dimethyl formamide (DMF). 65mg (0.28mmol) 4-acetoxy benzyl bromide was added. It was stirred at room temperature (RT) for 2 days. Solvent was partially removed through rotary evaporator and ethyl acetate was added to precipitate the product. Solid products were washed with ethyl acetate several times. Dark green products were obtained in quantitative yields.

^{1}H NMR (400 MHz, DMSO-d6) δ 9.16 (d, J = 6.5 Hz, 4H), 8.25 (d, J = 6.3 Hz, 4H), 7.94 (d, J = 16.4 Hz, 2H), 7.88 (d, J = 16.3 Hz, 2H), 7.61 (d, J = 8.6 Hz, 4H), 7.40 (d, J = 8.5 Hz, 2H), 7.32 – 7.02 (m, 8H), 5.87 (s, 4H), 3.86 (s, 3H), 2.28 (s, 6H), 1.54 (s, 6H).

MS (ESI): m/z Theoretical value: 415.17255 $(M)^{2+}$; Experimental value: 415.16751 (Δ: 12.1 ppm).

MS (ESI): m/z Theoretical value: 911.27020 $(M+Br^{-})^{+}$; Experimental value: 911.26048 (Δ: 10.67 ppm).

3.1.6 Synthesis of compound 3

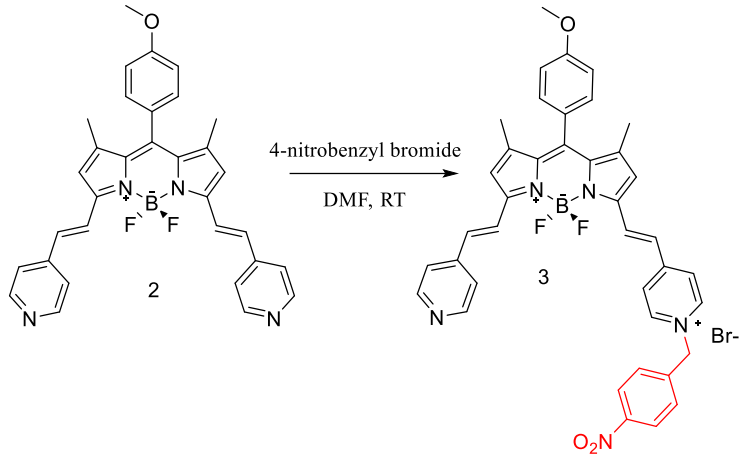

Scheme 3.6. Synthesis of Compound 3

60 mg (0.11 mmol) compound 2 was dissolved in 5ml DMF. 7 mg (0.033mmol) 4-nitrobenzly bromide was added. It was stirred over night at room temperature. The solvent was evaporated under vacuum. It was purified by silica column chromatography using a mobile phase mixture of DCM: MetOH (9:1; v: v) So, this method was repeated several times using the collected compound 2 from column chromatography. 40mg s green-black solid was obtained as with 54%yield

^{1}H NMR (400 MHz, DMSO-d_6) δ 9.08 (d, J = 6.2 Hz, 2H), 8.68 (b, 2H), 8.39 – 8.22 (m, 5H), 7.98 (d, J = 16.3 Hz, 1H), 7.86 – 7.67 (m, 4H), 7.55 (b, 2H), 7.39 (d, J = 8.2 Hz, 2H), 7.18 (s, 2H), 7.14 (d, J = 16.1 Hz, 2H), 6.00 (s, 2H), 3.86 (s, 3H), 1.54 (s, 3H), 1.51 (s, 3H).

^{13}C NMR (100 MHz, DMSO-d_6) δ 160.70, 154.58, 152.38, 151.05, 148.32, 145.72, 145.50, 143.11, 142.68, 142.06, 137.20, 130.29, 129.84, 125.75, 125.34, 124.65, 121.63, 120.84, 115.32, 55.80, 55.38, 15.22, 14.85.

MS (ESI): m/z Theoretical value: 668.26450 $(M)^{+}$; Experimental value: 668.26857(Δ: 6.09 ppm).

3.1.7. Synthesis of compound A2

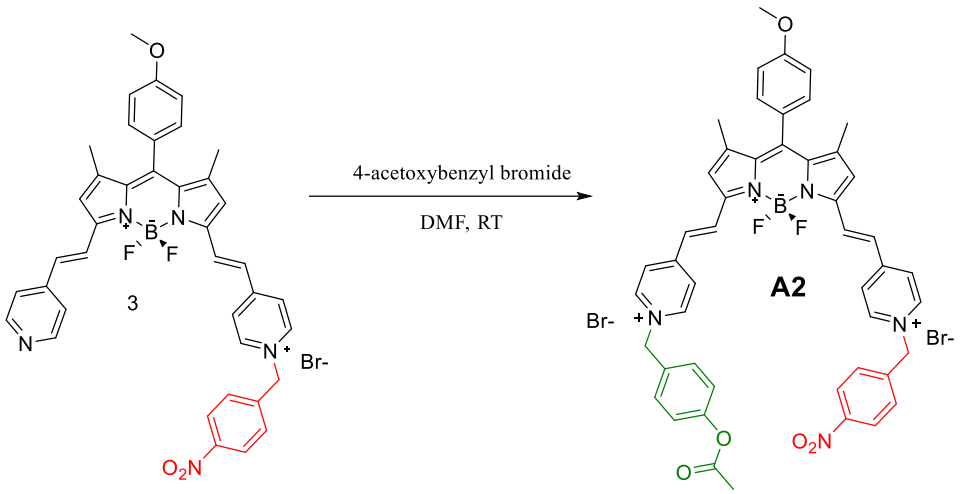

Scheme 3.7. Synthesis of Compound A2

32mg (0.05mmol) compound 3 was dissolved 3 mL DMF. 59 mg (0.25mmol) 4-acetoxybenzyl bromide was added. It was stirred at RT for 2 days. Starting material, compound 3, was completely consumed. DMF was removed under low vacuum. Residue was washed with Hexane-ethyl acetate-acetone. Green-black color was obtained with 53% quantitative yield

^{1}H NMR (400 MHz, DMSO-d6) δ 9.27 (dd, J = 6.7, 4.8 Hz, 4H), 8.40 – 8.16 (m, 6H), 8.04 – 7.90 (m, 4H), 7.85 (d, J = 8.8 Hz, 2H), 7.67 (d, J = 8.7 Hz, 2H), 7.38 (d, J = 8.5 Hz, 2H), 7.30 – 7.20 (m, 4H), 7.16 (d, J = 8.8 Hz, 2H), 6.13 (s, 2H), 5.94 (s, 2H), 3.84 (s, 3H), 2.27 (s, 3H), 1.49 (s, 6H).

^{13}C NMR (101 MHz, DMSO-d6) δ 169.6, 163.4, 162.8, 160.8, 157.5, 152.1, 151.7, 151.6, 148.3, 145.7, 145.4, 144.6, 142.0, 135.9, 135.3, 132.4, 132.1, 130.5, 130.4, 129.8, 128.5, 125.5, 124.6, 124.3, 123.1, 121.4, 115.4, 55.8, 34.8, 21.3.

MS (ESI): m/z Theoretical value: 408.66181 $(M)^{2+}$; Experimental value: 408.66540 (Δ: 8.78 ppm).

3.2. Molecular Design of PROTACs

In the second part of the thesis, the aim is to develop therapeutic agents that might have potential to overcome drug resistance in cancer cells. To accomplish this aim, new cereblon based PROTACs were designed to target different enzymes. The first of these PROTACs (B1) targets ALDH1A1 enzyme via dialkylamino benzaldehyde derivative (green), second PROTAC (B2) targets MDR1 efflux pumps via chrysin derivate (red) Last PROTAC (B3) targets human carboxyl esterase via benzil derivative(pink) (Figure 3.1). All PROTACs share to same cereblon targeting part which is a thalidomide derivative(blue).

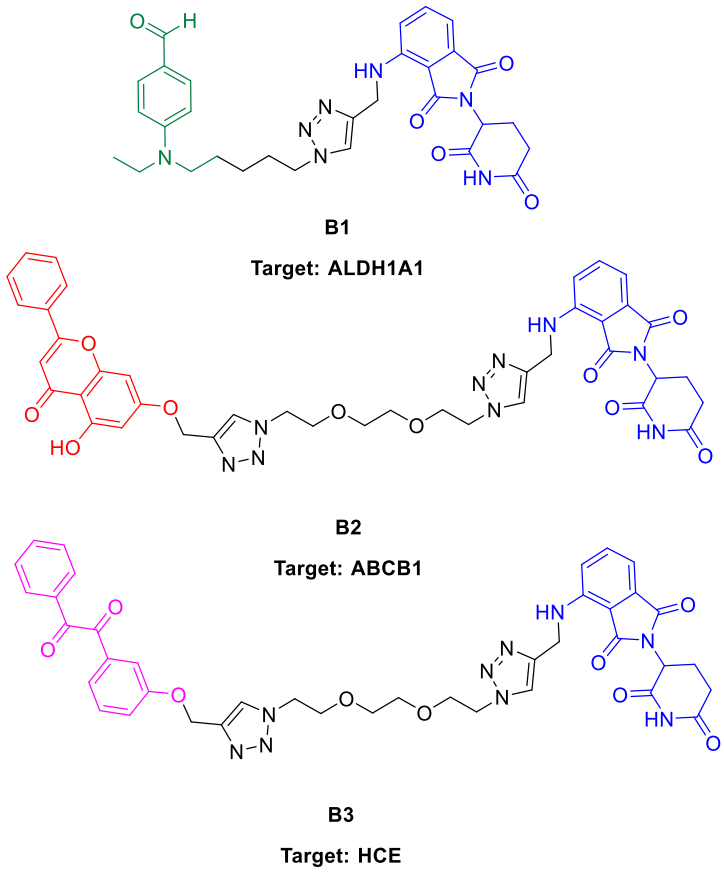

Figure 3.1. Chemical Structures of PROTACs Developed in Thesis Work.

So far, to the best of our knowledge, no protein degraders targeting any of these three enzymes are reported. Effect of the degradation is yet to be explored. Therefore, PROTACs that will be developed by the thesis work is structurally and functionally novel. If degradation of the target proteins can be optimized, this may pave the way for the development of therapeutics that can synergistically improve traditional chemotherapies and/or have therapeutic potential themselves.

3.2.1. Synthesis of ALDH1A1 PROTAC B1

Synthesis pathway of B1 PROTAC is shown in Scheme 3.8

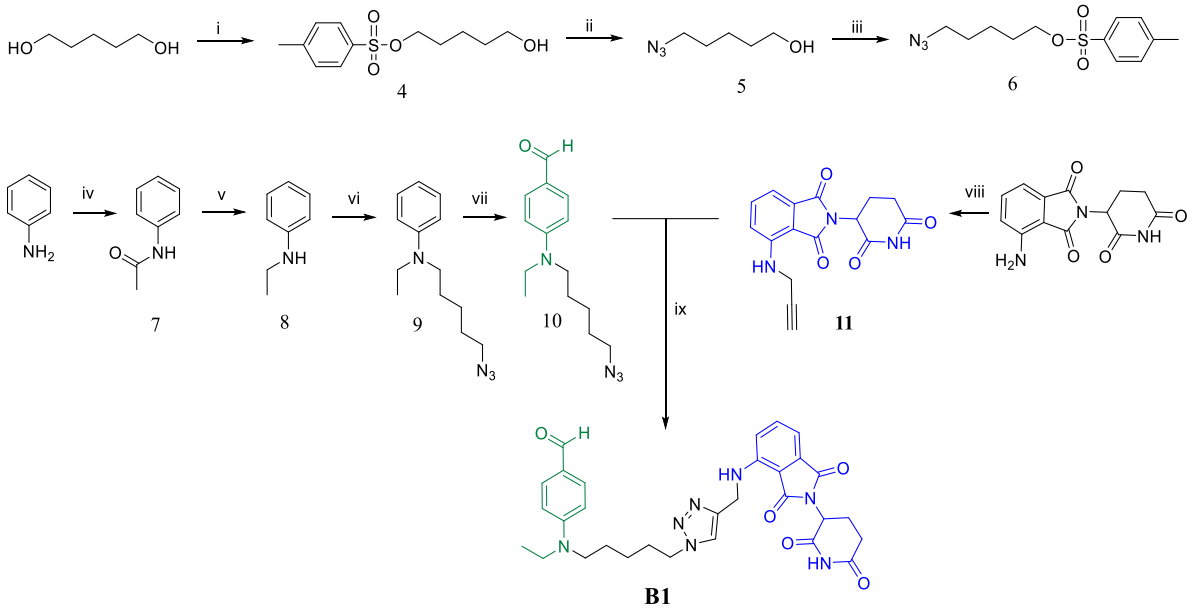

Scheme 3.8. Synthesis steps of ALDH1A1 PROTAC. i) TsCl, Et_3N, CH2Cl2, RT; ii) NaN_3, DMSO, 60ºC; iii) TsCl, Et_3N, CH_2Cl_2, RT; iv) acetyl chloride, Et_3N, DCM, RT; v) $LiAlH_4$, THF, 70ºC; vi) K_2CO_3, DMF, 80ºC; vii) $POCl_3$, DMF, 80ºC; viii) propargyl amine, DIEA, DMSO, 130ºC; ix) Cu(I)$MeCN_4PF_6$, CH_2Cl_2, RT

3.2.2 Synthesis of compound 4

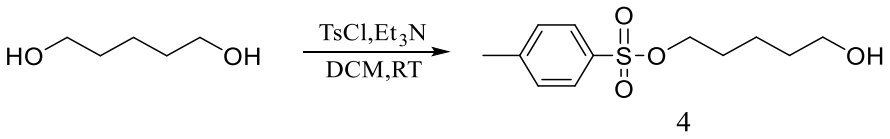

Scheme 3.9. Synthesis of Compound 4

2.1 mL (20mmol) 1,5-pentanediol was dissolved in 150 mL DCM. 2.76 mL (20mmol) triethylamine (Et_3N) was added. 3.8 g (20mmol) p-toluene sulfonyl chloride (TsCI) was added. It was stirred at RT overnight. Extraction was completed with water and DCM. The organic phase was collected and dried over sodium sulfate (Na_2SO_4), the solvent was evaporated under vacuum. The sample was purified by silica column chromatography using a mobile phase mixture of Hexane: EtoAc (6:1, v: v). 1.7 g yellow liquid product was obtained with 33% yield.

^{1}H NMR (400 MHz, Chloroform-*d*) δ 7.81 (d, *J* = 8.4 Hz, 2H), 7.37 (d, *J* = 7.9 Hz, 2H), 4.06 (t, *J* = 6.4 Hz, 2H), 3.64 (t, *J* = 6.4 Hz, 2H), 2.47 (s, 3H), 1.71 (dq, *J* = 8.0, 6.4 Hz, 2H), 1.61 – 1.51 (m, 2H), 1.49 – 1.34 (m, 2H).

^{13}C NMR (101 MHz, $CDCl_3$) δ 144.74, 133.16, 129.85, 127.90, 70.41, 62.60, 31.82, 28.61, 21.69, 21.65.

MS (ESI): m/z Theoretical value: 259.09985 $(M+H)^+$; Experimental value = 259.09915 $(M+H)^+$, (Δ = 2.70 ppm.)

3.2.3. Synthesis of compound 5

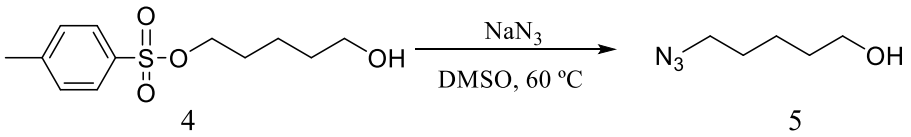

4 5

Scheme 3.10. Synthesis of Compound 5

980 mg (3.8mmol) Compound 4 was dissolved in 15 mL dimethyl sulfoxide (DMSO). 371 mg (5.7 mmol 1.5 mol equivalent) NaN_3 was added. The reaction mixture was stirred at 60ºC for 3 h, cooled, extracted with DCM and dried over Na_2SO_4, the solvent was evaporated under vacuum. 322 mg colorless liquid product was obtained with 66% yield.

^{1}H NMR (400 MHz, Chloroform-*d*) δ 3.69 (q, *J* = 2.6 Hz, 2H), 3.31 (t, *J* = 6.9 Hz, 2H), 1.79 – 1.60 (m, 4H), 1.53 – 1.45 (m, 2H), 1.31 (b, 1H).

^{13}C NMR (101 MHz, $CDCl_3$) δ 62.66, 51.40, 32.18, 28.66, 23.01.

MS (ESI): m/z Theoretical value: 130.09749 $(M+H)^+$; Experimental value = 130.09793 $(M+H)^+$, (Δ = 3.38 ppm.)

3.2.4. Synthesis of compound 6

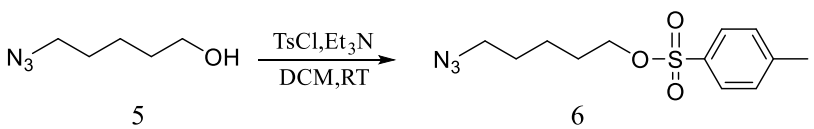

5 6

Scheme 3.10. Synthesis of Compound 6

322 mg (2.5 mmol) Compound 5 was dissolved in 10 mL DCM. 436 µL (3.125 mmol) EtN_3 was added. 538 mg (3.13 mmol) p-toluene sulfonyl chloride was added to the mixture. It

was stirred at RT overnight. Extraction was completed with water and DCM. The organic phase was collected and dried over Na_2SO_4, the solvent was evaporated under vacuum. It was purified by silica column chromatography using a mobile phase mixture of Hexane: EtOAc (3:1, v: v) as the mobile phase. 334 mg yellow liquid was obtained with 49% yield.

^{1}H NMR (400 MHz, Chloroform-*d*) δ 7.72 (d, *J* = 8.3 Hz, 2H), 7.28 (d, *J* = 7.9 Hz, 2H), 3.97 (t, *J* = 6.3 Hz, 2H), 3.16 (t, *J* = 6.8 Hz, 2H), 2.39 (s, 3H), 1.61 (m, 2H), 1.54 – 1.43 (m, 2H), 1.38 – 1.28 (m, 2H).

^{13}C NMR (101 MHz, $CDCl_3$) δ 144.81, 133.10, 129.87, 127.90, 70.10, 51.14, 28.42, 28.24, 22.72, 21.66.

MS (ESI): m/z Theoretical value:284.10634 $(M+H)^+$; Experimental value:284.10683 $(M+H)^+$, (Δ: 1.72 ppm).

3.2.5. Synthesis of compound 7

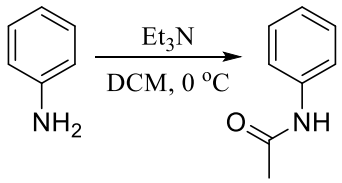

7

Scheme 3.11. Synthesis of Compound 7

20 mmol aniline was dissolved in 100 mL DCM. 30 mmol Et_3N was added. It was stirred in the ice-bath. 30 mmol acetyl chloride was added slowly. It was stirred at RT overnight. Extraction was completed with water and DCM. The organic phase was collected and dried over sodium sulfate (Na_2SO_4), the solvent was evaporated under vacuum. It was purified by silica column chromatography using a mobile phase mixture of Hexane: EtOAc (3:1, v: v) as the mobile phase. 2 g white viscous liquid was obtained with 74 % yield.

^{1}H NMR (400 MHz, Chloroform-*d*) δ 7.45 – 7.37 (m, 2H), 7.34 – 7.18 (m, 2H), 7.07 – 6.89 (m, 1H), 2.10 (s, 3H).

^{13}C NMR (101 MHz, $CDCl_3$) δ 168.39, 137.90, 129.00, 124.32, 119.90, 24.61.

MS (ESI): m/z Theoretical value: 136.07569 $(M+H)^+$; Experimental value = 136.07341 $(M+H)^+$, (Δ: 16.76 ppm).

3.2.6. Synthesis of compound 8

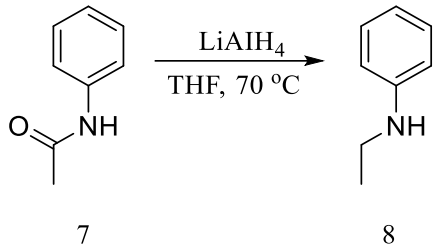

7 8

Scheme 3.12. Synthesis of Compound 8

541 mg (4 mmol) compound 7 was dissolved in 15 mL THF. It cooled in the ice bath. 380mg (10 mmol) lithium aluminum hydride ($LiAlH_4$) was added slowly. The reaction was refluxed at 70ºC for 2 hours. Then, the reaction was quenched with 2 mL water. The extraction was completed with water (pH 9) and DCM. The organic phase was collected and dried over sodium sulfate (Na_2SO_4), the solvent was evaporated under vacuum. It was purified by silica column chromatography using a mobile phase mixture of Hexane: EtOAc (23:2, v: v) as the mobile phase. 198 mg yellow liquid product was obtained with 40% yield.

^{1}H NMR (400 MHz, Chloroform-d) δ 7.10 (dd, J = 8.6, 7.4 Hz, 2H), 6.73 – 6.58 (m, 1H), 6.53 (dd, J = 8.7, 1.0 Hz, 2H), 3.45 (s, 2H), 3.08 (q, J = 7.1 Hz, 1H), 1.18 (t, J = 7.1 Hz, 3H).

^{13}C NMR (101 MHz, CDCl3) δ 148.47, 129.24, 117.22, 112.76, 38.48, 14.92.

MS (ESI): m/z Theoretical value: 122.09643 $(M+H)^+$; Experimental value = 122.09583 $(M+H)^+$, (Δ: 4.91 ppm).

3.2.7. Synthesis of compound 9

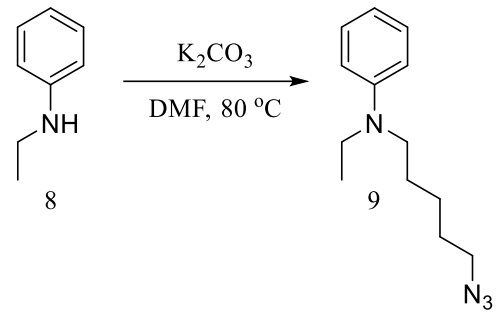

Scheme 3.13. Synthesis of Compound 9

180 mg (1.5 mmol) compound 8 was dissolved in 8 mL DMF. 334 mg (1.2 mmol) compound 6 was added. 276 mg (2 mmol 2 mole eq) was added. The reaction was stirred at 80 ºC overnight. Extraction was completed with water (pH 9) and DCM. The organic phase was collected and dried over sodium sulfate, the solvent was evaporated under vacuum. It was purified by silica column chromatography using a mobile phase mixture of Hexane: EtOAc (23:2, v: v) as the mobile phase. 32 mg yellow liquid was obtained with 14% yield.

^{1}H NMR (400 MHz, Chloroform-*d*) δ 7.14 (dd, *J* = 9.0, 7.2 Hz, 2H), 6.68 – 6.50 (m, 3H), 3.29 (q, *J* = 7.1 Hz, 2H), 3.20 (m, 4H), 1.69 – 1.51 (m, 4H), 1.41 – 1.31 (m, 2H), 1.07 (t, *J* = 7.0 Hz, 3H).

^{13}C NMR (101 MHz, $CDCl_3$) δ 146.86, 128.25, 114.47, 110.86, 50.39, 49.19, 44.00, 27.84, 26.14, 23.36, 11.26

MS (ESI): m/z Theoretical value: 233.17607 $(M+H)^+$; Experimental value = 233.17590 $(M+H)^+$, (Δ: = 0.73 ppm).

3.2.8. Synthesis of compound 10

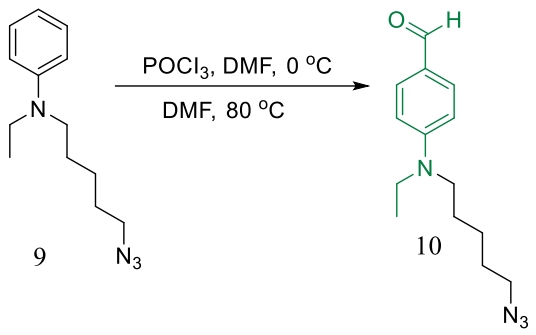

Scheme 3.14. Synthesis of Compound 10

145 µL (1.876 mmol) DMF was added to reaction round bottom flask or a viel. The reaction was cooled to 0ºC in ice-bath. While it was stirred, 190 mL $POCl_3$ was added. It was stirred for 1 h in ice-bath. 43 mg (0.2 mmol) Compound 9 was added. It was stirred at 80ºC. After 2 h, reaction was checked by TLC Hexane: EtOAc (23:2, v: v) until the compound 9 was consumed. Extraction was completed with water (pH>7) and DCM. The organic phase was collected and dried over sodium sulfate, the solvent was evaporated under vacuum. The crude sample was purified by silica column chromatography using a mobile phase mixture of Hexane: EtOAc (23:2, v: v) 7 mg yellow liquid product was obtained with 13% yield.

^{1}H NMR (400 MHz, Chloroform-d) δ 9.63 (s, 1H), 7.64 (d, J = 9.0 Hz, 2H), 6.59 (d, J = 8.6 Hz, 2H), 3.38 (q, J = 7.1 Hz, 2H), 3.29 (t, J = 7.7 Hz, 2H), 3.23 (t, J = 6.7 Hz, 2H), 1.58 (m, 4H), 1.45 – 1.31 (m, 2H), 1.14 (t, J = 7.1 Hz, 3H).

^{13}C NMR (101 MHz, $CDCl_3$) δ 190.01, 152.32, 132.29, 124.77, 110.68, 51.32, 50.30, 45.29, 28.80, 27.05, 24.28, 12.25.

MS (ESI): m/z Theoretical value: 261.17099 $(M+H)^+$; Experimental value = 261.16933 $(M+H)^+$, (Δ: 6.36 ppm).

3.2.9. Synthesis of compound 11

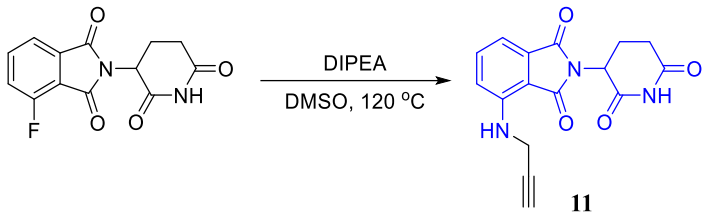

Scheme 3.15. Synthesis of Compound 11

553 mg (2 mmol) 2-(2,6-dioxo-piperidin-3-yl)-4-fluoroisoindoline-1,3-dione was dissolved in 8 mL DMSO. DIPEA (6mmol) and propargyl amine (2.2 mmol 1.1 eq.) was added to the reaction. The reaction was stirred at 130 ºC for 16 h. The reaction was cooled to room temperature. Extraction was completed with water and diethyl ether. The organic phase was collected and dried over sodium sulfate, the solvent was evaporated under vacuum. It was purified by silica column chromatography using a mobile phase mixture of Hexane: Ethyl acetate (3:2, v: v) as mobile phase. 500 mg yellow solid was obtained with 80% yield

^{1}H NMR (400 MHz, Chloroform-*d*) δ 8.02 (s, 1H), 7.50 (dd, *J* = 8.5, 7.2 Hz, 1H), 7.13 (dd, *J* = 7.2, 0.6 Hz, 1H), 6.96 (d, *J* = 8.4 Hz, 1H), 6.38 (t, *J* = 6.1 Hz, 1H), 4.85 (dd, *J* = 12.2, 5.4 Hz, 1H), 4.03 (dd, *J* = 6.1, 2.5 Hz, 2H), 2.90 – 2.59 (m, 3H), 2.20 (t, *J* = 2.4 Hz, 1H), 2.09 – 2.01 (m, 1H).

^{13}C NMR (101 MHz, $CDCl_3$) δ 170.92, 169.25, 168.17, 167.44, 145.56, 136.15, 132.43, 117.18, 112.75, 111.41, 79.14, 72.19, 48.96, 32.32, 31.42, 30.94 (acetone), 22.77.

MS (ESI): m/z Theoretical value: 312.0984 $(M+H)^{+}$; Experimental value: 312.09749 (Δ: 6.09 ppm).

3.2.2. Synthesis of compound B1

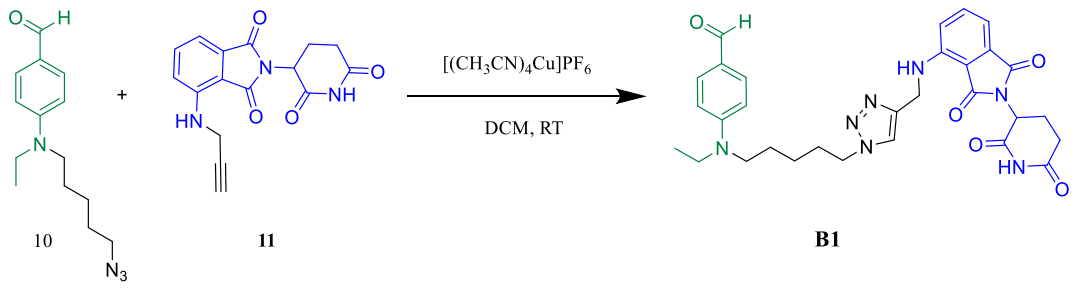

Scheme 3.15. Synthesis of Compound B1

6.5 mg (0.027 mmol) compound 10 was dissolved in 1 mL DCM. 17 mg (0.054 mmol) compound 11 and 21 mg (0.054 mmol) tetrakis(acetonitrile)copper(I)hexafluorophosphate were added. It was stirred overnight at RT. Extraction was completed with water (EDTA containing) and DCM. The organic phase was collected and dried over sodium sulfate, the solvent was evaporated under vacuum. It was purified by silica column chromatography using a mobile phase EtOAc. 14 mg yellow solid was obtained with. 90% yield

^{1}H NMR (400 MHz, Chloroform-*d*) δ 9.62 (s, 1H), 8.36 (b, 1H), 7.63 (d, J = 9.0 Hz, 2H), 7.42 (dd, J = 7.7, 0.9 Hz, 1H), 7.39 (s, 1H), 7.06 (dd, J = 7.2, 0.6 Hz, 1H), 6.92 (d, J = 8.5 Hz, 1H), 6.62 (t, J = 6.0 Hz, 1H), 6.56 (d, J = 9.0 Hz, 2H), 4.95 – 4.78 (m, 1H), 4.56 (d, J = 5.9 Hz, 2H), 4.28 (t, J = 7.0 Hz, 2H), 3.34 (q, J = 7.1 Hz, 2H), 3.32 – 3.16 (m, 2H), 2.93 – 2.52 (m, 3H), 2.09 – 2.00 (m, 1H), 1.88 (dq, J = 10.7, 7.2 Hz, 2H), 1.70 – 1.45 (m, 2H), 1.38 – 1.24 (m, 2H), 1.11 (t, J = 7.1 Hz, 3H).

^{13}C NMR (101 MHz, CDCl3) δ 190.10, 171.14, 169.42, 168.51, 167.47, 152.26, 146.15, 145.23, 136.25, 132.44, 124.79, 121.55, 117.10, 112.35, 110.83, 110.70, 63.73, 50.10, 48.96, 45.30, 38.73, 31.43, 30.08, 26.85, 23.97, 22.76, 12.23.

MS (ESI): m/z Theoretical value: 572.26159 $(M+H)^{+}$; Experimental value: 572.26190 (Δ: 0.54 ppm).

3.3.1. Synthesis of MDR1 PROTAC B2

Synthesis pathway of B2 PROTAC is shown in Scheme 3.16 and the details are given below.

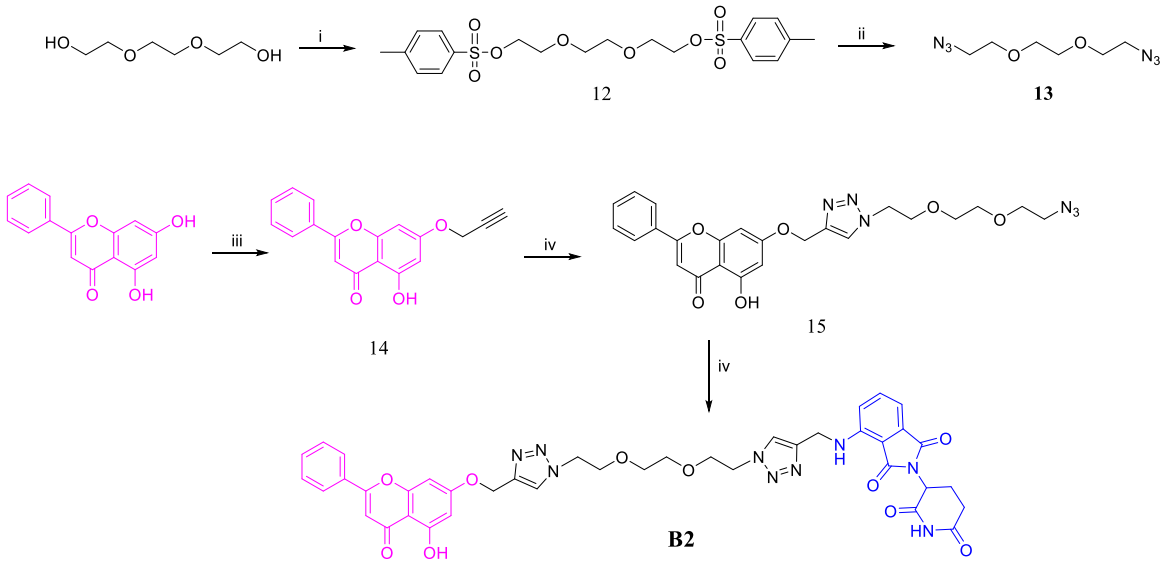

Scheme 3.16. Synthesis steps of ABCB1 PROTAC. i) TsCl, Et3N, CH2Cl2, RT; ii) NaN3, DMSO, 60ºC; iii) propargyl bromide, K_2CO_3, DMF; iv) Cu(I)MeCN4PF6, CH_2Cl_2, RT vi) Cu(I)$MeCN_4PF_6$, CH_2Cl_2, RT

3.3.2. Synthesis of compound 12

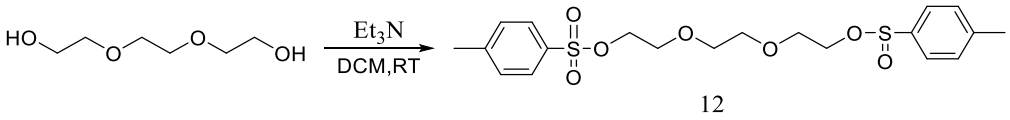

Scheme 3.16. Synthesis of Compound 12

510 mL (3.75 mmol) Triethylene glycol (510 mL, 3.75 mmol, 1 eq.) was dissolved in 25 mL DCM. 2.145g (11.25 mmol) p-toluene sulfonyl chloride and 1.139 mL (11.25 mmol) triethylamine were added. The reaction was stirred at room temperature for 24 h. Extraction was completed with water and DCM. The organic phase was collected and dried over sodium sulfate, the solvent was evaporated under vacuum. It was purified by silica column chromatography using a mobile phase mixture of Hexane: Ethyl acetate (1:1; v: v). 1.3 g white solid was obtained with 76% yield.

^{1}H NMR (400 MHz, Chloroform-*d*) δ 7.72 (d, *J* = 8.3 Hz, 4H), 7.41 – 7.24 (m, 4H), 4.09 – 4.04 (m, 4H), 3.70 – 3.53 (m, 4H), 3.46 (s, 4H), 2.37 (s, 6H).

^{13}C NMR (101 MHz, $CDCl_3$) δ 144.88, 132.98, 129.86, 127.97, 70.70, 69.21, 68.75, 21.65.

MS (ESI): m/z Theoretical value: 481.0967 $(M+Na)^+$; Experimental value: 481.09634$(M+Na)^+$ (Δ: 0.75 ppm).

3.2.3. Synthesis of compound 13

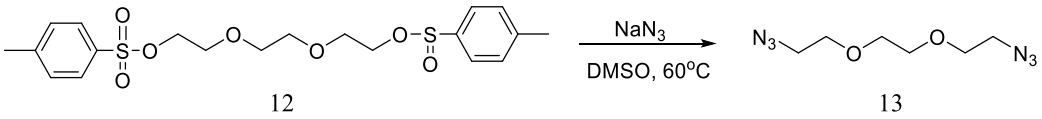

Scheme 3.17. Synthesis of Compound 13

459 mg (1 mmol) Compound 12 was dissolved in 10 mL DMSO. 163 mg sodium azide (2.5 mmol) was added. The reaction was stirred at 60 ºC for 3 h. The reaction was cooled to room temperature. Extraction was completed with water and DCM. The organic phase was collected and dried over sodium sulfate, the solvent was evaporated under vacuum. 148 mg light yellow liquid was obtained as with 74% yield.

^{1}H NMR (400 MHz, Chloroform-*d*) δ 3.73 – 3.55 (m, 8H), 3.36 – 3.30 (m, 4H).

^{13}C NMR (101 MHz, $CDCl_3$) δ 70.76, 70.16, 50.71.

MS (ESI): m/z Theoretical value: 223.0920 $(M+H)^+$; Experimental value: 223.09143$(M+Na)^+$, Δ = 2.55 ppm.

3.3.4. Synthesis of compound 14

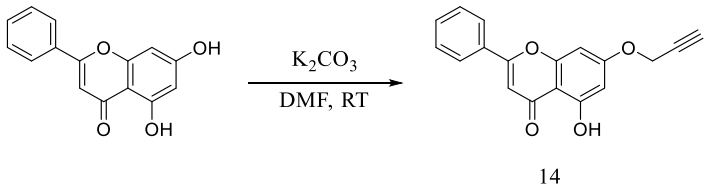

Scheme 3.18. Synthesis of Compound 14

600 mg (2.36 mmol) chrysin was dissolved in 10 mL DMF. (489 mg, 3.5 mmol) Potassium carbonate K_2CO_3 and 296 mL (3.44 mmol) propargyl bromide (80 wt% solution in toluene) was added sequentially. The reaction was stirred at room temperature for 12 h. The reaction was monitored by TLC using DMC: Ethyl acetate mobile phase (1:9; v: v) until chrysin was totally consumed. DMF was removed under reduced pressure. Extraction was completed

with water and DCM. The organic phase was collected and dried over sodium sulfate, the solvent was evaporated under vacuum. It was purified by silica column chromatography using a mobile phase mixture of DMC: Ethyl acetate (1:9; v: v) as the mobile phase. 610 mg yellow solid was obtained with 89% yield

^{1}H NMR (400 MHz, Chloroform-*d*) δ 12.66 (s, 1H), 7.81 (dd, *J* = 8.1, 1.6 Hz, 2H), 7.57 – 7.30 (m, 3H), 6.60 (s, 1H), 6.51 (d, *J* = 2.3 Hz, 1H), 6.37 (d, *J* = 2.2 Hz, 1H), 4.70 (d, *J* = 2.4 Hz, 2H), 2.53 (t, *J* = 2.4 Hz, 1H).

^{13}C NMR (101 MHz, $CDCl_3$) δ 182.53, 164.16, 163.35, 162.23, 157.66, 131.93, 131.25, 129.12, 126.34, 106.22, 105.96, 98.95, 93.56, 76.73, 76.58, 56.21.

MS (ESI): m/z Theoretical value: 293.0814 $(M+H)^+$; Experimental value:293.08088 $(M+H)^+$, (Δ: 2.55 ppm).

3.3.5. Synthesis of compound 15

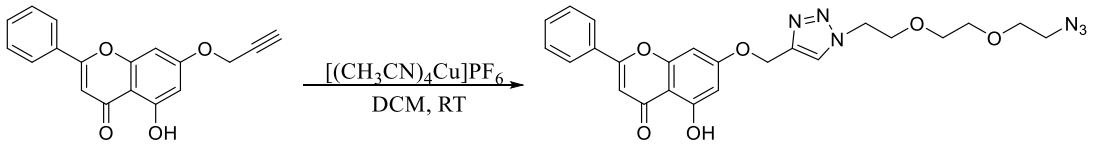

14 15

Scheme 3.19. Synthesis of Compound 15

146 mg (0.5 mmol) compound 14 and 200 mg (1 mmol) compound 13 were dissolved in 6 ml DCM. 186 mg (0.5 mmol) tetrakis(acetonitrile)copper(I)hexafluorophosphate was added. The reaction was stirred overnight at RT. Extraction was completed with water (EDTA containing) and DCM. The organic phase was collected and dried over sodium sulfate, the solvent was evaporated under vacuum. It was purified by silica column chromatography using a mobile phase mixture of Hexane: Acetone (1:1, v: v). 53 mg light yellow was obtained with 22% yield.

^{1}H NMR (400 MHz, Chloroform-*d*) δ 12.65 (s, 1H), 7.90 – 7.70 (m, 3H), 7.62 – 7.32 (m, 3H), 6.61 (s, 1H), 6.59 (d, *J* = 2.2 Hz, 1H), 6.38 (d, *J* = 2.3 Hz, 1H), 5.23 (s, 2H), 4.59 – 4.45 (m, 2H), 3.93 – 3.76 (m, 2H), 3.60 – 3.47 (m, 6H), 3.32 – 3.26 (m, 2H).

^{13}C NMR (101 MHz, $CDCl_3$) δ 206.99 (acetone peak), 182.52, 164.17, 164.15, 162.16, 157.81, 131.91, 131.25, 129.12, 126.36, 124.32, 105.93, 99.10, 93.34, 70.55, 70.53, 70.09, 69.44, 62.43, 50.66, 50.46, 30.94 (acetone peak).

MS (ESI): m/z Theoretical value: 493.1836 $(M+H)^+$; Experimental value = 493.18282 $(M+H)^+$, (Δ: 1.58 ppm)

3.3.6. Synthesis of compound B2

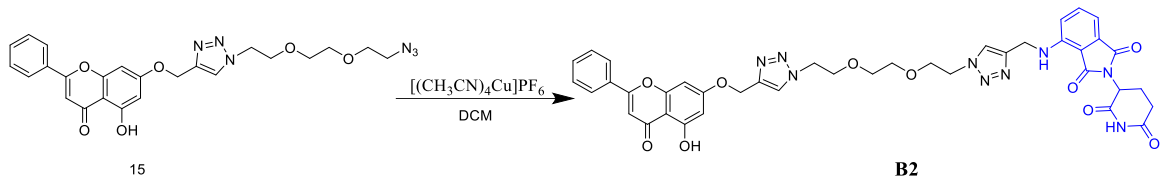

Scheme 3.20. Synthesis of Compound B2

38 mg (0.08 mmol) compound 15 and 37.5 mg (0.12 mmol) compound 11 were dissolved in 10 mL DCM. 60 mg (0.16 mmol) Tetrakis (acetonitrile)copper(I)hexafluorophosphate was added. The reaction was stirred at room temperature for 24. The reaction was monitored by TLC Hexane: Acetone (2:1; v: v) until compound 15 is consumed. Extraction was completed with water (EDTA containing) and DCM. The organic phase was collected and dried over sodium sulfate, the solvent was evaporated under vacuum. It was purified by silica column chromatography using a mobile phase mixture of Hexane: Acetone (2:1; v: v). 15mg yellow solid was obtained with 23% yield.

^{1}H NMR (400 MHz, Cloroform-*d*) δ 12.65 (s, 1H), 8.26 (s, 1H), 7.81 (dd, J = 8.1, 1.7 Hz, 2H), 7.71 (s, 1H), 7.52 (s, 1H), 7.49 – 7.42 (m, 3H), 7.38 (dd, J = 8.5, 7.1 Hz, 1H), 7.02 (d, J = 7.0 Hz, 1H), 6.94 (d, J = 8.5 Hz, 1H), 6.64 (t, J = 6.0 Hz, 1H), 6.59 (s, 1H), 6.55 (d, J = 2.3 Hz, 1H), 6.35 (d, J = 2.3 Hz, 1H), 5.21 (s, 2H), 4.88 – 4.78 (m, 1H), 4.55 (d, J = 5.9 Hz, 2H), 4.46 – 4.24 (m, 5H), 3.79 – 3.67 (m, 4H), 3.42 (s, 4H), 2.86 – 2.60 (m, 3H), 2.14 – 1.94 (m, 1H).

MS (ESI): m/z Theoretical value: 802.25906 $(M-H)^-$, Experimental value: 802.26173 $(M-H)^-$, (Δ: 1.58 ppm).

3.4.1. Synthesis of carboxylesterase PROTAC B3

Synthesis pathway of B2 PROTAC is shown in Scheme 3.21 and the details are given below.

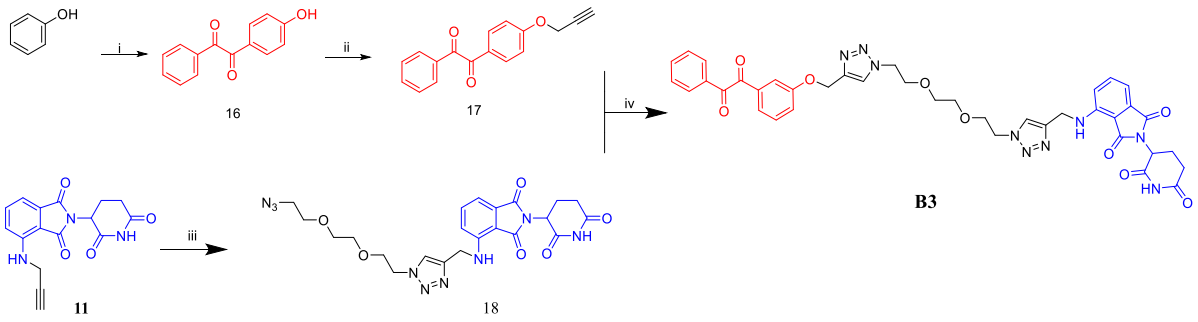

Scheme 3.21. Synthesis steps of carboxylesterase PROTAC. i) acetophenone, I_2, Zn, $CuBr_2$, H_3BO_3, DMSO, 100ºC; ii) propargyl bromide, K2CO3, MeCN, 70ºC; iv) CuSO4, C6H7NaO6, CH_2Cl_2: THF, RT

3.4.2. Synthesis of compound 16

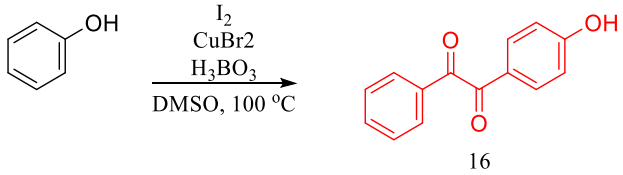

Scheme 3.22. Synthesis of Compound 16

2 mmol phenol, 1 mmol Acetophenone, 1.5 mmol Iodine, 0.2 mmol copper(II) bromide $CuBr_2$, 1 mmol Boric acid were dissolved in 3 mL DMSO. It was stirred for 6 hours at 100ºC. The extraction was completed with water (saturated with NaCI) and EtOAc. The organic phase was collected and dried over sodium sulfate, the solvent was evaporated under vacuum. It was purified by silica column chromatography using a mobile phase mixture of Hexane: EtOAc (7:3, v: v) as the mobile phase. The compound was used for further synthesis without purification(Xiang et al., 2016).

3.4.3. Synthesis of compound 17

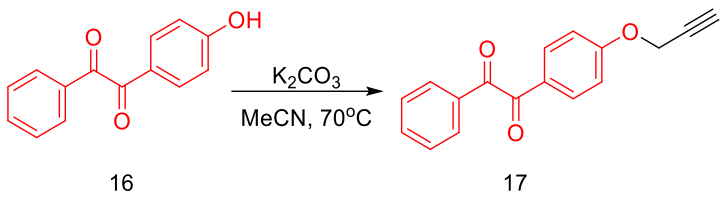

Scheme 3.23. Synthesis of Compound 17

35 mg (0.15 mmol) compound 16 was dissolved 7 mL acetonitrile 24 µL (0.225 mmol) propargyl bromide and 42 mg (0.3 mmol) K_2CO_3 were added. The reaction was refluxed at 70ºC for 4 hours. Then acetonitrile was removed. then crude residue was purified by silica gel column chromatography using Hexane: EtOAc (15:1, v: v) as the mobile phase. 40 mg yellow oily liquid was obtained with 81% yield.

^{1}H NMR (400 MHz, Cloroform-*d*) δ 8.27 – 7.91 (m, 4H), 7.77 – 7.58 (m, 1H), 7.54 – 7.42 (m, 2H), 7.07 (d, J = 9.0 Hz, 2H), 4.78 (d, J = 2.4 Hz, 2H), 2.56 (t, J = 2.4 Hz, 1H).

^{13}C NMR (101 MHz, $CDCl_3$) δ 194.71, 193.11, 162.74, 134.79, 133.14, 132.32, 129.94, 128.99, 126.81, 115.22, 77.23, 76.50, 55.99.

MS (ESI): m/z Theoretical $(M+H)^+$: 265.08592; Experimental m/z $(M+H)^+$: 265.08631, (Δ:1.47 ppm).

3.4.4. Synthesis of compound 18

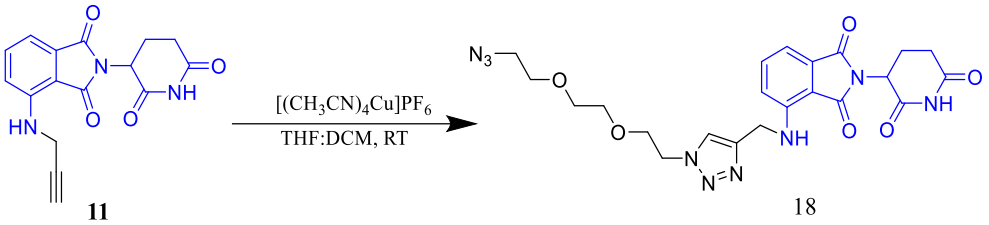

Scheme 3.24. Synthesis of Compound 18

700 mg (2.25 mmol) compound 11 was dissolved in 4 mL THF:6ml DCM. 2.25 mmol compound 13 and 839 mg (2.25 mmol) tetrakis (acetonitrile)copper(I)hexafluorophosphate was added. It was stirred overnight. Extraction was completed with water (EDTA containing) and DCM. The organic phase was collected and dried over sodium sulfate, the solvent was

evaporated under vacuum. It was purified by silica column chromatography using a mobile phase mixture of Hexane: Ethyl Acetate (1:4, v:v). 60 mg yellow solid was obtained.

^{1}H NMR (400 MHz, Cloroform-*d*) δ 8.13 (s, 1H), 7.69 (s, 1H), 7.50 (dd, J = 8.5, 7.1 Hz, 1H), 7.18 – 7.07 (m, 1H), 7.04 (d, J = 8.5 Hz, 1H), 6.69 (t, J = 6.0 Hz, 1H), 4.92 (dd, J = 12.1, 5.3 Hz, 1H), 4.63 (d, J = 6.0 Hz, 2H), 4.53 (dd, J = 5.5, 4.6 Hz, 2H), 3.86 (dd, J = 5.5, 4.5 Hz, 2H), 3.68 – 3.53 (m, 6H), 3.35 (dd, J = 5.5, 4.3 Hz, 2H), 3.04 – 2.59 (m, 3H), 2.25 – 2.06 (m, 1H).

^{13}C NMR (101 MHz, $CDCl_3$) δ 170.94, 169.34, 168.25, 167.50, 146.25, 144.88, 136.20, 132.41, 122.94, 117.22, 112.25, 110.75, 70.52, 70.50, 70.07, 69.45, 50.66, 50.39, 48.92, 38.73, 31.42, 22.77.

MS (ESI): m/z Theoretical value: 512.20005 $(M-H)^-$, Experimental value: 512.19953 $(M-H)^-$, (Δ: 1.02 ppm).

3.4.5. Synthesis of compound B3

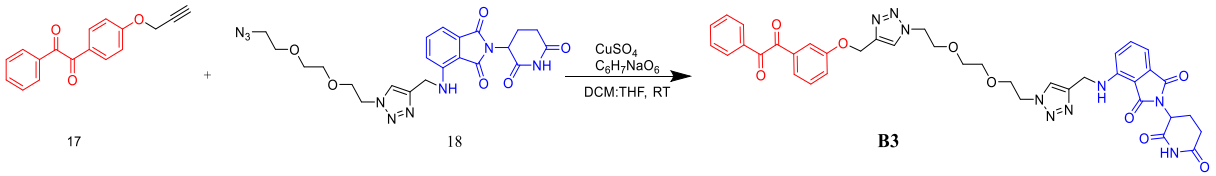

Scheme 3.24. Synthesis of Compound B3

51 mg (0.1 mmol) compound 17 was dissolved in 6 mL DCM and 3 mL THF. 33 mg (0.125 mmol) compound 18 was added. 0.6mmol $CuSO_4$ and 0.6 mmol sodium ascorbate were added. It was stirred at RT for 2 days. Compound 17 was completely consumed. Extraction was completed with water (EDTA containing) and DCM. The organic phase was collected and dried over sodium sulfate, the solvent was evaporated under vacuum. It was purified by silica column chromatography using EtOAc as the mobile phase. 21 mg yellow solid product was obtained with 27% yield.

^{1}H NMR (400 MHz, Cloroform-*d*) δ 8.47 (s, 1H), 8.04 – 7.88 (m, 4H), 7.74 (s, 1H), 7.69 – 7.62 (m, 1H), 7.59 (s, 1H), 7.55 – 7.40 (m, 3H), 7.15 – 6.95 (m, 4H), 6.72 (t, J = 6.0 Hz, 1H), 5.28 (s, 2H), 5.02 – 4.86 (m, 1H), 4.62 (d, J = 5.9 Hz, 2H), 4.55 – 4.39 (m, 4H), 3.77 (ddd, J = 5.6, 4.6, 2.4 Hz, 4H), 3.47 (s, 4H), 3.05 – 2.64 (m, 3H), 2.12 (ddd, J = 7.6, 6.3, 3.8 Hz, 1H).

^{13}C NMR (101 MHz, $CDCl_3$) δ 194.79, 193.08, 171.21, 169.35, 168.56, 167.48, 163.53, 146.19, 145.00, 142.86, 136.20, 134.83, 133.10, 132.39, 129.92, 129.00, 126.46, 124.18,

122.85, 117.25, 115.17, 112.20, 110.66, 70.31, 69.30, 62.16, 60.41, 50.34, 48.94, 38.64, 31.41, 22.74, 21.06, 14.21.

MS (ESI): m/z Theoretical value: 776.27870 $(M-H)^-$, Experimental value: 776.27788 $(M-H)^-$, (Δ:1.06 ppm).

3.5.1. Spectral analysis

Stock solution of the probes compound 2, A1 and A2 were prepared in DMSO. Absorbance of each stock solutions is checked to determine exact concentrations from the Beer-Lambert Law.

$$A = \varepsilon C l \qquad \textbf{Formula 1}$$

In Formula 1, A refers to absorbance value at the maximum absorbance wavelength, ε refers to extinction coefficient, C refers to concentration of the sample, l is the light path taken to be 1 cm for the quartz cuvette used in the experiments. Zinc Phthalocyanine (ZnPc) was used as reference compound to calculate fluorescence quantum yields of the compounds. Formula 2 is used for calculations:

$$\Phi_F(s) = \Phi_F(r)\,(A_r\, I_s\, n_s^2)/(A_s\, I_r\, n_r^2) \qquad \textbf{Formula 2}$$

In Formula 2, the abbreviation r refers to the reference compound and s refers to the molecules. Φ_F is the fluorescence quantum yield of ZnPc and it is taken to be 0.28 for this compound in ethanol. n values are tabulated refractive indexes of the solvents. A is the absorbance at the excitation wavelength and I is the integrated fluorescence area calculated using the Origin software. Time-resolved fluorescence spectrometry analysis was used to determine fluorescence lifetime (Φ_F) of the probes. The analysis was done at Bilkent University National Nanotechnology Research Center (UNAM) using 625 nm laser source.

Spectroscopic analysis and selectivity of the probes were analyzed in 25% water in DMSO for A1 and A2 to visualize Compound 2 formation. Fluorescence spectra were recorded by exciting samples at 600 nm unless otherwise given. To analyze the effect of target enzyme and some abundant cellular components on A1 fluorescence 10 U/mL carboxylesterase enzyme, 0.5 mM of glucose, 120 mM NaCl, 20 mg/mL BSA, 0.1 mM GSH were used in the presence of 3.75 μM probe.

3.5.2. Preparing drug resistant Hep3B cells

Sorafenib was used to generate drug resistant human hepatocellular carcinoma Hep3B cells. The same dose was applied on cell for weeks and dose gradually increased over weeks. RNA isolation was done when the applied drug dose reached 2.75μM and the level of drug resistance marker gene Multi-Drug Resistance 1 (MDR1) was checked by RT-PCR. This gene encodes membrane pump responsible for drug efflux (Tang et al., 2020). Statistically significant overexpression of this gene compared to untreated Hep3B cells is considered as gain of sorafenib resistance.

3.5.3. Fluorescence microscopy imaging

For fluorescence cell imaging with A1, Hep3B cells were seeded on 6-well plate with a cell density of $20x10^5$ cells/well using the High-glucose DMEM medium supplemented with 10% FBS and 0.1% gentamycin antibiotic. Cells were incubated in humidified incubator at 37ºC for at least 24 h. One group of cells were treated with benzil (200 μM, esterase inhibitor) for 2h under the same incubation conditions and others are untreated. Then, 4 μM A1 was applied to all wells. After 30 min incubation, cells are washed with Phosphate Saline Buffer (PBS) three times and cells are fixed with 4% formaldehyde for 20 min. Cells are washed again with PBS three times and the cells are incubated with nucleus stain DAPI (7.5 μM) for 10 min. After washing three times with PBS, 1 mL PBS was added and cell images are obtained using Zeiss microscopy, Axiocam 305 camera. Spectra are recorded selecting DAPI (excitation wavelength 353 nm, emission wavelength 465 nm) and AF610 channels (excitation wavelength 612, emission wavelength 630 nm).

For fluorescence cell imaging with A2 sensor (4 μM), either sorafenib resistant Hep3B cells (R (+)) or normal Hep3B cells (R (-)) are used. Cells are either exposed to hypoxic environment at least 16 h prior to probe addition using 100 μM $CoCl_2.6H_2O$ or incubated under normoxic conditions. For appropriate groups, esterase inhibitor benzil (200 μM) is added to the cell medium 2 h prior to probe addition. After 30 minutes of probe incubation, the cells were fixed and the procedures applied to the A1 microscopy analysis were repeated.

Micrographs were analyzed using ImageJ software and the statistical analysis were performed using GrapPad software. P values greater than or equal to 0.05 were considered as statistically significant.

3.5.4. Gene expression analysis

Sorafenib drug resistance of Hep3B is confirmed by Real Time Polymerase Chain Reaction (RT-PCR) method. Gene expression was analyzed when the sorafenib dose reaches 2.75 μM concentration. To isolate RNA from cells, cells were seeded on 6-well plate in HG-DMEM supplemented with 10% FBS and 0.1% gentamycin and incubated at 37ºC for at least 24 h. Medium of the wells were discarded and cells were collected using Trypsin-EDTA. RNA was isolated with GeneJEt RNA purification kit (Thermo Scientific). cDNA was synthesized (Takara: 6110A-50) and relative gene expression was analyzed with RT-PCR (SYBR Green Supermix, Bio-Rad). β-Actin was used as reference housekeeping gene. Primer set used for PCR analysis is given Table 3.1

Gene	Forward Primer (5' to 3')	Reverse Primer (5' to 3')
MDR1	CCCATCATTGCAATAGCAGG	TGTTCAAACTTCTGCTCCTGA
HCE2	AACCTGTCTGCCTGTGACCAAG	ACATCAGCAGCGTTAACATTTTCTG
HIF1α	TATGACCAGAAGAACTTTTAGC	CACCTCTTTTGGCAAGCATCCTG
ACTB	CACCATTGGCAATGAGCGGTTC	AGG TCT TTG CGGATGTCCACGT

Table 3.1. Primer sequences used for RT-PCR analysis

3.5.5. Cell viability analysis

Hep3B or resistant Hep3B cells were seeded with a seeding density of $5x10^3$ cells/well on 96-well plate in HG-DMEM supplemented with 10% FBS and 1% gentamycin and incubated at 37ºC in humidified incubator for at least 24 h. Then, 100 mL fresh medium contains different doses of the compounds were added to each well. Compound stocks were prepared in DMSO. The final DMSO concentrations in the cell do not exceed 1% to avoid toxicity. Cells were further incubated for 24 h. 100 mL medium containing of 5 mg/mL 3-(4,5-dimethylthiazol-2-yl)-2,5-diphenyltetrazolium bromide (MTT,) was added to each well and the cells were further incubated in the dark for 4 h. 100 mL DMSO was added to each well to dissolve resulting formazan crystals. After 15 min incubation absorbance at 570 nm was recorded using ELISA plate reader (Thermo Instruments, ABD). Experiments were done with at least three replicates. Average values of each dose were normalized to untreated cell control group to determine relative viability. Formula 3 is used to determine percent cell viability

$$\textbf{\% Cell Viability} = A_d/A_c*100 \qquad \textbf{Formula 3}$$

Where, A_d is the absorbance of the dose applied cells at 570 nm and A_c is the absorbance of untreated cells at 570 nm.

3.5.6. Western blot analysis

Protein was isolated form Hep3B cell with RIPA buffer (ElabScience) or cell lysis buffer (ElabScience) with protease inhibitors cocktail. Protein concentration was evaluated with UV/VIS nano spectrophotometer (MicroDigital). The SDS-PAGE was performed with 6% bis-acrylamide gel. Protein was transferred to PDVF membrane (Thermo Scientific™) via semi-dry transfer system (Trans-Blot® Turbo™ Transfer System) at 25V for 10 min. Membrane was blocked with 3% skim milk powder (SERVA) for 2 hours at 4°C. Membrane is incubated with primary antibodies (ALDH1A1 Polyclonal Antibody (E-AB-60451); MDR1/ABCB1 Antibody (G-1): sc-13131; CES1 Antibody (A-11): sc-365249) for 16 hours at 4°C. It was washed with TBST. Membrane is incubated with secondary antibody conjugated HRP (Goat anti-Rabbit IgG (H+L) Secondary Antibody, HRP,65-6120; Goat anti-Mouse IgG (H+L) Secondary Antibody, HRP,62-6520) for 3 hours and washed with TBST. Membrane is incubated with chemiluminescent agent (West Pico Plus Chemiluminescent) and was monitored with chemiluminescent imager (ChemiDoc™ Touch Imaging System).

4. RESULTS AND DISCUSSION

4.1. Gene Expression Analysis

One of the major aims of the project is to monitor drug resistant cancer cells. Therefore, sorafenib resistant Hep3B cells were prepared, and gene expression profile was analyzed to verify the development of resistance. PCR results show that MDR1 gene expression is significantly increased in Hep3B cells exposed to increasing amount of sorafenib up to 2.75µM over the course of weeks (Figure 4.1).

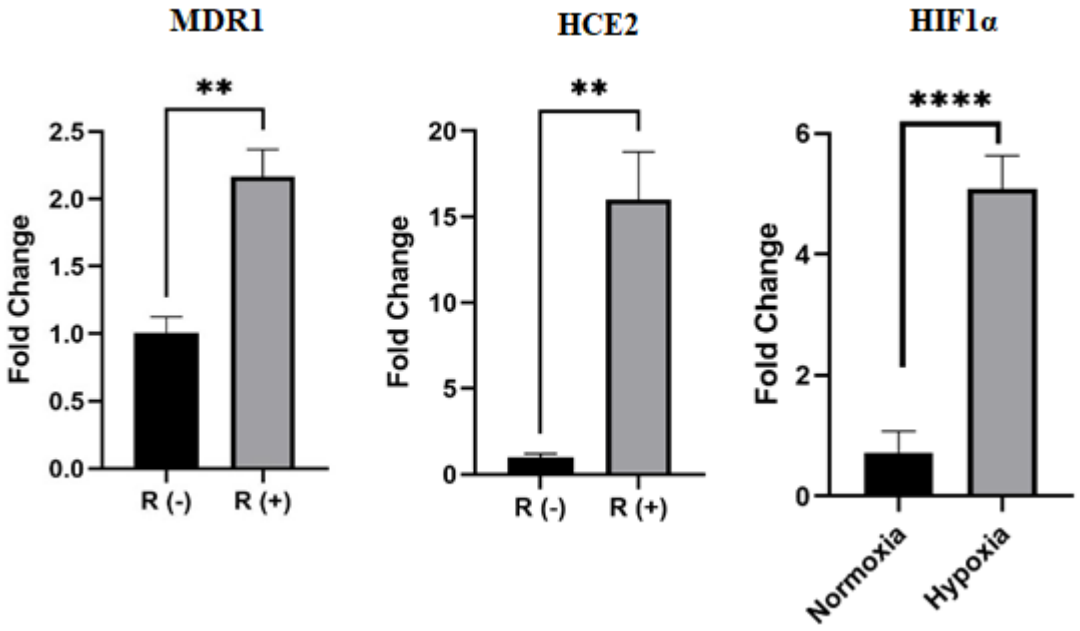

Figure 4.1. Relative mRNA levels of MDR1, HCE2 genes in sorafenib resistant (R(+)) and normal Hep3B cells (R(-)) and HIF1a expression in normoxic and hypoxic Hep3B cells. Hypoxia is generated by incubating cells with 100 mM CoCl2.6H2O for 24 h. ($n \geq 3$)

The same analysis was performed for Human carboxylesterase gene and similarly, expression of this gene is also shown to significantly increase in resistant cells (Figure 4.1).

To verify the generation of hypoxia in Hep3B cells, expression of hypoxia marker HIF1a was analyzed. Cells were incubated with 100 mM $CoCl_2.6H_2O$ for 24 h and RNA is isolated. RT-PCR analysis indicates significant overexpression of HIF1a in hypoxic cells as shown in Figure 4.1.

4.2. Spectroscopic Analysis of the Probes

UV-absorbance and fluorescence analysis of the probes, compound 2, A1 and A2 in DCM, DMSO and 10% water in DMSO were given in Figures 4.2. In DMSO, the maximum absorbance peak of A1 is at 663 nm and the maximum fluorescence peak is at 703 nm, when excited at 600 nm. In apolar DCM, peak absorbance and emission wavelengths display a bathochromic shift. These solvent dependent spectral properties are usually observed in ICT-based probes.

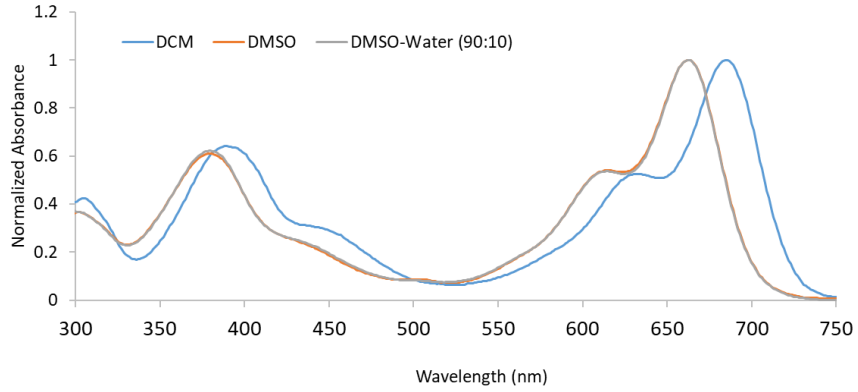

Figure 4.2. Normalized UV-Vis absorbance spectra of A1 in DCM, DMSO and 10% water in DMSO (Sahin et. al. 2025).

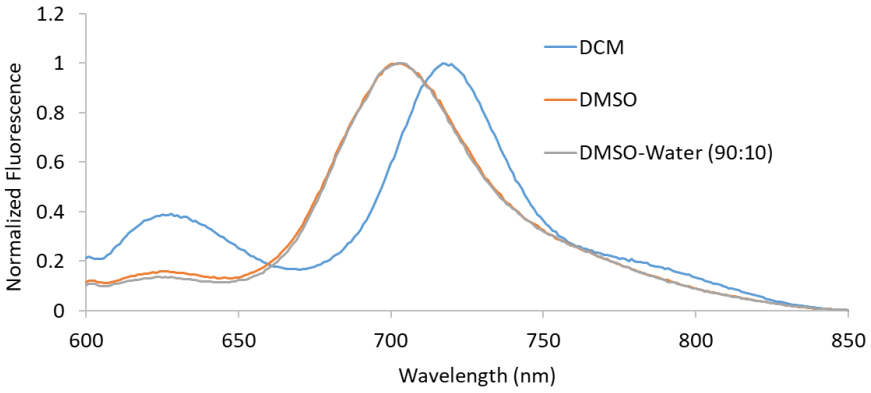

Figure 4.3. Normalized fluorescence spectra of A1 in DCM, DMSO and 10% water in DMSO (excited at 600 nm) (Sahin et. al. 2025).

Fluorescence intensity of A1 in PBS: DMSO solvent mixture (25:75; v: v) was measured in the presence of varying concentrations of carboxylesterase enzyme (0.5-10 U/mL) (Figure 4.4.). The samples were incubated for 30 min and spectra were recorded by exciting at 600 nm.

While the emission peak at 704 nm was decreasing, the peak at 629 nm was increasing depending on the increase of enzyme concentration. Ratio of fluorescence intensity at 622 nm to 704 nm was calculated and the obtained values are plotted with respect to enzyme concentrations (0-10 U/mL). An obvious correlation between the ratio of intensities to dose of enzyme is obtained as shown in Figure 4.4.

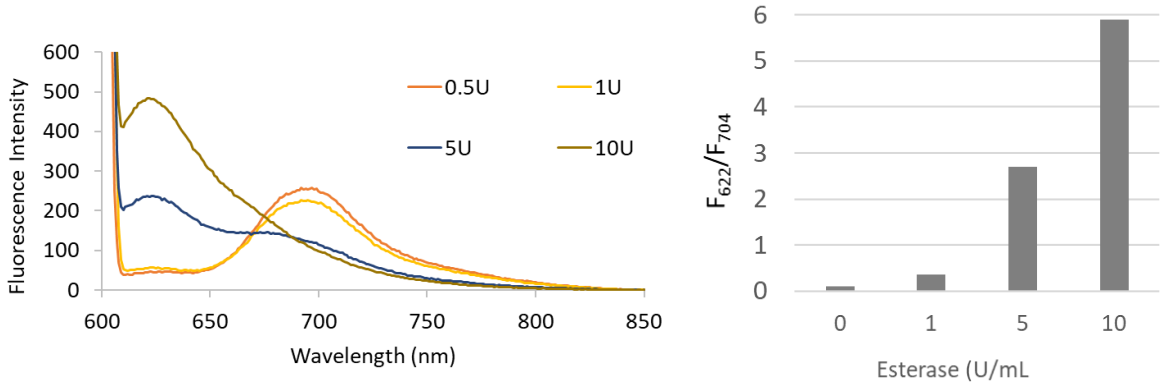

Figure 4.4. Change in the fluorescence of A1 (3.75 μM) upon treatment with different concentrations of the enzyme (0.5-10 U/mL) and the resulting ratio of fluorescence intensity at 622 nm to the emission at 704 nm. An obvious enzyme dependent ratiometric response is generated (Sahin et. al. 2025).

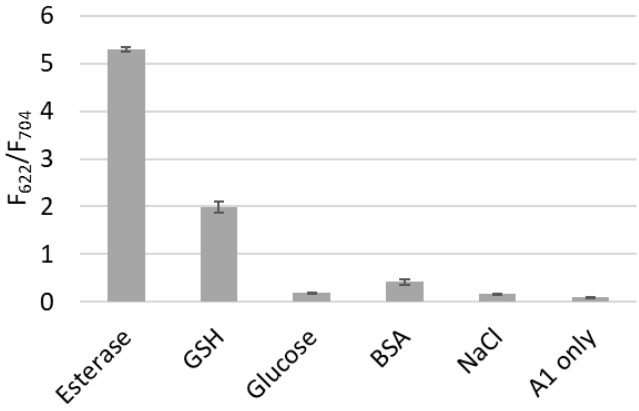

Figure 4.5. Change in the fluorescence of A1 (3.75 mM) within 30 min. upon treatment with different possibly competing analytes (excited at 600 nm) (Sahin et. al. 2025).

Selectivity of the probe A1 is analyzed using abundant biological analytes. For this purpose, glutathione, glucose, albumin, NaCl are used in biologically relevant concentrations. As shown in Figure 4.5., none of these analytes display significant change in ratiometric fluorescent output. Only, GSH display some enhancement which is attributed to ester hydrolysis

through thioester formation. Since this analyte is also a drug resistance marker, the partial interference is not considered as a disadvantage.

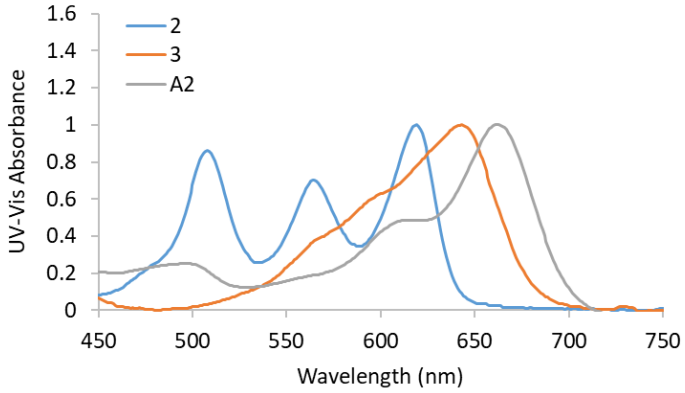

Figure 4.6. Normalized UV-Vis absorbance spectra of 2, 3 and A2 in 25% PBS in DMSO (Sahin et. al. 2025)

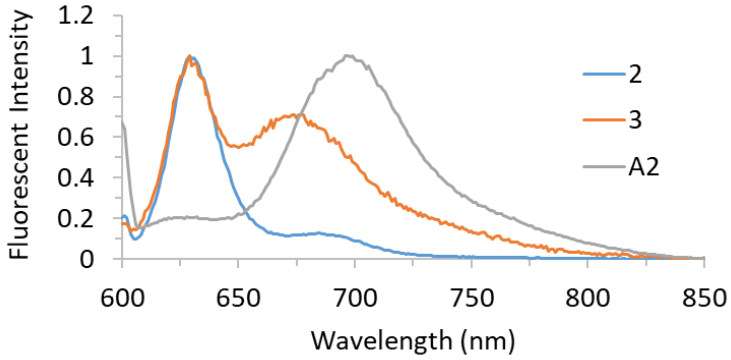

Figure 4.7. Normalized fluorescence spectra of 2, 3 and A2 in 25% PBS in DMSO. Fluorescence spectra are obtained by exciting at 600 nm (Sahin et. al. 2025).

Figure 4.8. The spectral characteristics of the probes as observed by naked eye under day light (a) and under UV (Sahin et. al. 2025).

UV-Vis absorbance and fluorescence of compounds 2, 3 and A2 are analyzed in 25% PBS in DMSO as shown in Figure 4.6. and Figure 4.7. Relatively poor solubility of uncharged

compound 2 in aqueous solution resulted in splitting of absorbance spectra. As expected, the degree of pyridinium groups determines the scale of bathochromic spectral shift. Absorbance and emission peaks shift towards right as the compounds are converted from the uncharged pyridine form to mono and di-charged pyridinium forms, indicating the role of electron withdrawing pyridinium moiety on the spectral alteration. A2 emits at 697 nm which lies 68 nm above pyridine bearing compound 2.

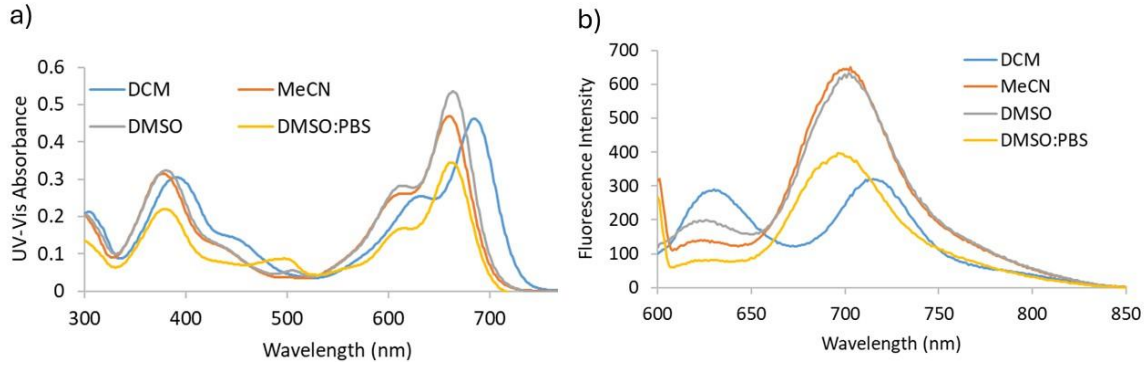

Figure 4.9. Solvatochromism of probe A2. In apolar solvents a bathochromic shift in absorbance is observed. (Sahin et. al. 2025).

Similar to A1, compound A2 has distinct absorption and emission spectra depending on the solvent polarity. In apolar DCM, a bathochromic shift is observed, which is thought to be associated with stabilization/destabilization of HOMO/LUMO levels by the solvents. The spectroscopic data of the probes in DMSO is summarized in Table 4.1. Compound 2 has the highest quantum yield, 0.67 in DMSO. The lifetime of the same compound is measured to be 4.87 ns in DMSO.

Compound	e, $M^{-1}cm^{-1}$	F_F[b]	t_F (ns)
A2	71000	0.13	2.13
3	77000	0.14	2.08
2	15200[7]	0.67	4.87
A1	81000	0.20	2.38

Table 4.1. Spectroscopic data of probes 2, 3, A1 and A2 in DMSO (Sahin et. al. 2025).

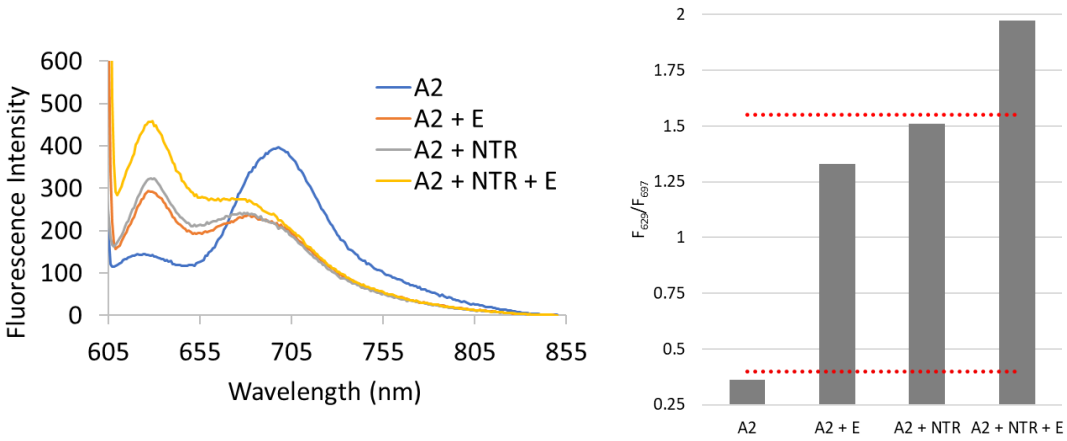

Figure 4. Fluorescence A2 (5 µM) in presence of NTR or/and carboxylesterase enzyme (25 mg/mL and 5U/mL, respectively). Relative response ratio of A2 and the threshold level set to discriminate presence of mono and dual enzyme (Sahin et. al. 2025).

Fluorescence intensity of A2 in PBS: DMSO solvent mixture (25:75; v: v) was measured in the presence of carboxylesterase enzyme (5 U/mL) or/and nitroreductase enzyme (25 µg/ml) Figure 4.9. Samples were incubated for 1 hour and each spectrum was obtained exciting at 600 nm. Enzyme treated samples display a decrease of emission intensity at 697 nm while peak at 629 nm was shown to increase. Although the fluorescence intensity at 629 nm to the intensity at 697 nm significantly increased when any of the enzymes are used, this ratio does not exceed 1.55. However, when both enzymes were used this ratio reaches above 1.9. This data suggests that by setting a threshold, presence of single or dual enzymes can be discriminated.

4.3. Results of Cytotoxicity Analysis

Cytotoxicity of probes A1 was analyzed in Hep3B liver cancer cells. Hep3B cells were incubated with different concentrations of the probes for 24 hours and cytotoxic effect was measured by using MTT assay. As shown in Figure 4.10 at 4 µM (application dose) cytotoxicity is negligible, indicating that the probe is safe enough for use in bioimaging applications. Beyond this dose, cytotoxicity increases significantly.

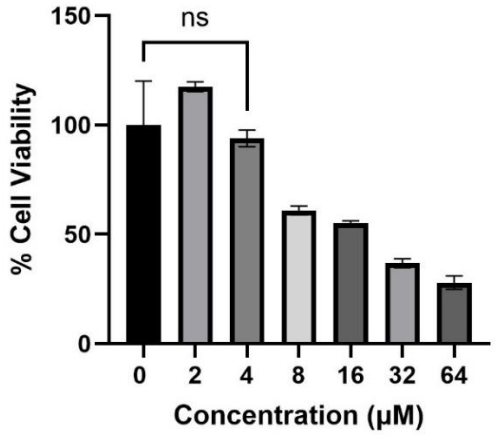

Figure 4.10. Cytotoxicity of prob A1 to Hep3B cells after 24h application (n = 3). (Sahin et. al. 2025).

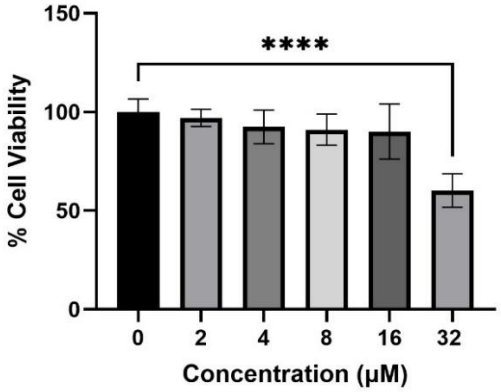

Figure 4.11. Cytotoxicity of prob A2 to Hep3B cells after 24h application (n = 6). (Sahin et. al. 2025).

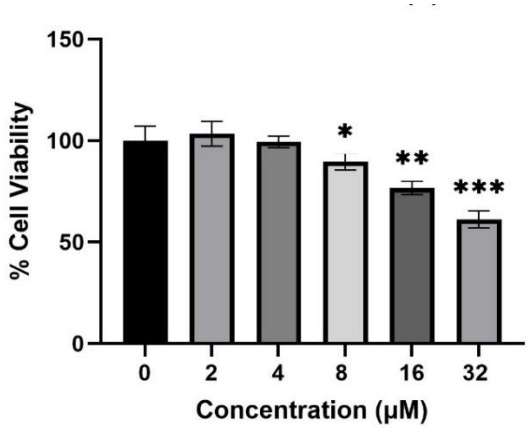

Figure 4.12. Cytotoxicity of prob A2 to sorafenib resistant Hep3B cells after 24h application (n = 6). (Sahin et. al. 2025).

Cytotoxicity of A2 was analyzed in Hep3B liver cancer cells and sorafenib resistant HEP3B cells. Cells were incubated with different concentrations of the probes for 24 hours and cytotoxic effect was measured by using MTT assay. As shown in Figure 4.11. and Figure 4.12. at 4 μM (application dose) cytotoxicity is negligible, indicating that the probe is safe enough for use in bioimaging applications. In drug resistant cells, cytotoxicity is becoming significant beyond 16 μM (Figure 4.12.).

4.4. Results of Fluorescence Imaging

Cellular response of A1 was evaluated in Hep3B cell with high esterase activity. As shown in Figure 4.13, 4 μM probe A1 was applied to cell for 30 min in both in the presence and absence of esterase inhibitor, benzil. Emission intensity of the probe is significantly reduced in benzil-treated cells indicating the esterase dependency of fluorescence response.

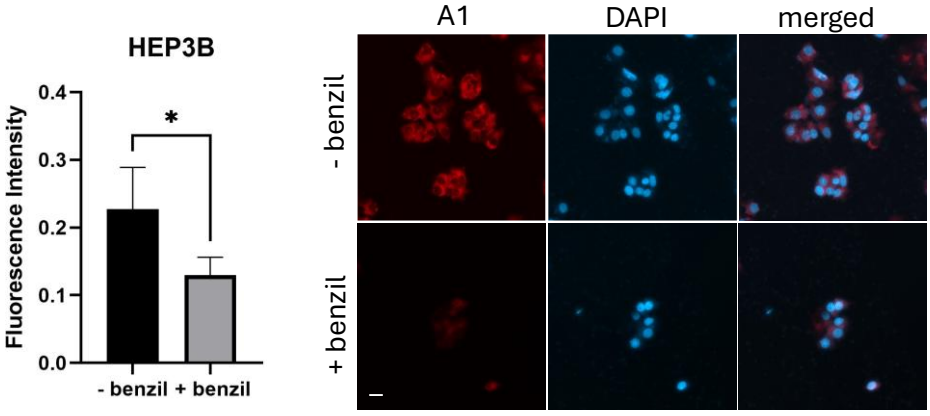

Figure 4.13. Response of probe A1 (4 μM) in Hep3B cells after 30 min incubation. Pre-treatment of benzil (esterase inhibitor, applied 2h before probe addition) decreases the fluorescence intensity. For DAPI visualization samples were excited at 353 nm, emission was collected at 465 nm whereas to monitor probe emission AF610 channels was used (excitation at 612 nm, emission at 630 nm). Scale bar 100 μm. n = 4. (Sahin et. al. 2025).

Cellular response of A2 was evaluated in normoxic, hypoxic and/or sorafenib resistant Hep3B cells as shown in Figure 4.14. 4 μM A2 was applied to cell for 30min. While esterase activity was controlled with benzil, nitroreductase activity was controlled with pre-treatment with 100 mM $CoCI_2.6H_2O$. Maximum fluorescence intensity was observed in hypoxic cells in the absence of benzil. This result is considered as esterase overexpressing cells with hypoxic cancer associated microenvironment can easily be discriminated against the other groups (Figure 4.15). When the emission threshold is set as 14, drug resistant cells with cancer

microenvironment can be discriminated against the rest. When the threshold is set as 9, presence of any enzyme can be detected. When the inputs and outputs are digitalized, the corresponding responses can be read as molecular AND/OR gates (Erbas-Cakmak et. al. 2018).

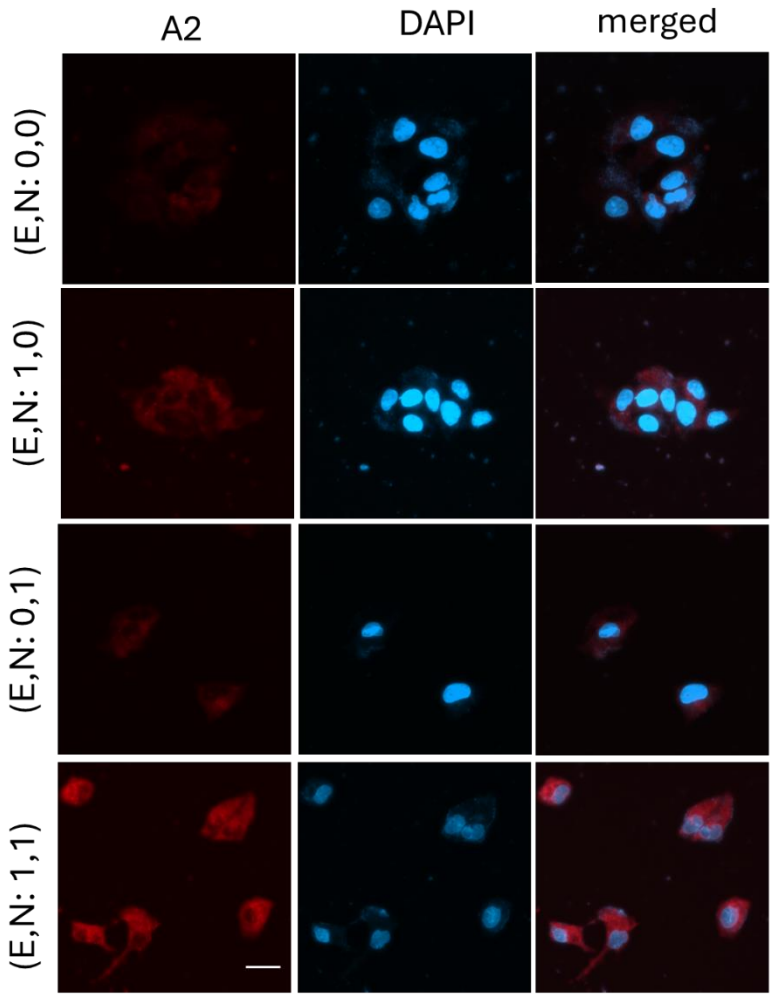

Figure 4.14. Cellular response of A2 (4 μM) in Hep3B cells. For esterase overexpressing cells sorafenib resistant Hep3B cells were used. For nitroreductase activity, hypoxic microenvironment was generated by pre-treatment of the cells with 100 mM $CoCI_2.6H_2O$**.** (Sahin et. al. 2025).

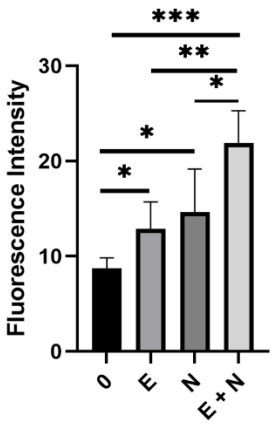

Marker 1 (E)	Marker 2 (NTR)	State 1 (AND) Output ≥ 14	State 2 (OR) Output ≥ 9
0	0	0	0
1	0	0	1
0	1	0	1
1	1	1	1

Figure 4.15. Cellular response of A2 (4 µM) in Hep3B cells having different cellular status (i.e. drug resistance, cancer microenvironment). (Sahin et. al. 2025).

4.5. Cytotoxic Analysis of the PROTACS

Cytotoxicity of PROTACs were analyzed in Hep3B cells. The IC_{50} values are determined to be above 80 µM for all the PROTACs (Figure 4.16., Figure 4.17., and Figure 4.18.).

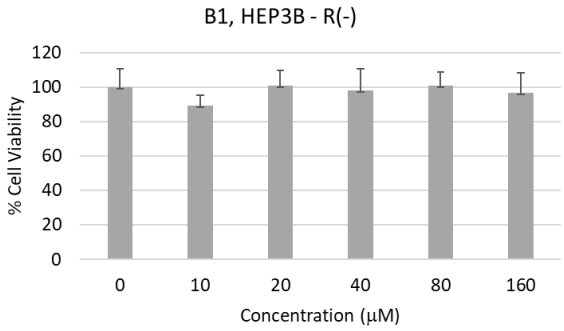

Figure 4.16. Cytotoxicity of ALDH1A1 targeting PROTAC B1 to Hep3B cells after 24h application (n = 5).

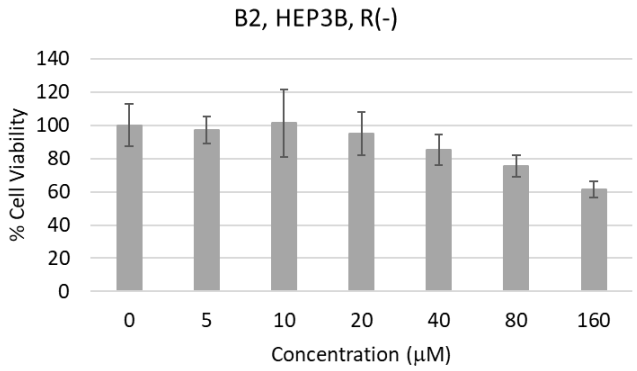

Figure 4.17. Cytotoxicity of MDR1 targeting PROTAC B2 to Hep3B cells after 24h application (n = 4).

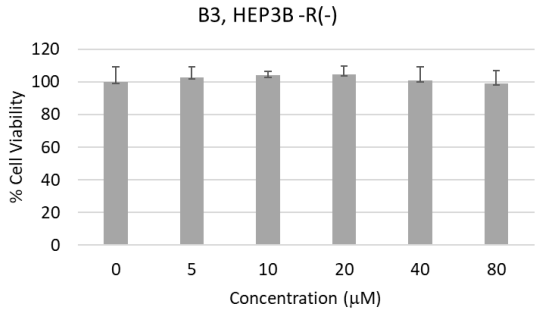

Figure 4.18. Cytotoxicity of esterase targeting PROTAC B3 to Hep3B cell after 24h application (n = 6).

4.5. Western Blot Analysis of PROTACs

Western blot analysis of ALDH1A1 PROTAC was completed (Figure 4.19)

Figure 4.19. Western Blot results of ALDH1A1 targeting B1 PROTAC when 0, 50, 150, 200, 250, 300, 350 and 400 nM doses were applied to Hep3B cells.

Even if degradation was observed in both 150 nM and 250 nM, band intensity of 250 nM undermines trust the results. Therefore, western blot analysis should be repeated.

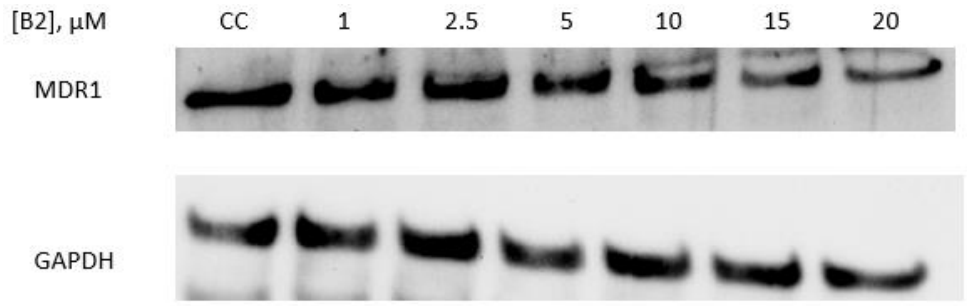

Figure 4.20. Western Blot results of MDR1 targeting B2 PROTAC when 0, 1, 2.5, 5, 10,15 and 20 µM doses were applied to Hep3B cells.

Intensity of 15 mM and 20 mM concentration lower. This might indicate the degradation of MDR1 protein at these doses of the PROTAC.

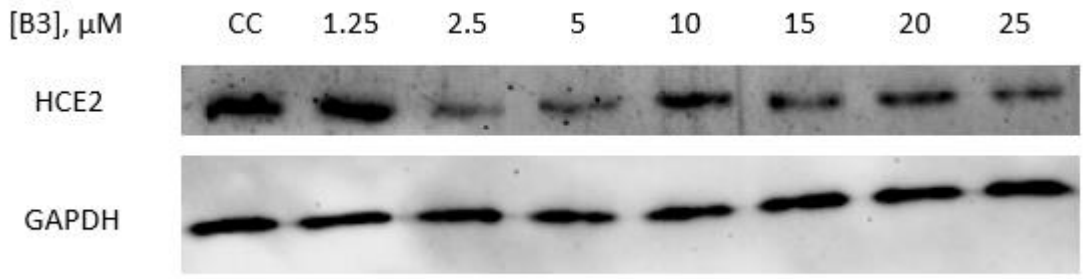

Figure 4.21. Western Blot results of esterase targeting B3 PROTAC when 0, 1.25, 2.5, 5, 10, 15, 20 and 25 µM doses were applied to Hep3B cells.

Western blot analysis indicates that it might be HCE2 degradation at 2.5µM and 5µM dose-applied cells.

5. CONCLUSIONS AND RECOMMENDATIONS

5.1. Conclusion

In the first part of the thesis projects, new ratiometric fluorescent probes with distyryl pyridinium BODIPY core structures were developed. The diagnosis of cancer cells, especially drug-resistant cells, was achieved. ICT based ratiometric fluorescent enzymes probes display a large spectral shift upon treatment with enzymes. None of the probes are toxic to cells at the application dose. Probes can have distinct fluorescence output in hypoxic and/or drug-resistant cells when an appropriate threshold is set. By this, drug resistance cells can be discriminated against normal cancer cells.

In the second part of the thesis projects, new PROTACs were developed. Proximity-based therapeutic approaches can be used for tuning a specific protein's turnover rate in the cell. Up to date, PROTACs against ALDH1, human carboxylesterase or MDR1 have not been developed. Considering the involvement of these proteins in drug metabolization and resistance, regulating their level in the cell may provide a therapeutic potential. PROTACs were synthesized successfully and the primary experiments in the cell culture were initiated.

5.2. Recommendation

Thesis project provides a novel strategy for the discrimination of different cellular states with the use of multi-responsive fluorescent ratiometric sensors. This idea can be expanded into a diverse range of diseases. The number of parameters detected by the probe can be increased. Additionally, biological responses to PROTACs developed in this thesis can be extensively studied.

6. REFERENCES

Al-Shamma, S. A., Zaher, D. M., Hersi, F., Abu Jayab, N. N., & Omar, H. A. (2023). Targeting aldehyde dehydrogenase enzymes in combination with chemotherapy and immunotherapy: An approach to tackle resistance in cancer cells. *Life Sciences*, *320*, 121541.

Daly, B., Ling, J., & De Silva, A. P. (2015). Current developments in fluorescent PET (photoinduced electron transfer) sensors and switches. *Chemical Society Reviews*, *44*(13), 4203–4211.

Dean, M. (2005). The Genetics of ATP-Binding Cassette Transporters. *Methods in Enzymology*, *400*, 409–429.

Deniz, E., Isbasar, G. C., Bozdemir, Ö. A., Yildirim, L. T., Siemiarczuk, A., & Akkaya, E. U. (2008). Bidirectional switching of near IR emitting boradiazaindacene fluorophores. *Organic Letters*, *10*(16), 3401–3403.

Emran, T. Bin, Shahriar, A., Mahmud, A. R., Rahman, T., Abir, M. H., Siddiquee, M. F. R., Ahmed, H., Rahman, N., Nainu, F., Wahyudin, E., Mitra, S., Dhama, K., Habiballah, M. M., Haque, S., Islam, A., & Hassan, M. M. (2022). Multidrug Resistance in Cancer: Understanding Molecular Mechanisms, Immunoprevention and Therapeutic Approaches. *Frontiers in Oncology*, *12*, 891652.

Erbas-Cakmak, S., Cakmak, F. P., Topel, S. D., Uyar, T. B., & Akkaya, E. U. (2015). Selective photosensitization through an AND logic response: optimization of the pH and glutathione response of activatable photosensitizers. *Chemical Communications*, *51*(61), 12258–12261.

Gao, M., & Tang, B. Z. (2017). Fluorescent Sensors Based on Aggregation-Induced Emission: Recent Advances and Perspectives. *ACS Sensors*, *2*(10), 1382–1399.

Gil-Rivas, A., De Pascual-Teresa, B., Ortín, I., & Ramos, A. (2023). *molecules New Advances in the Exploration of Esterases with PET and Fluorescent Probes*.

Guo, B., Shen, T., Liu, Y., Jing, J., Shao, C., & Zhang, X. (2023). An endoplasmic reticulum-specific ratiometric fluorescent probe for imaging esterase in living cells. *Spectrochimica Acta Part A: Molecular and Biomolecular Spectroscopy*, *291*, 122389.

Holohan, C., Van Schaeybroeck, S., Longley, D. B., & Johnston, P. G. (2013). Cancer drug resistance: an evolving paradigm. *Nature Reviews Cancer 2013 13:10*, *13*(10), 714–726.

Ibrahim, A. I. M., Sadiq, M., Frame, F. M., Maitland, N. J., & Pors, K. (2018). Expression and regulation of aldehyde dehydrogenases in prostate cancer. *Journal of Cancer Metastasis*

and Treatment, *4*(8), 44.

Kachwal, V., & Tan, J. C. (2023). Stimuli-Responsive Electrospun Fluorescent Fibers Augmented with Aggregation-Induced Emission (AIE) for Smart Applications. *Advanced Science*, *10*(1), 2204848.

Kim, S., Kim, H., Choi, Y., & Kim, Y. (2015). A New Strategy for Fluorogenic Esterase Probes Displaying Low Levels of Non-specific Hydrolysis. *Chemistry – A European Journal*, *21*(27), 9645–9649.

Klinhom, N., Saengsuwan, N., Sriyab, S., Prompinit, P., Hannongbua, S., & Suramitr, S. (2019). Photophysical properties for excited-state intramolecular proton transfer (ESIPT) reaction of N-salicylidene-o-aminophenol: Experimental and DFT based approaches. *Spectrochimica Acta Part A: Molecular and Biomolecular Spectroscopy*, *206*, 359–366.

Kong, F., Li, Y., Yang, C., Li, X., Wu, J., Liu, X., Gao, X., Xu, K., & Tang, B. (2019). A fluorescent probe for simultaneously sensing NTR and hNQO1 and distinguishing cancer cells. *Journal of Materials Chemistry B*, *7*(43), 6822–6827.

Kowada, T., Maeda, H., & Kikuchi, K. (2015). BODIPY-based probes for the fluorescence imaging of biomolecules in living cells. *Chemical Society Reviews*, *44*(14), 4953–4972.

Li, M., Fan, J., Du, J., Cao, J., & Peng, X. (2018). Inhibiting proton interference in PET chemosensors by tuning the HOMO energy of fluorophores. *Sensors and Actuators B: Chemical*, *259*, 626–632.

Li, X., Wang, H., Zhang, Y., Cao, Q., & Chen, Y. (2021). A GSH-responsive PET-based fluorescent probe for cancer cells imaging. *Chinese Chemical Letters*, *32*(4), 1541–1544.

Liu, Y., Teng, L., Chen, L., Ma, H., Liu, H. W., & Zhang, X. B. (2018). Engineering of a near-infrared fluorescent probe for real-time simultaneous visualization of intracellular hypoxia and induced mitophagy. *Chemical Science*, *9*(24), 5347–5353.

Liu, Y., Yao, Y., Sha, J., Liang, G., & Sun, X. (2025). Dual-Locked Enzyme-Activatable Fluorescence Probes for Precise Bioimaging. *ACS Biomaterials Science and Engineering*.

Loudet, A., & Burgess, K. (2007). BODIPY dyes and their derivatives: Syntheses and spectroscopic properties. *Chemical Reviews*, *107*(11), 4891–4932.

Luo, X., Hu, E., Deng, F., Zhang, C., & Xian, Y. (2025). A dual-enzyme activated fluorescent probe for precise identification of tumor senescence. *Chemical Science*, *16*(15), 6507–6514.

Muralikrishnan, V., Hurley, T. D., & Nephew, K. P. (2020). Targeting Aldehyde Dehydrogenases to Eliminate Cancer Stem Cells in Gynecologic Malignancies. *Cancers 2020, Vol. 12, Page 961*, *12*(4), 961.

Nanayakkara, A. K., Follit, C. A., Chen, G., Williams, N. S., Vogel, P. D., & Wise, J. G. (2018). Targeted inhibitors of P-glycoprotein increase chemotherapeutic-induced mortality of multidrug resistant tumor cells. *Scientific Reports*, *8*(1), 1–18.

Nishino, K., Yamasaki, S., Nakashima, R., Zwama, M., & Hayashi-Nishino, M. (2021). Function and Inhibitory Mechanisms of Multidrug Efflux Pumps. *Frontiers in Microbiology*, *12*, 737288.

Peng, L., Xu, S., Zheng, X., Cheng, X., Zhang, R., Liu, J., Liu, B., & Tong, A. (2017). Rational Design of a Red-Emissive Fluorophore with AIE and ESIPT Characteristics and Its Application in Light-Up Sensing of Esterase. *Analytical Chemistry*, *89*(5), 3162–3168.

Potter, P. M., & Wadkins, R. M. (2006). Carboxylesterases - Detoxifying Enzymes and Targets for Drug Therapy. *Current Medicinal Chemistry*, *13*(9), 1045–1054.

Qiao, J., Wang, M., Cui, M., Fang, Y., Li, H., Zheng, C., Li, Z., Xu, Y., Hua, H., & Li, D. (2021). Small-molecule probes for fluorescent detection of cellular hypoxia-related nitroreductase. *Journal of Pharmaceutical and Biomedical Analysis*, *203*, 114199.

Rueff, J., & Rodrigues, A. S. (2016). Cancer drug resistance: A brief overview from a genetic viewpoint. *Methods in Molecular Biology*, *1395*, 1–18.

Schneider, S. M., Lee, B. H., & Nicola, A. V. (2021). Viral entry and the ubiquitin-proteasome system. *Cellular Microbiology*, *23*(2), e13276.

Sedgwick, A. C., Wu, L., Han, H. H., Bull, S. D., He, X. P., James, T. D., Sessler, J. L., Tang, B. Z., Tian, H., & Yoon, J. (2018a). Excited-state intramolecular proton-transfer (ESIPT) based fluorescence sensors and imaging agents. *Chemical Society Reviews*, *47*(23), 8842–8880.

Sedgwick, A. C., Wu, L., Han, H. H., Bull, S. D., He, X. P., James, T. D., Sessler, J. L., Tang, B. Z., Tian, H., & Yoon, J. (2018b). Excited-state intramolecular proton-transfer (ESIPT) based fluorescence sensors and imaging agents. *Chemical Society Reviews*, *47*(23), 8842–8880.

Sun, X., Gao, H., Yang, Y., He, M., Wu, Y., Song, Y., Tong, Y., & Rao, Y. (2019a). PROTACs: great opportunities for academia and industry. *Signal Transduction and Targeted Therapy 2019 4:1*, *4*(1), 1–33.

Sun, X., Gao, H., Yang, Y., He, M., Wu, Y., Song, Y., Tong, Y., & Rao, Y. (2019b). PROTACs: great opportunities for academia and industry. *Signal Transduction and Targeted Therapy 2019 4:1*, *4*(1), 1–33.

Takara, K., Sakaeda, T., & Okumura, K. (2006). An update on overcoming MDR1-mediated multidrug resistance in cancer chemotherapy. *Current Pharmaceutical Design*, *12*(3),

273–286.

Tang, W., Chen, Z., Zhang, W., Cheng, Y., Zhang, B., Wu, F., Wang, Q., Wang, S., Rong, D., Reiter, F. P., De Toni, E. N., & Wang, X. (2020). The mechanisms of sorafenib resistance in hepatocellular carcinoma: theoretical basis and therapeutic aspects. *Signal Transduction and Targeted Therapy 2020 5:1*, *5*(1), 1–15.

Thomas, H., Coley, H. M., Parker Kodiak, J., Pastel, A., & Ellefson, J. (2003). Overcoming Multidrug Resistance in Cancer: An Update on the Clinical Strategy of Inhibiting P-Glycoprotein. *Cancer Control*, *10*(2), 159–165.

Uddin, M. H., Kim, B., Cho, U., Azmi, A. S., & Song, Y. S. (2020). Association of ALDH1A1-NEK-2 axis in cisplatin resistance in ovarian cancer cells. *Heliyon*, *6*(11), e05442.

Udhayakumari, D. (2024). Mechanistic Innovations in Fluorescent Chemosensors for Detecting Toxic Ions: PET, ICT, ESIPT, FRET and AIE Approaches. *Journal of Fluorescence*, 1–30.

Verma, P., Shukla, N., Kumari, S., Ansari, M. S., Gautam, N. K., & Patel, G. K. (2023). Cancer stem cell in prostate cancer progression, metastasis and therapy resistance. *Biochimica et Biophysica Acta (BBA) - Reviews on Cancer*, *1878*(3), 188887.

Visvader, J. E., & Lindeman, G. J. (2008). Cancer stem cells in solid tumours: accumulating evidence and unresolved questions. *Nature Reviews Cancer 2008 8:10*, *8*(10), 755–768.

Wang, F., Zhang, X., Wang, Y., Chen, Y., Lu, H., Meng, X., Ye, X., & Chen, W. (2023). Activation/Inactivation of Anticancer Drugs by CYP3A4: Influencing Factors for Personalized Cancer Therapy. *Drug Metabolism and Disposition*, *51*(5), 543–559.

Wang, X., Zhang, H., & Chen, X. (2019). Drug resistance and combating drug resistance in cancer. *Cancer Drug Resistance*, *2*(2), 141.

Wang, Y. H., & Wan, P. (2013). Solvent-dependent excited state intramolecular proton transfer (ESIPT) pathways from phenol to carbon in 2,5-dihydroxyphenyl arenes. *Photochemical & Photobiological Sciences*, *12*(9), 1571–1588.

Wangngae, S., Chansaenpak, K., Khrootkaew, T., Lai, R. Y., & Kamkaew, A. (2022). Hemicyanine-based pH-responsive probes for rapid hypoxia detection in cancer cells. *Bioorganic Chemistry*, *129*, 106173.

Wu, S., & Fu, L. (2018). Tyrosine kinase inhibitors enhanced the efficacy of conventional chemotherapeutic agent in multidrug resistant cancer cells. *Molecular Cancer*, *17*(1).

Wu, Y., Ge, C., Zhang, Y., Wang, Y., & Zhang, D. (2023). ICT-based fluorescent probes for intracellular pH and biological species detection. *Frontiers in Chemistry*, *11*, 1304531.

Xiang, J. C., Cheng, Y., Wang, M., Wu, Y. D., & Wu, A. X. (2016). Direct Construction of 4-

Hydroxybenzils via Para-Selective C-C Bond Coupling of Phenols and Aryl Methyl Ketones. *Organic Letters*, *18*(17), 4360–4363.

Yadav, R., Munan, S., Kardam, V., Dutta Dubey, K., & Samanta, A. (2023). Esterase Specific Fluorescent Probe: Mechanistic Understanding Using QM/MM Calculation and Cell States Discrimination. *Chemistry - A European Journal*, *29*(32), e202300244.

Yao, X., Mao, J., Zhang, H., Xiao, Y., Wang, Y., & Liu, H. (2024). Development of novel N-aryl-2,4-bithiazole-2-amine-based CYP1B1 degraders for reversing drug resistance. *European Journal of Medicinal Chemistry*, *272*, 116488.

Yu, Z., Pestell, T. G., Lisanti, M. P., & Pestell, R. G. (2012). Cancer stem cells. *The International Journal of Biochemistry & Cell Biology*, *44*(12), 2144–2151.

Yue, H., Hu, Z., Hu, R., Guo, Z., Zheng, Y., Wang, Y., & Zhou, Y. (2022). ALDH1A1 in Cancers: Bidirectional Function, Drug Resistance, and Regulatory Mechanism. *Frontiers in Oncology*, *12*, 918778.

Zeng, S., Huang, W., Zheng, X., Liyan cheng, Zhang, Z., Wang, J., & Shen, Z. (2021). Proteolysis targeting chimera (PROTAC) in drug discovery paradigm: Recent progress and future challenges. *European Journal of Medicinal Chemistry*, *210*, 112981.

Zhao, M., Ma, J., Li, M., Zhang, Y., Jiang, B., Zhao, X., Huai, C., Shen, L., Zhang, N., He, L., & Qin, S. (2021). Cytochrome p450 enzymes and drug metabolism in humans. *International Journal of Molecular Sciences*, *22*(23), 12808.

Zhou, L., Zhang, W., & Qian, J. (2024). A fluorescent probe for bioimaging of GSH in cancer cells. *Spectrochimica Acta Part A: Molecular and Biomolecular Spectroscopy*, *305*, 123457.

7.APPENDIX

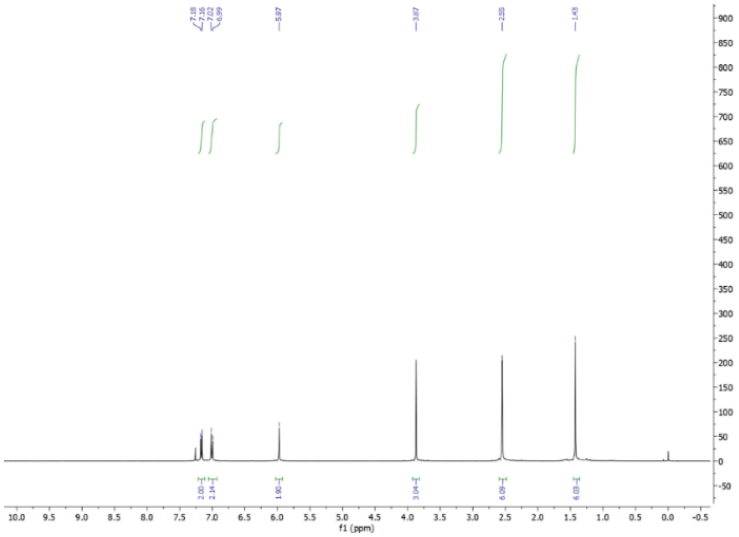

APPENDIX-1. ^{1}H NMR Spectrum of Compound 1 (400 MHz, $CDCl_3$).

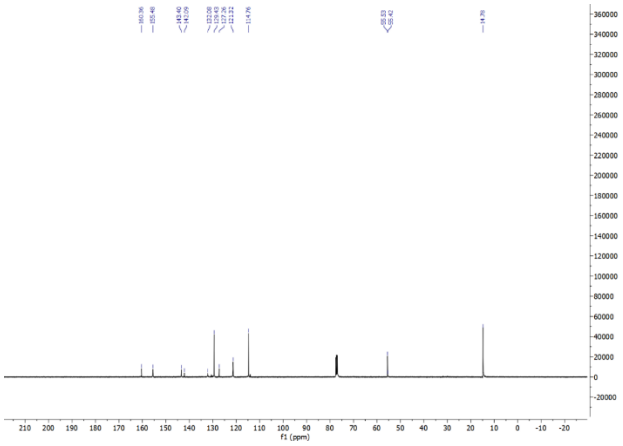

APPENDIX-2. ^{13}C NMR Spectrum of Compound 1 (101 MHz, $CDCl_3$).

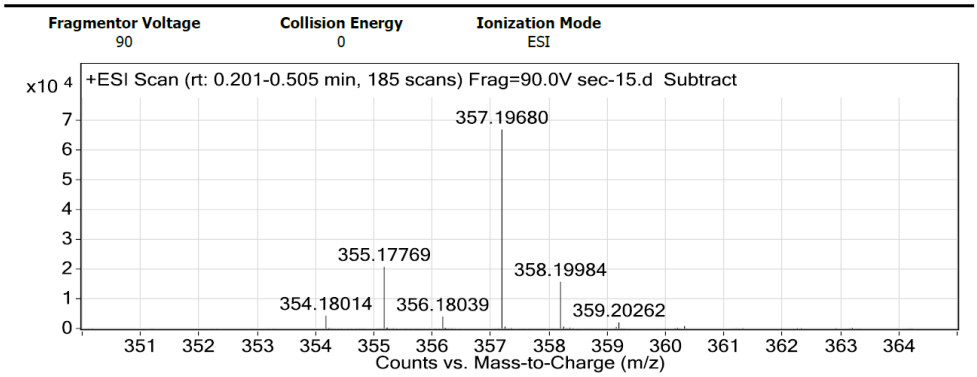

APPENDIX-3. QTOF-LC/MS Spectra of Compound 1

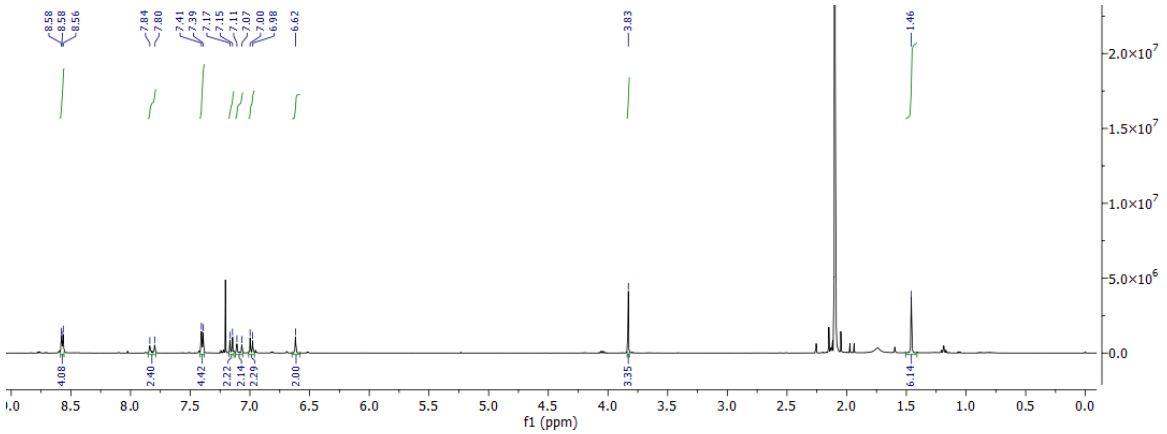

APPENDIX-4. ^{1}H NMR Spectrum of Compound 2 (400 MHz, $CDCl_3$).

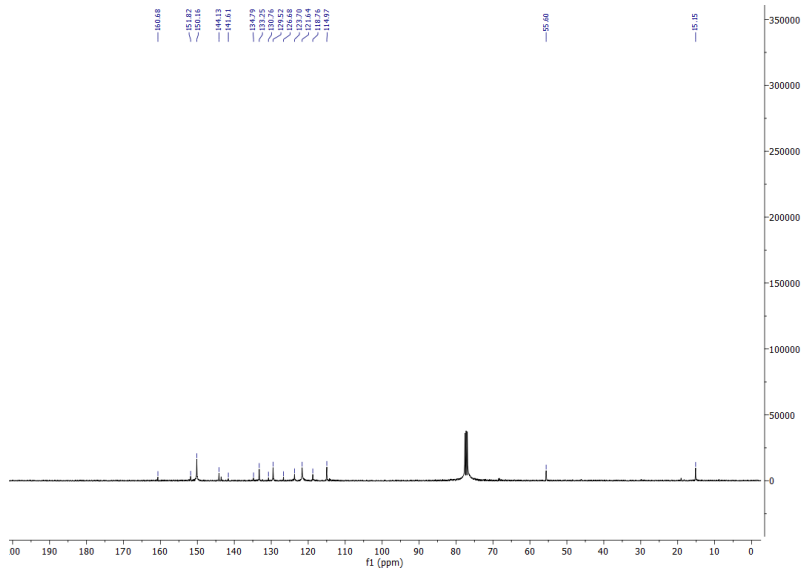

APPENDIX-5. ^{13}C NMR Spectrum of Compound 2 (101 MHz, $CDCl_3$).

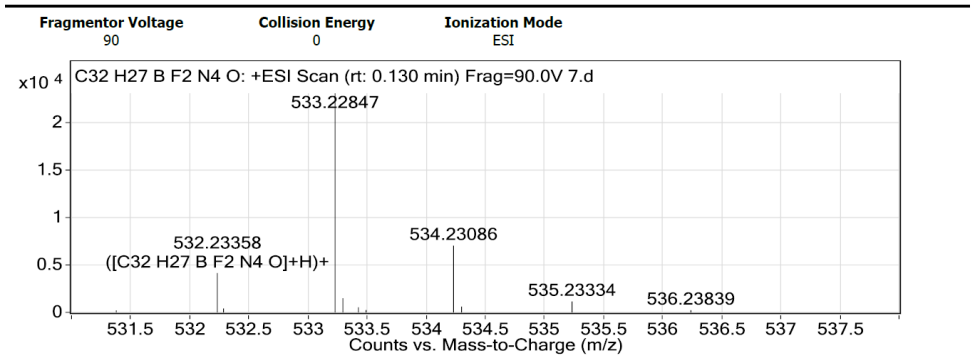

APPENDIX-6. QTOF-LC/MS Spectra of Compound 2

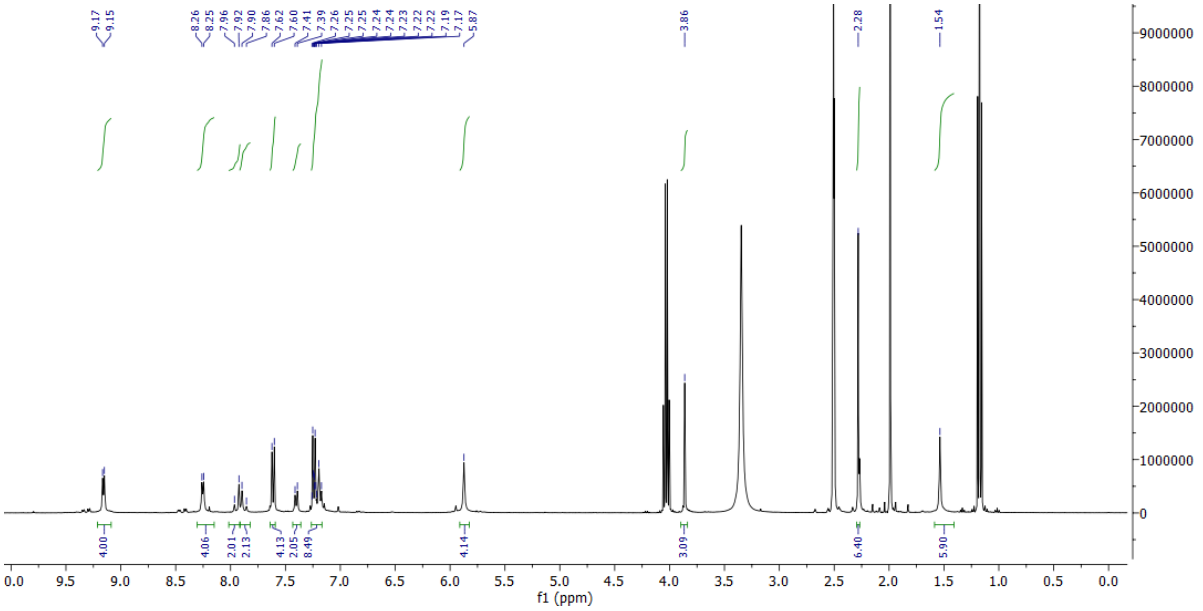

APPENDIX-7. ^{1}H NMR Spectrum of Compound **A1** (400 MHz, $CDCl_3$).

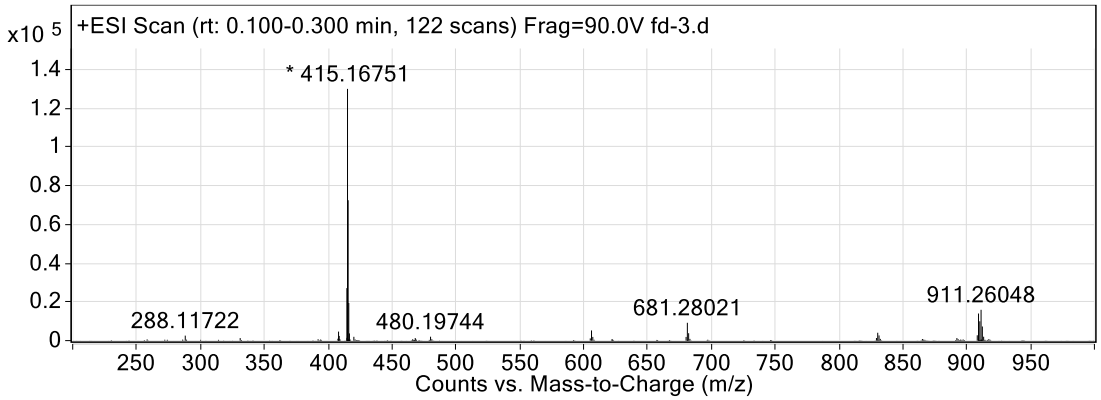

APPENDIX-8. QTOF-LC/MS Spectra of Compound **A1**

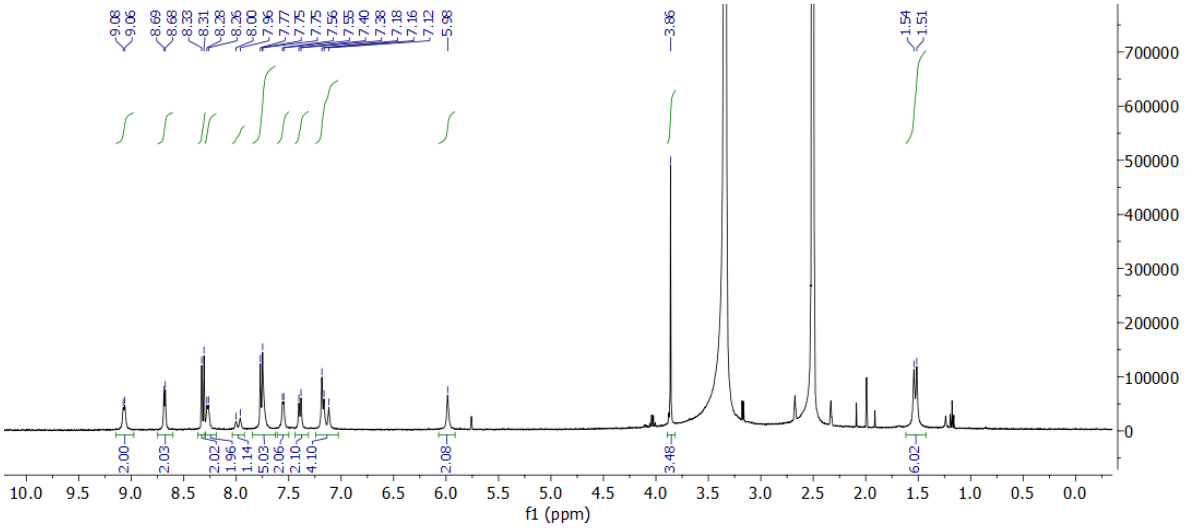

APPENDIX-10. ^{1}H NMR Spectrum of Compound 3 (400 MHz, DMSO-d_6).

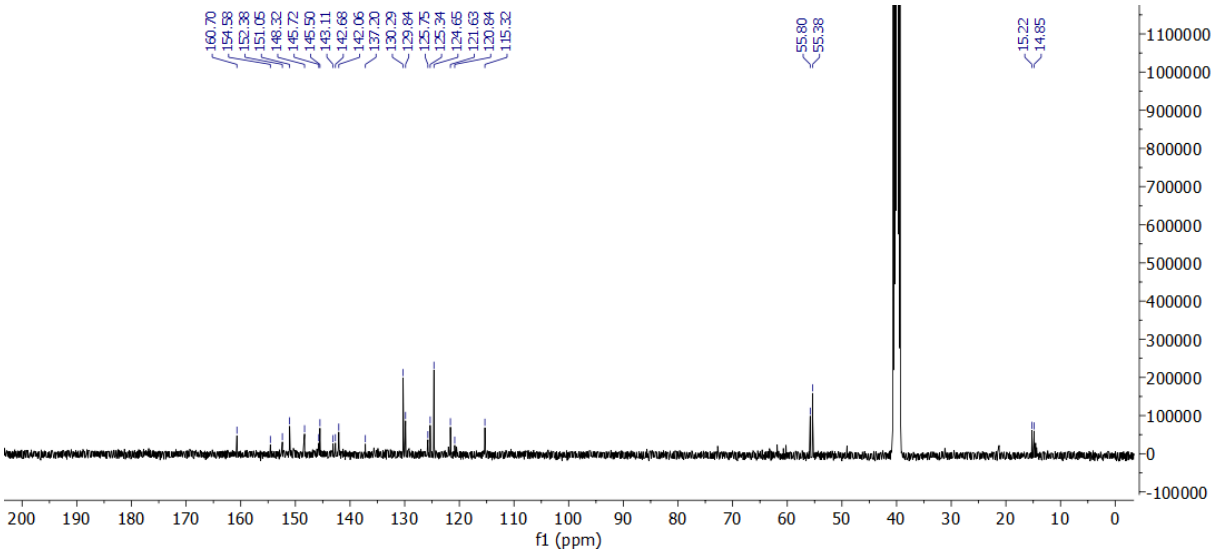

APPENDIX-11. ^{13}C NMR Spectrum of Compound 3 (101 MHz, DMSO-d_6).

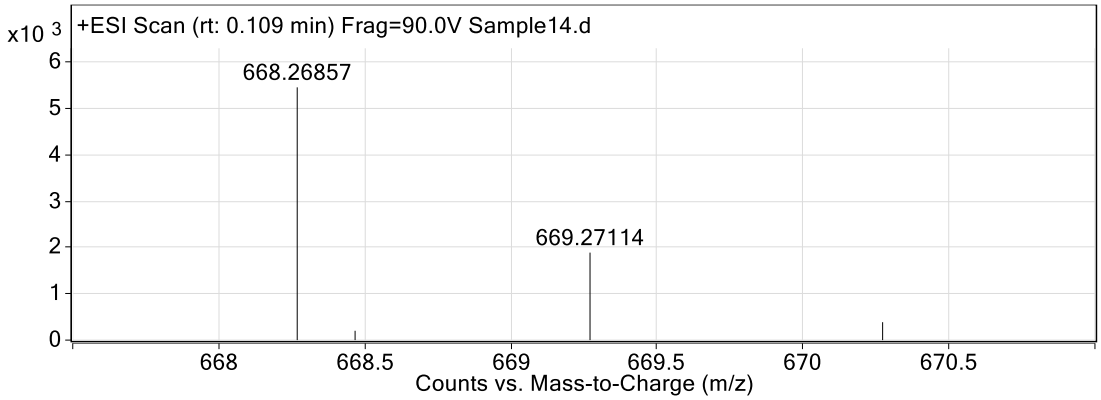

APPENDIX-12. QTOF-LC/MS Spectra of Compound 3

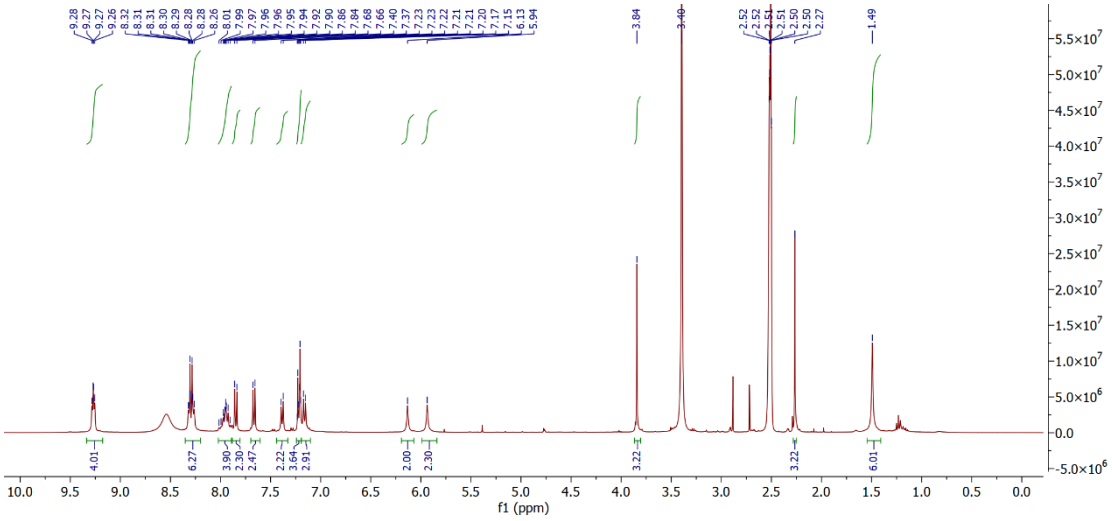

APPENDIX-13. ^{1}H NMR Spectrum of **A2** (400 MHz, DMSO-d_6).

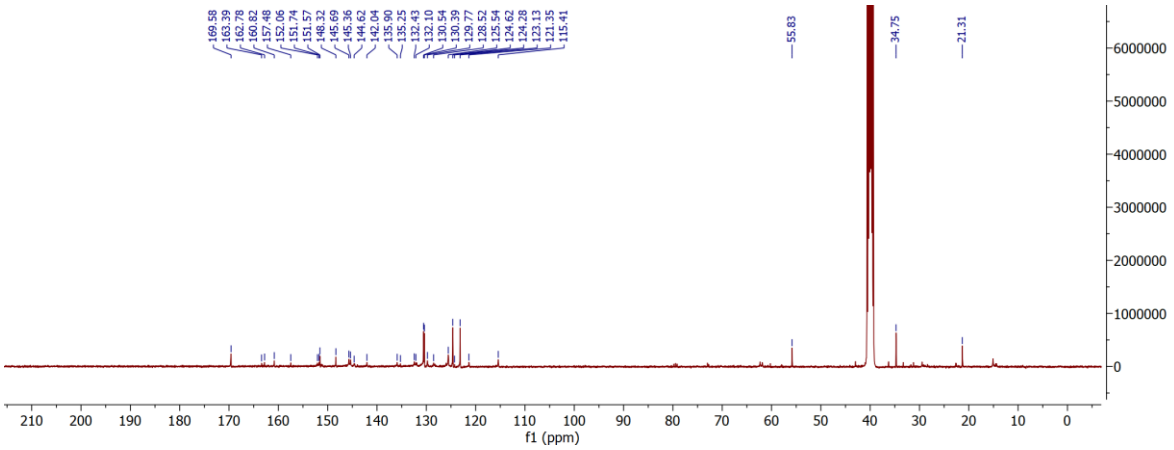

APPENDIX-14. ^{13}C NMR spectrum of **A2** (101 MHz, DMSO-d_6).

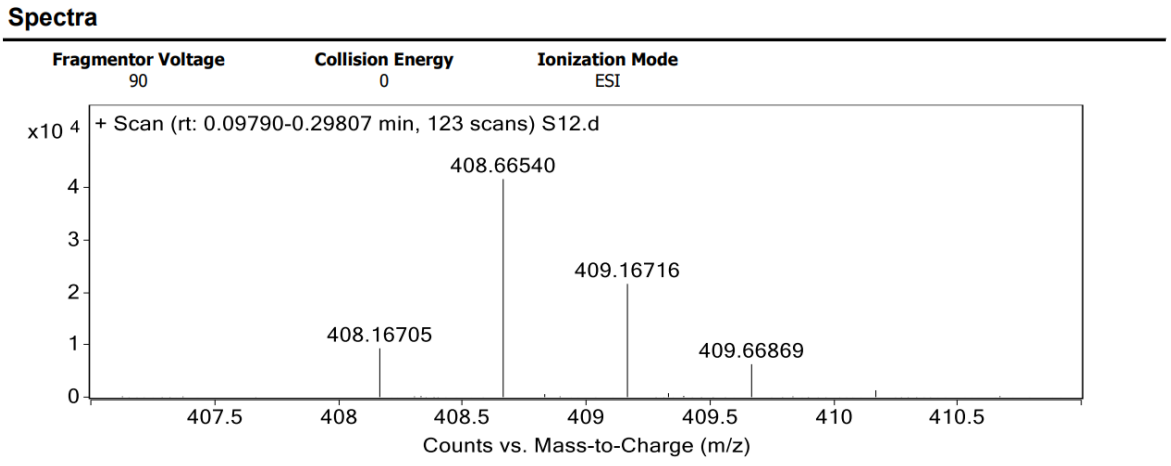

APPENDIX-15. QTOF-LC/MS Spectra of **A2**

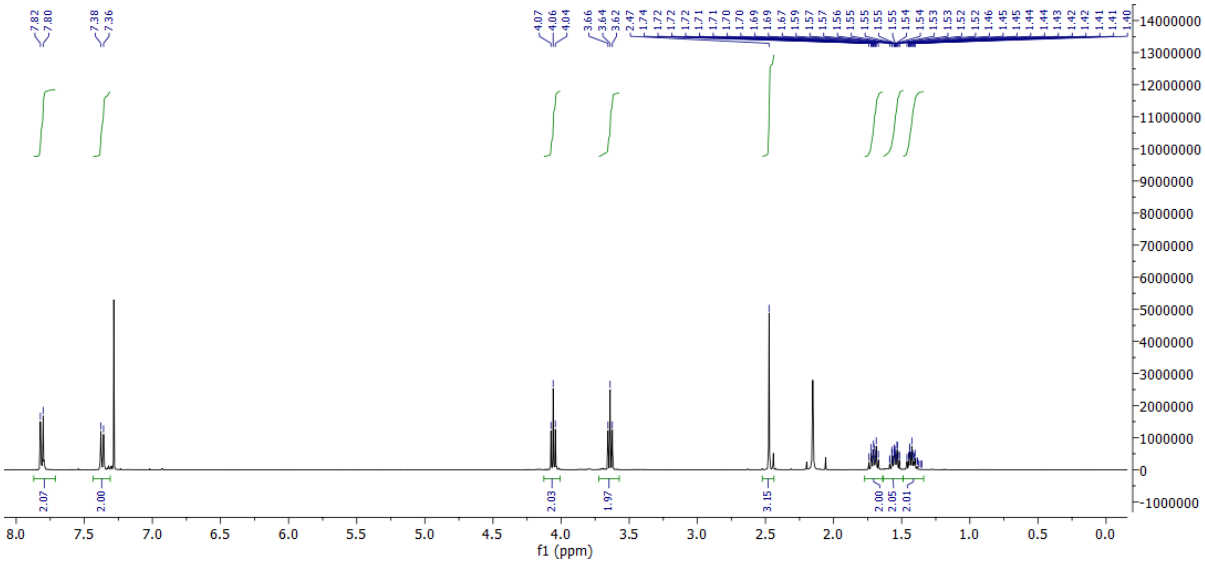

APPENDIX-16. ^{1}H NMR Spectrum of Compound 4 (400 MHz, $CDCl_3$)

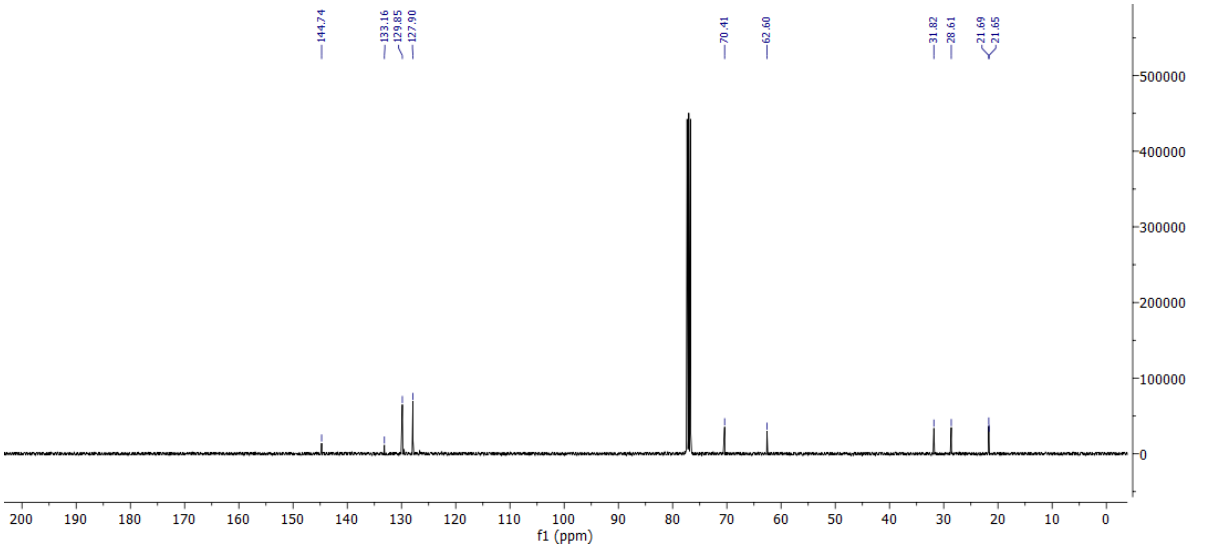

APPENDIX-17. ^{13}C NMR Spectrum of Compound 4 (101 MHz, $CDCl_3$)

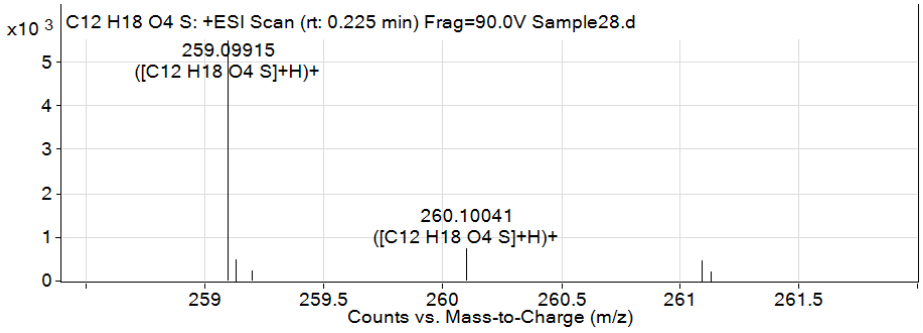

APPENDIX-18. QTOF-LC/MS Spectra of Compound 4

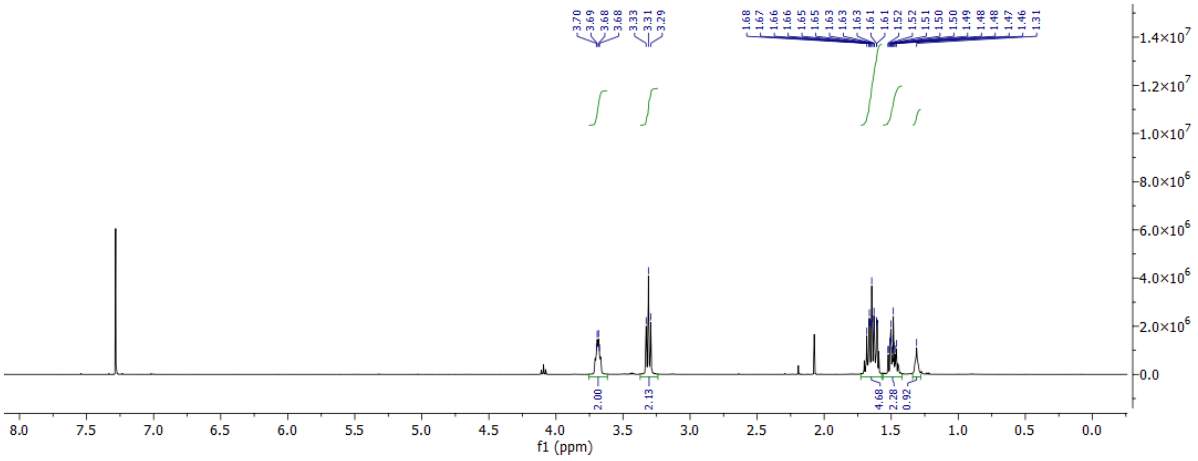

APPENDIX-19. ^{1}H NMR spectrum of Compound 5 (400 MHz, $CDCl_3$).

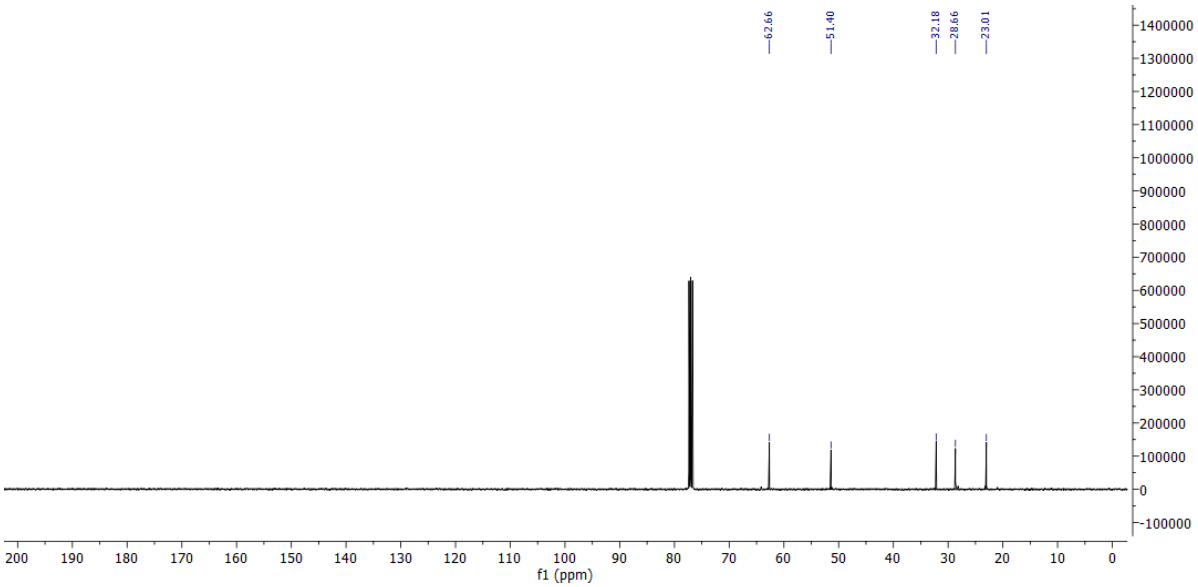

APPENDIX-20. ^{13}C NMR spectrum of Compound 5 (101 MHz, $CDCl_3$).

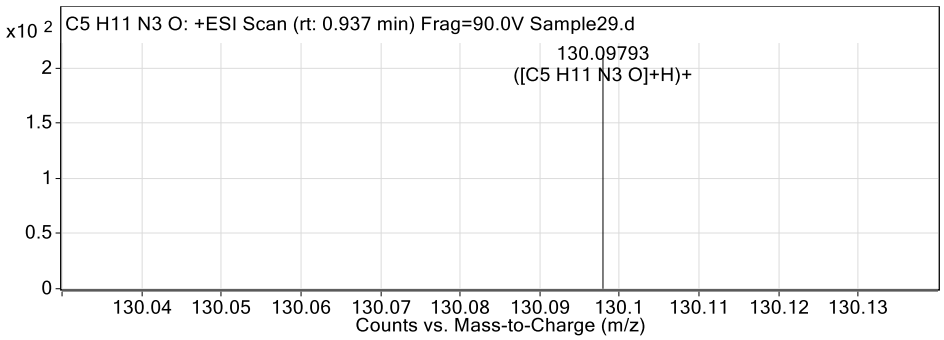

APPENDIX-21. QTOF-LC/MS Spectra of Compound 5

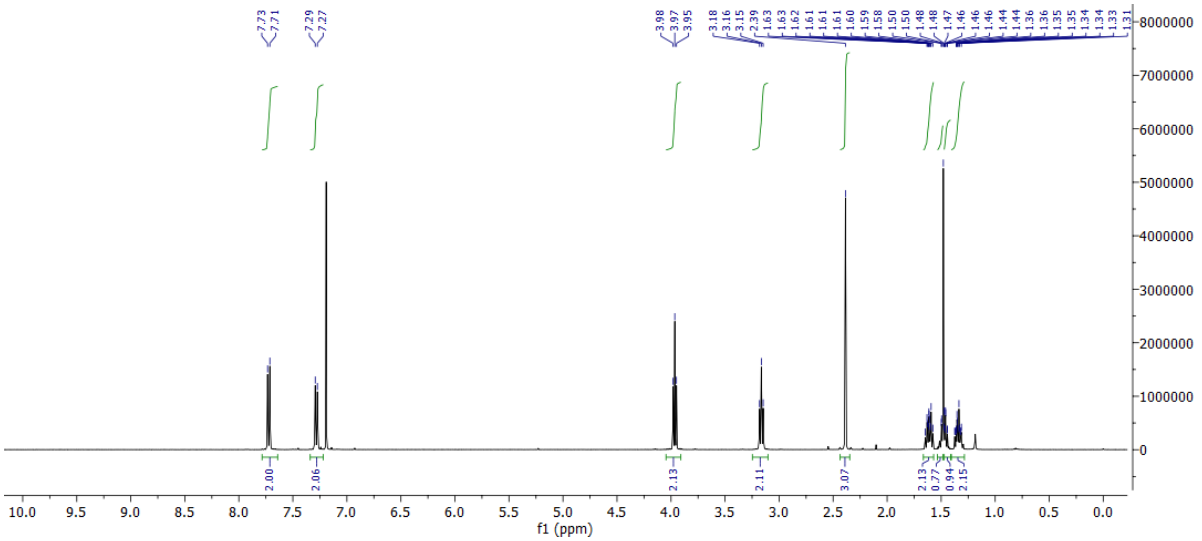

APPENDIX-22. ^{1}H NMR Spectrum of Compound 6 (400 MHz, $CDCl_3$)

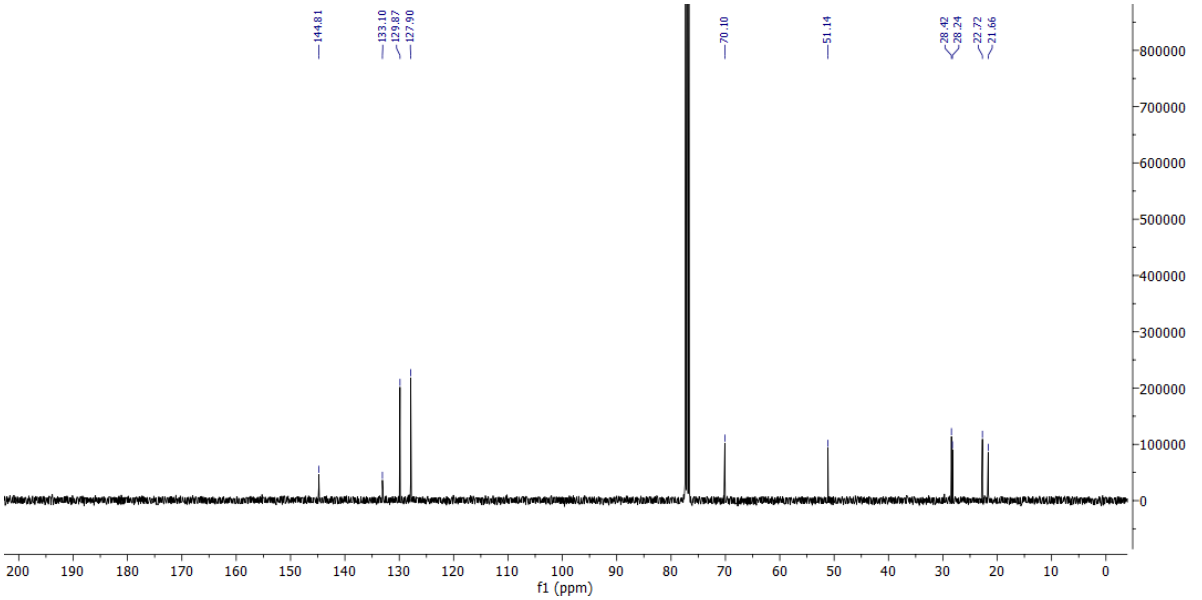

APPENDIX-23. ^{13}C NMR spectrum of Compound 6 (101 MHz, $CDCl_3$)

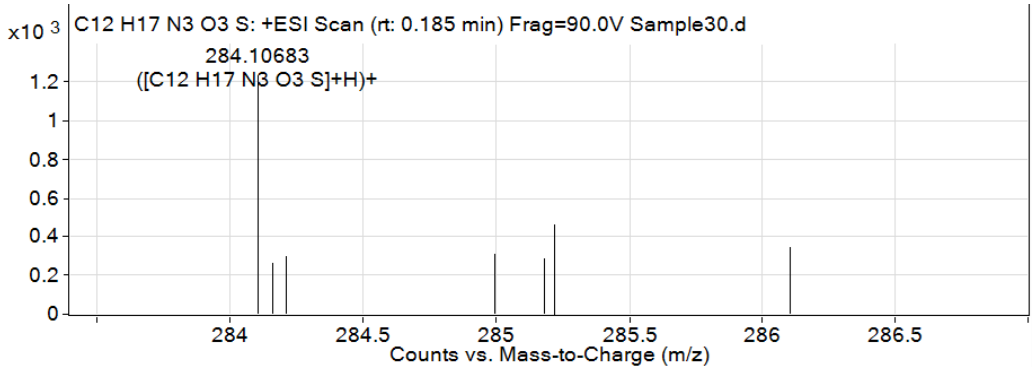

APPENDIX-24. QTOF-LC/MS Spectra of Compound 6

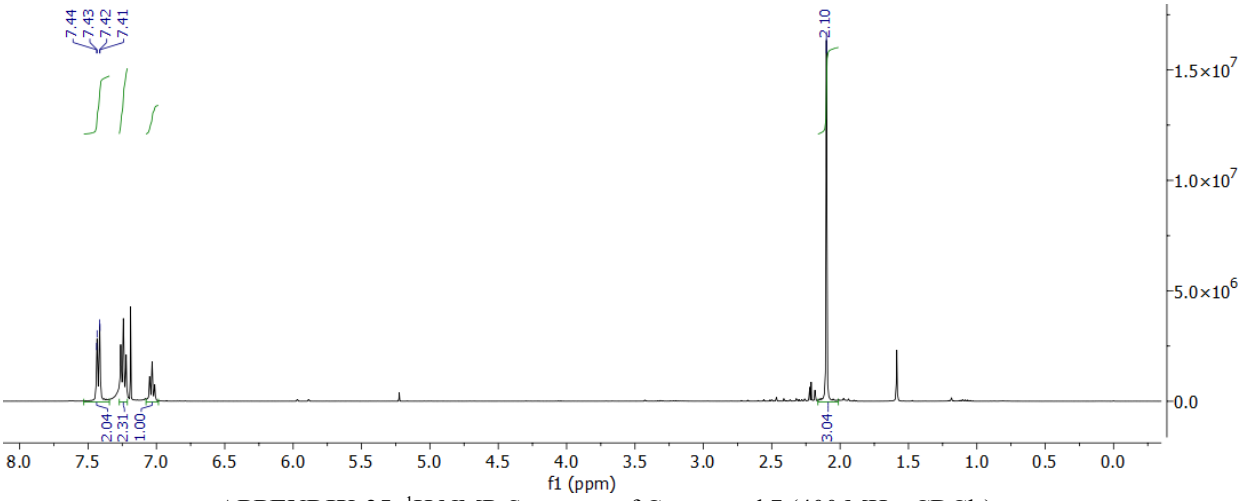

APPENDIX-25. ^{1}H NMR Spectrum of Compound 7 (400 MHz, $CDCl_3$).

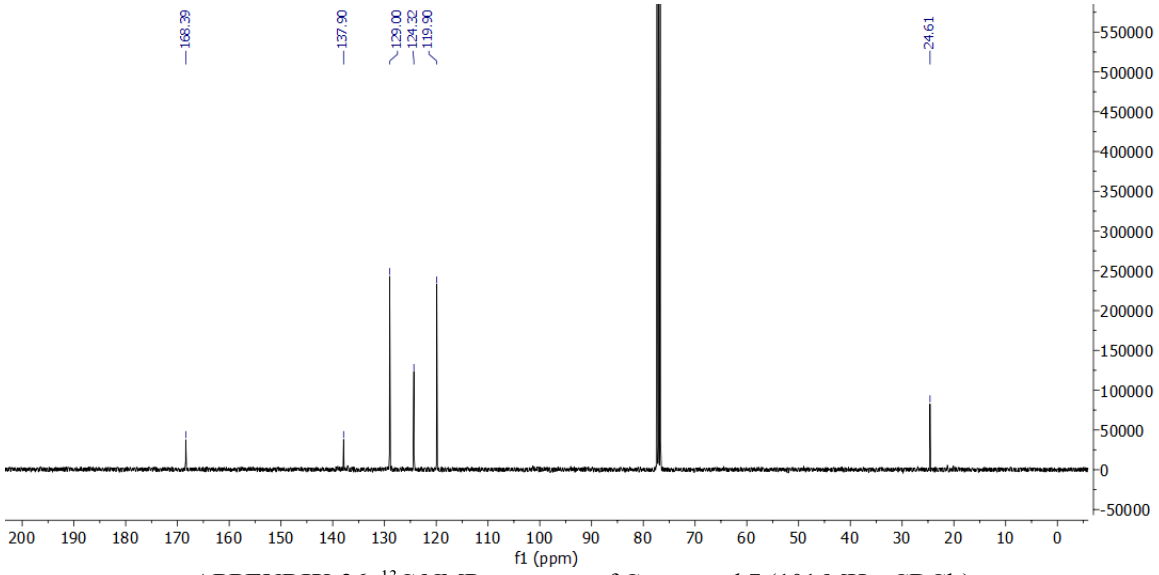

APPENDIX-26. ^{13}C NMR spectrum of Compound 7 (101 MHz, $CDCl_3$).

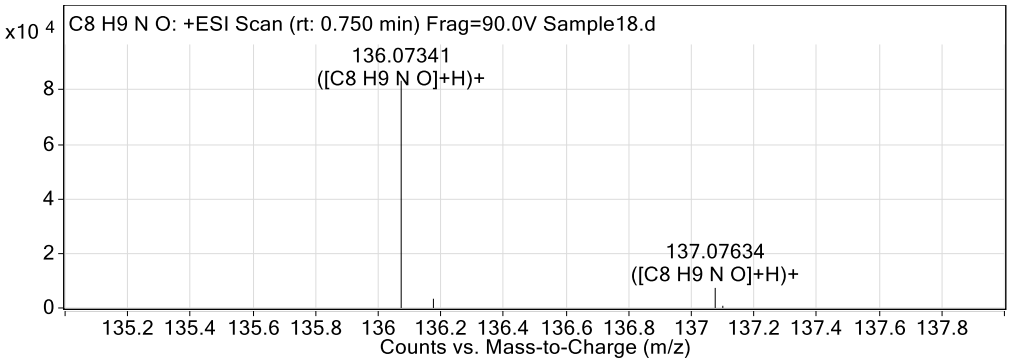

APPENDIX-27. QTOF-LC/MS Spectra of Compound 7

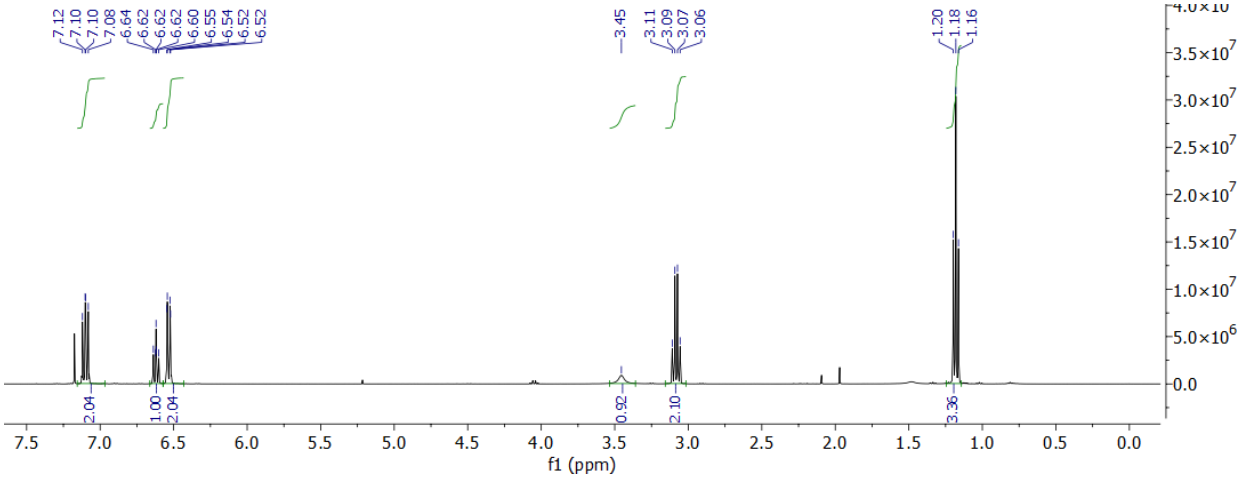

APPENDIX-28. ^{1}H NMR Spectrum of Compound 8 (400 MHz, $CDCl_3$).

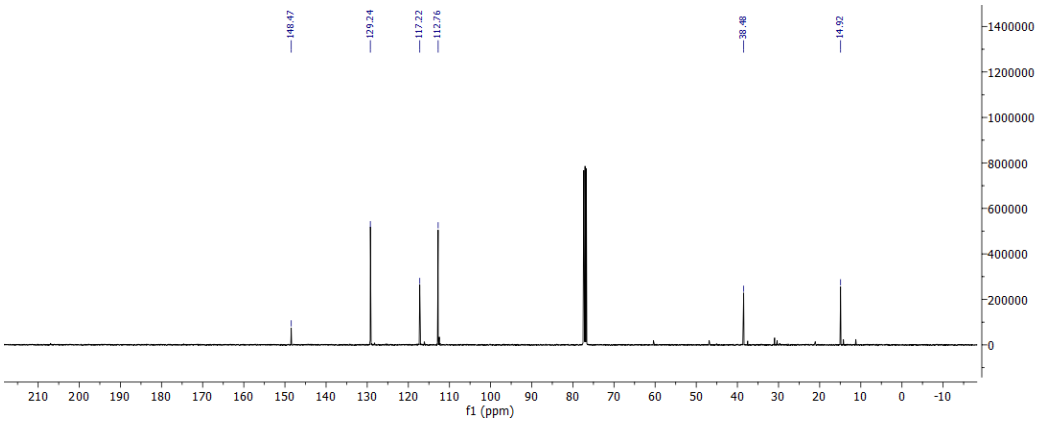

APPENDIX-29. ^{13}C NMR spectrum of Compound 8 (101 MHz, $CDCl_3$).

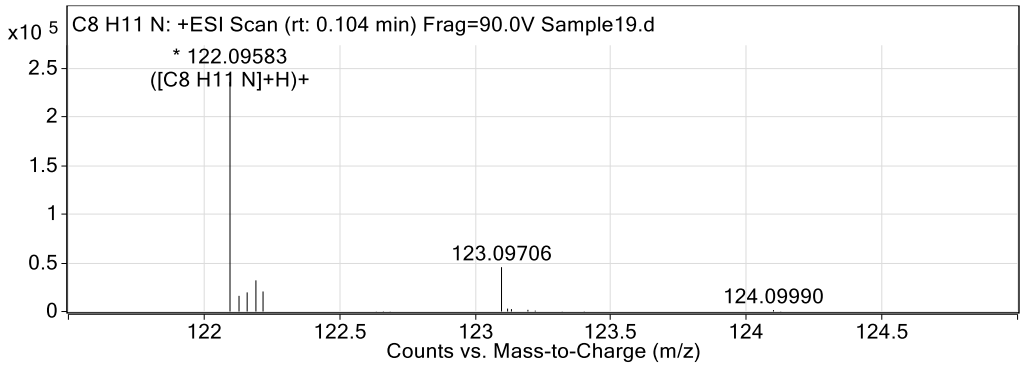

APPENDIX-30. QTOF-LC/MS Spectra of Compound 8

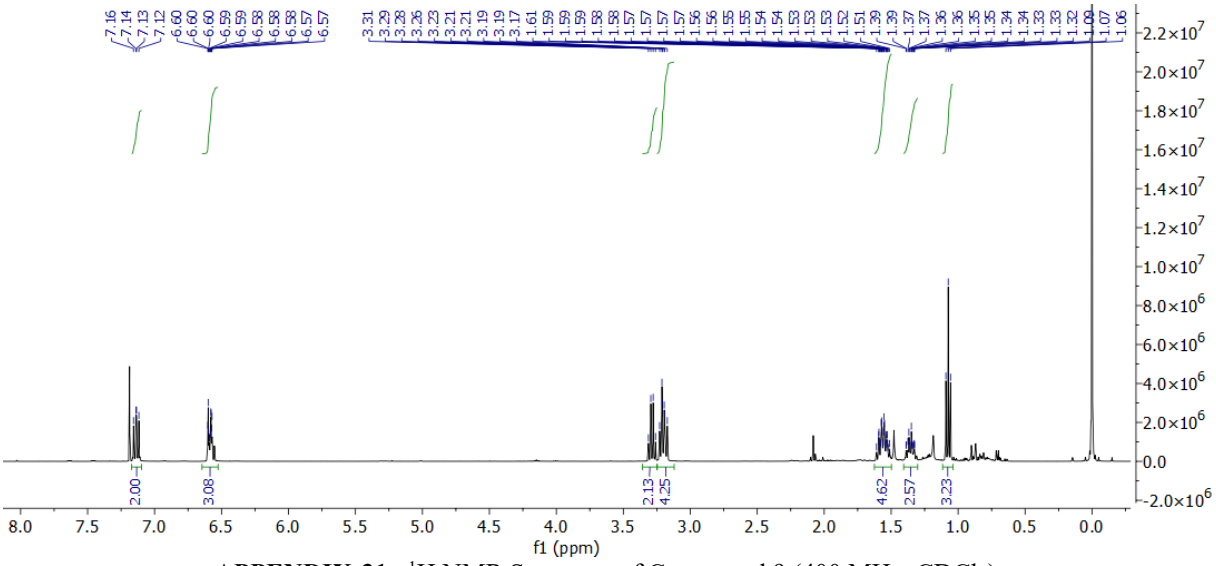

APPENDIX-31. ^{1}H NMR Spectrum of Compound 9 (400 MHz, $CDCl_3$).

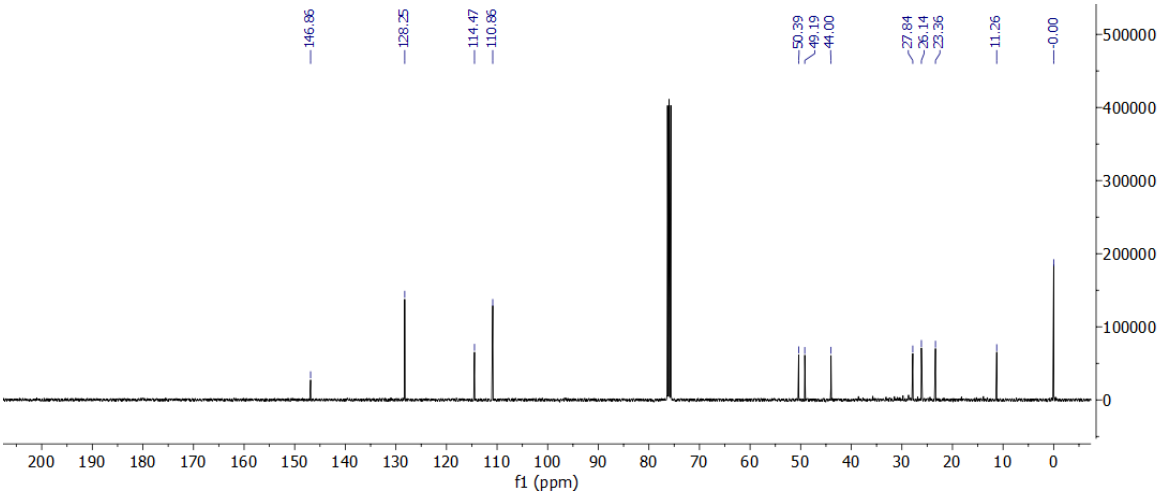

APPENDIX-32. ^{13}C NMR Spectrum of Compound 9 (101 MHz, $CDCl_3$).

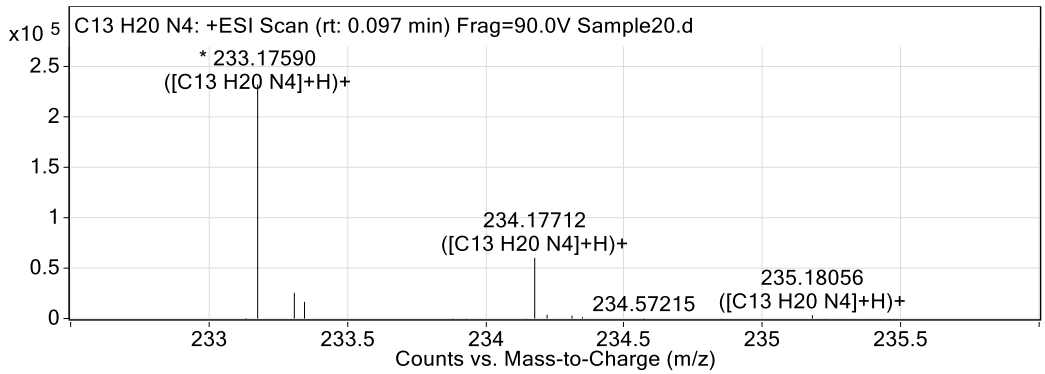

APPENDIX-33. QTOF-LC/MS Spectra of Compound 9

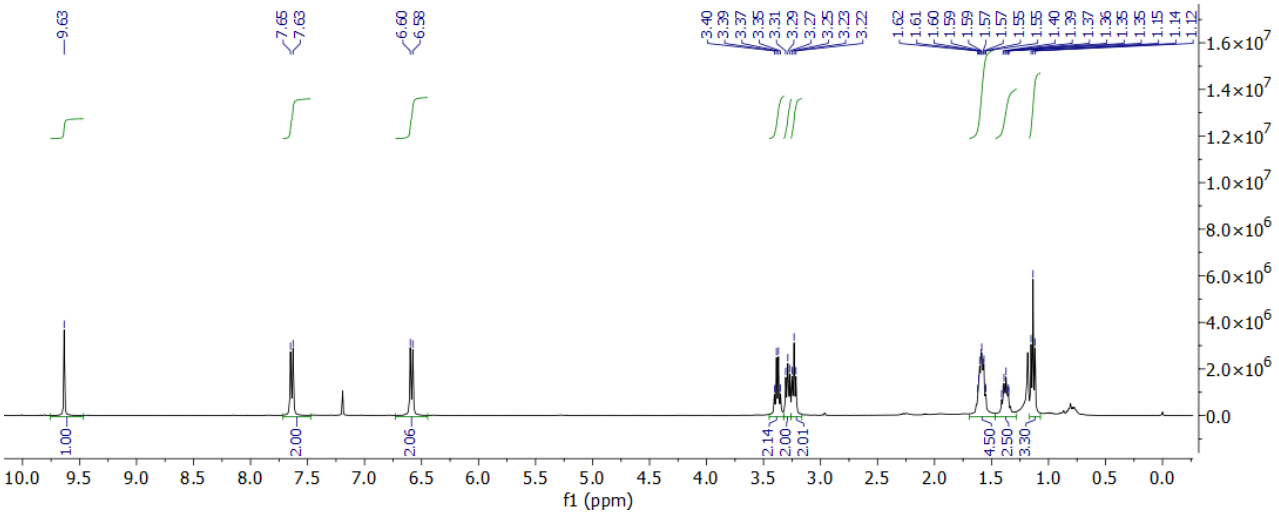

APPENDIX-34. ^{1}H NMR Spectrum of Compound 10 (400 MHz, $CDCl_3$).

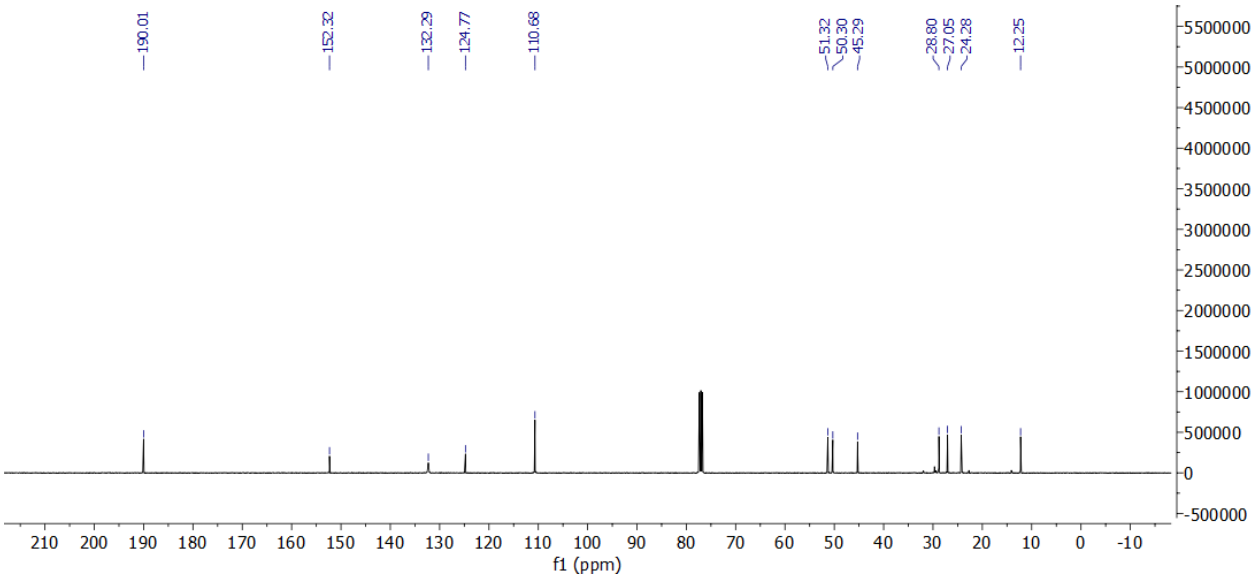

APPENDIX-35. ^{13}C NMR Spectrum of Compound 10 (101 MHz, $CDCl_3$).

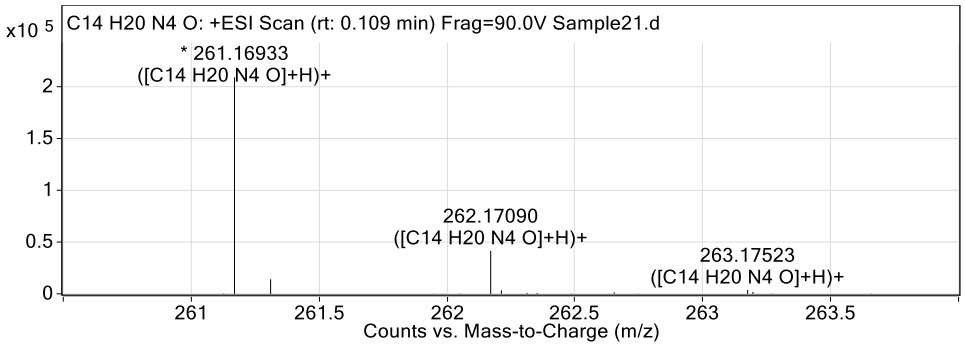

APPENDIX-36. QTOF-LC/MS Spectra of Compound 10

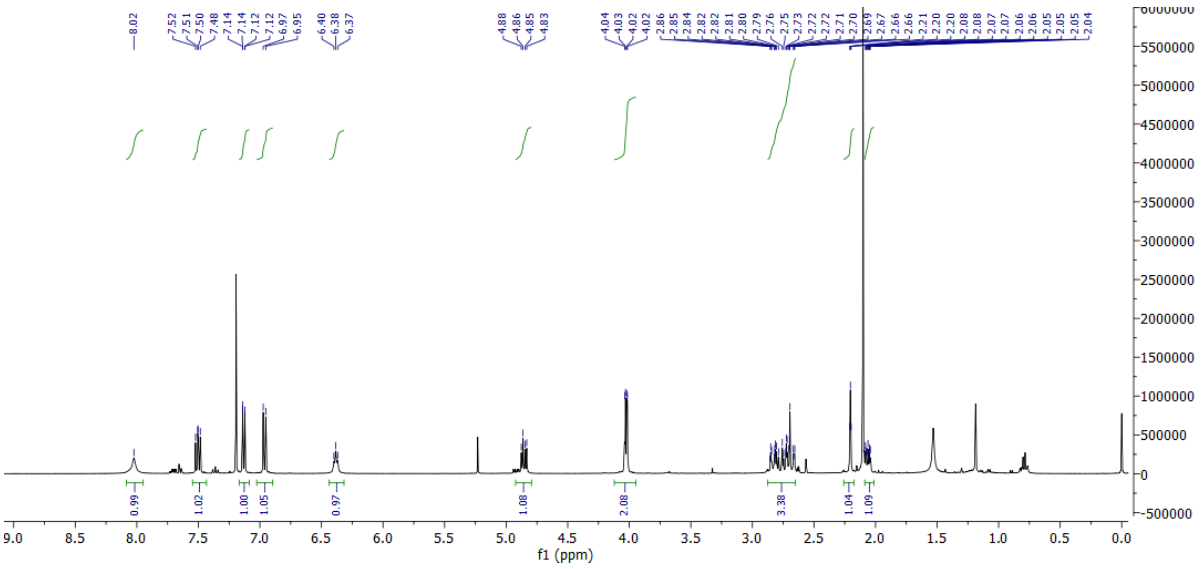

APPENDIX-37. ^{1}H NMR Spectrum of Compound 11 (400 MHz, $CDCl_3$).

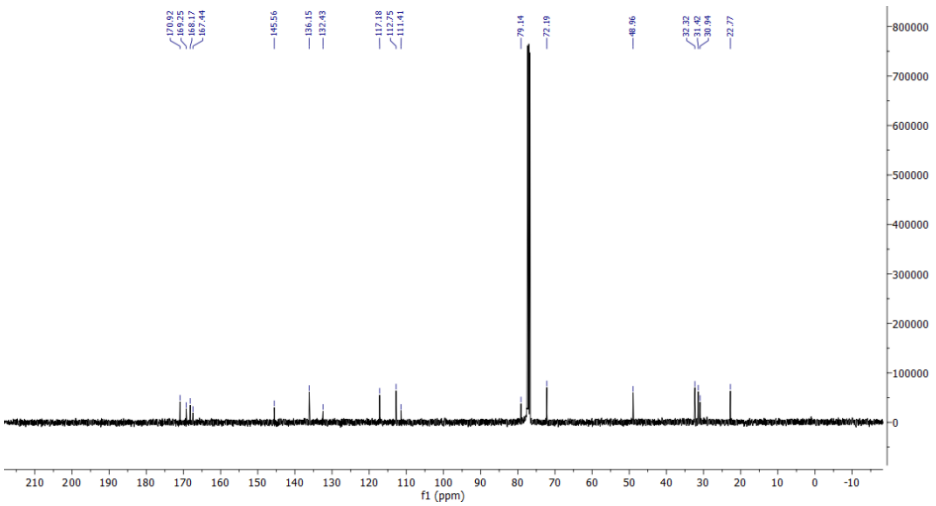

APPENDIX-38. ^{13}C NMR Spectrum of Compound 11 (100 MHz, $CDCl_3$).

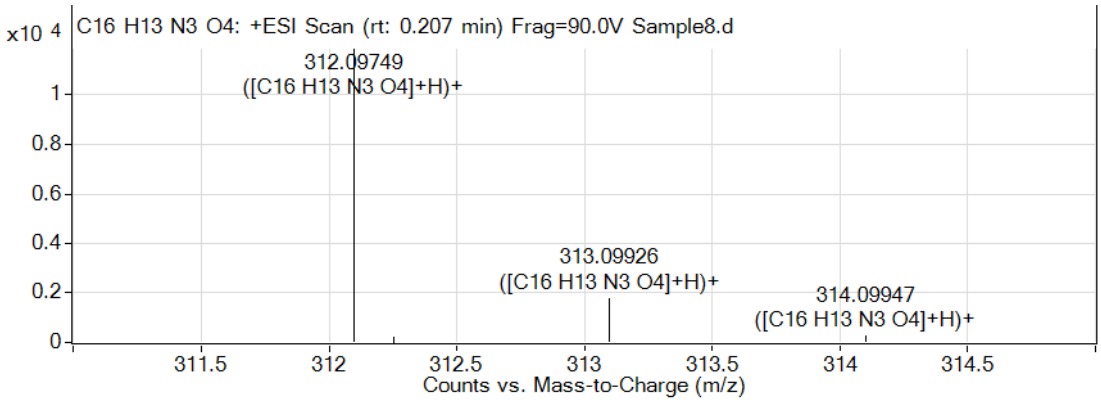

APPENDIX-39. QTOF-LC/MS Spectra of Compound 11

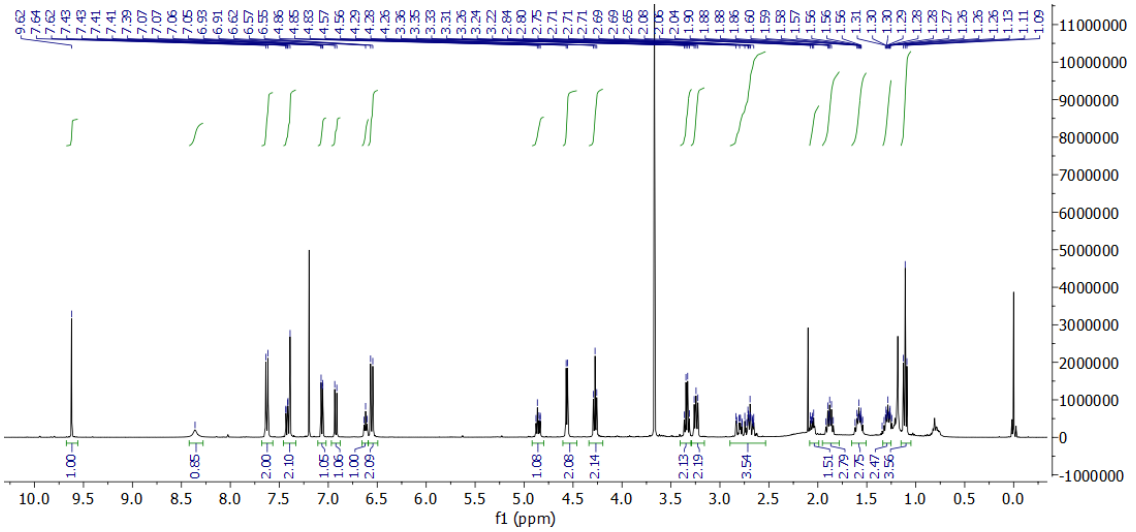

APPENDIX-40. ^{1}H NMR Spectrum of Compound **B1**

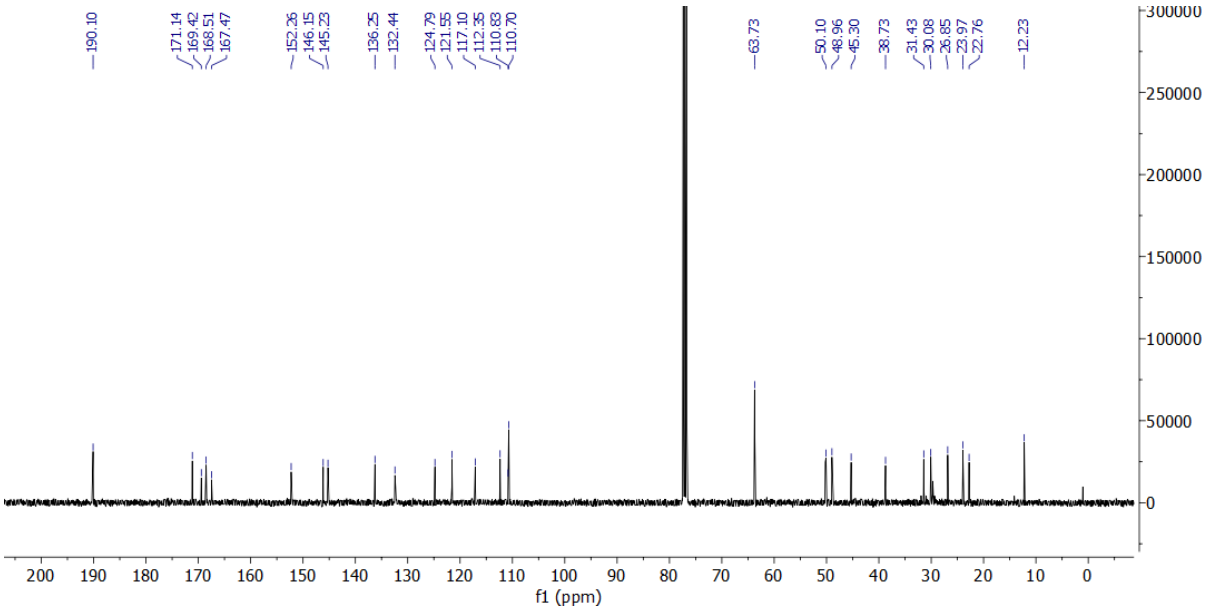

APPENDIX-41. ^{13}C NMR Spectrum of Compound **B1** (101 MHz, $CDCl_3$).

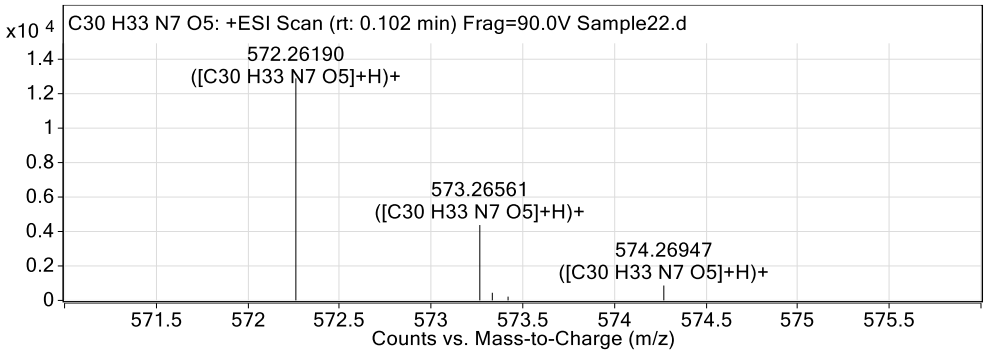

APPENDIX-42. QTOF-LC/MS Spectra of Compound **B1**

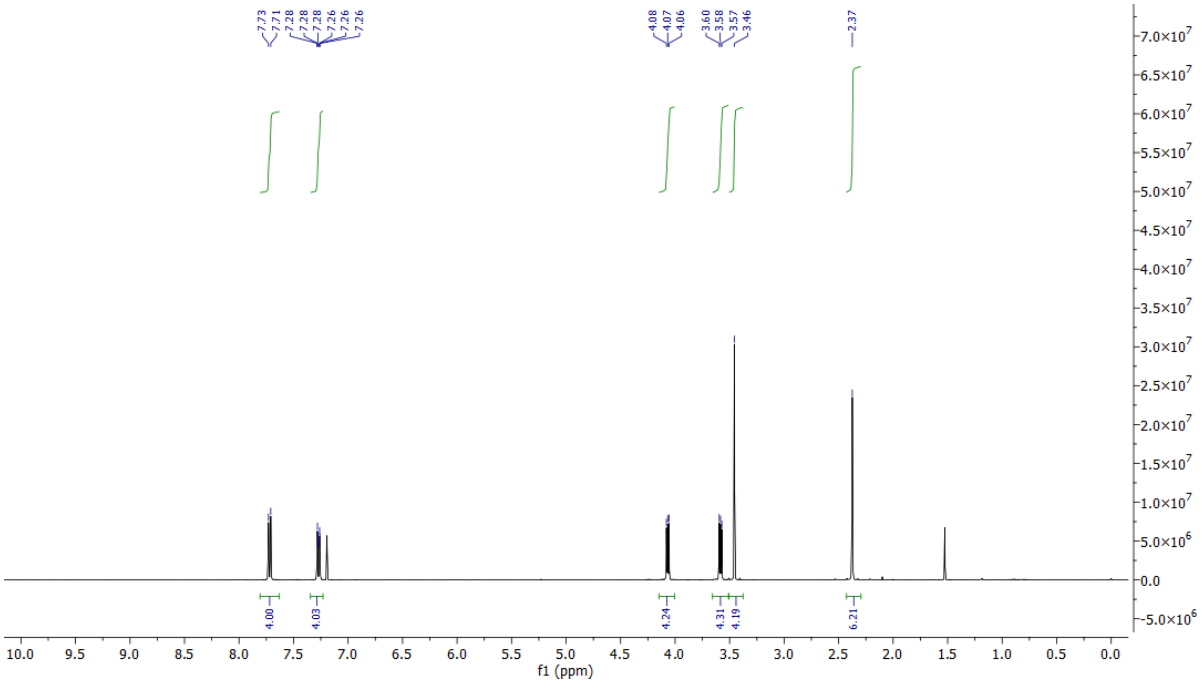

APPENDIX-43. ^{1}H NMR Spectrum of Compound 12 **(**400 MHz, $CDCl_3$)

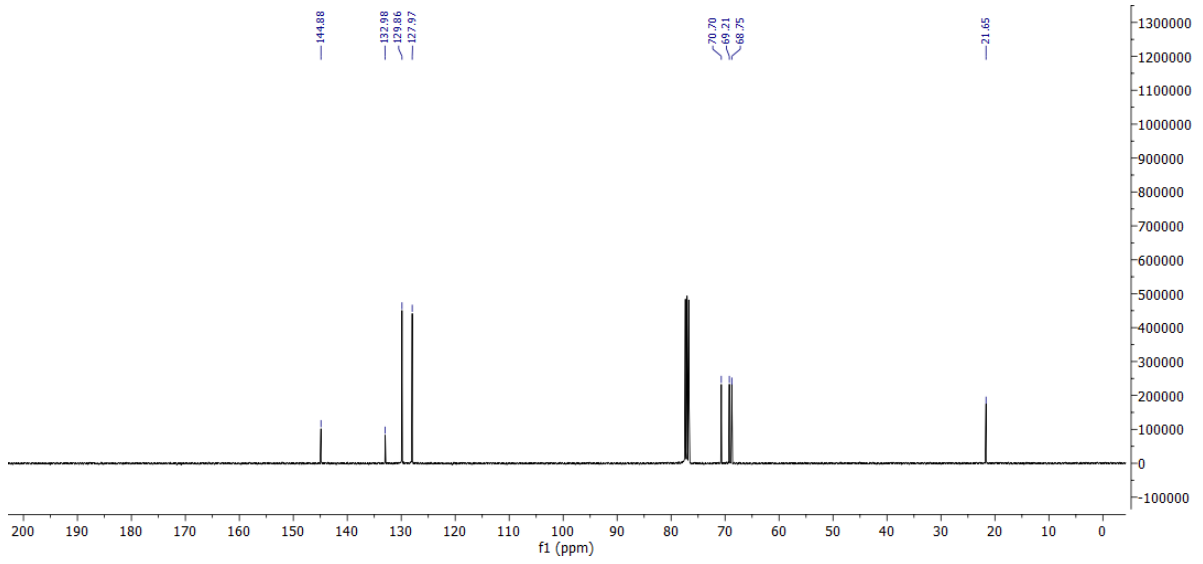

APPENDIX-44. ^{13}C NMR Spectrum of Compound 12 (100 MHz, $CDCl_3$)

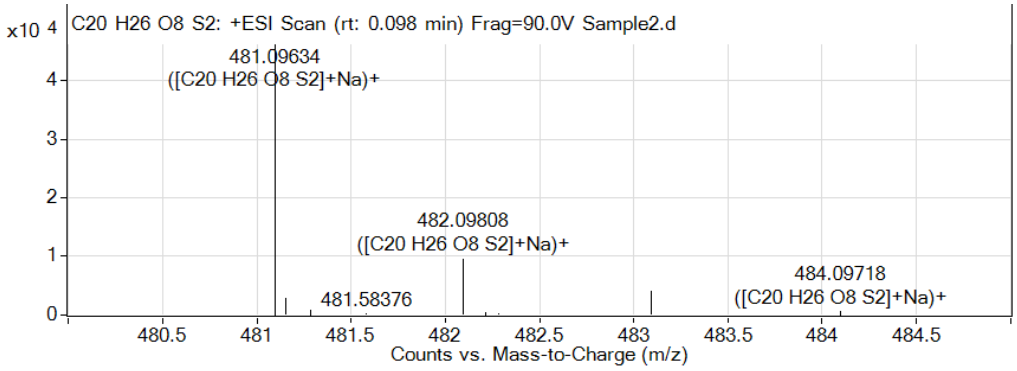

APPENDIX-45. QTOF-LC/MS Spectra of Compound 12

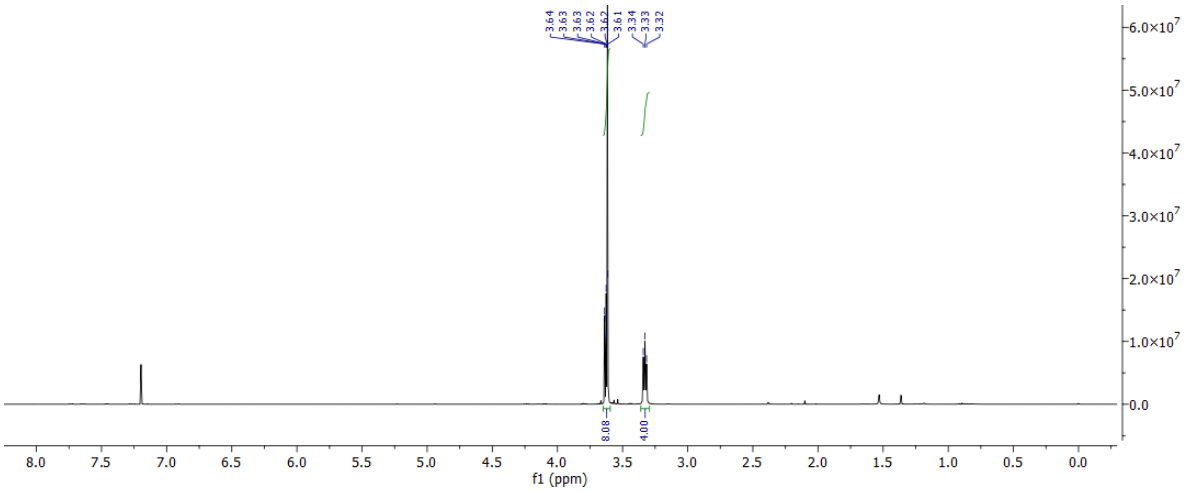

APPENDIX-46. ^{1}H NMR Spectrum of Compound 13 **(**400 MHz, $CDCl_3$)

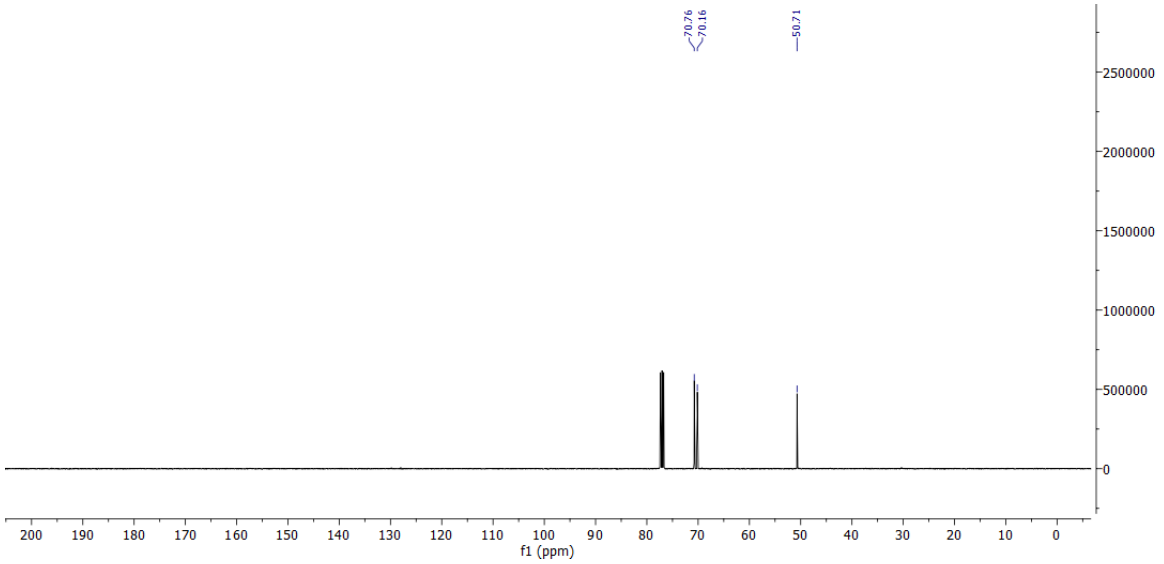

APPENDIX-47. ^{13}C NMR Spectrum of Compound 12(101 MHz, $CDCl_3$)

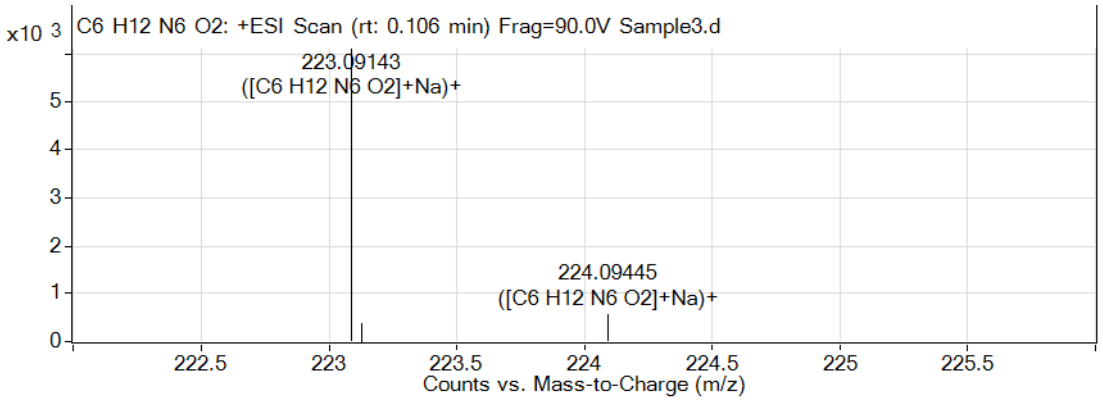

APPENDIX-47. QTOF-LC/MS Spectra of Compound 13

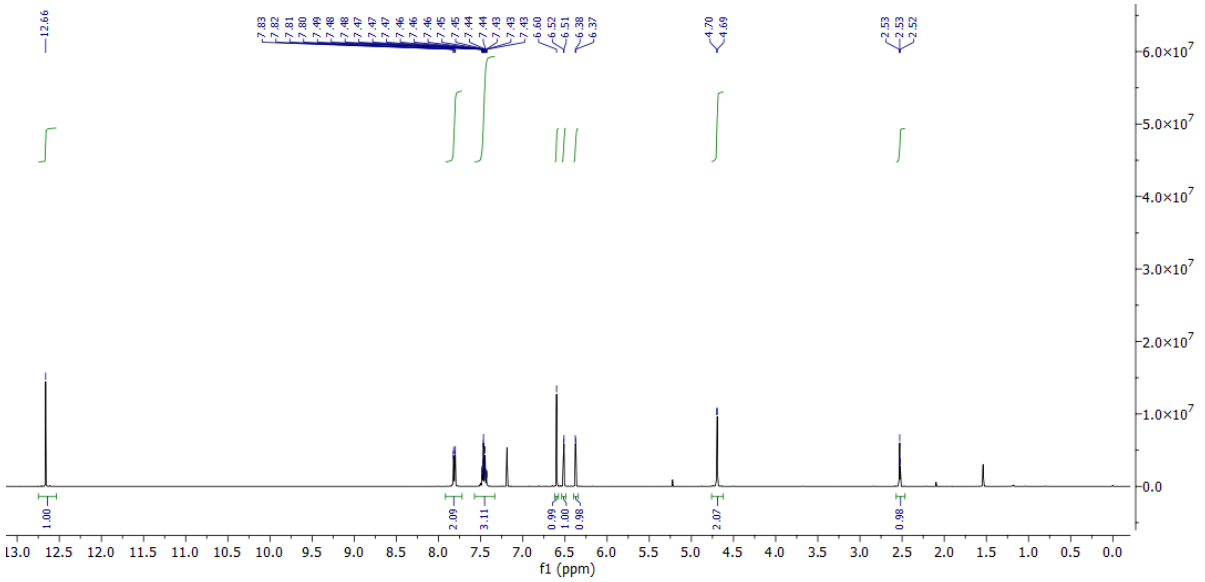

APPENDIX-49. ^{1}H NMR Spectrum of Compound 14 **(**400 MHz, $CDCl_3$)

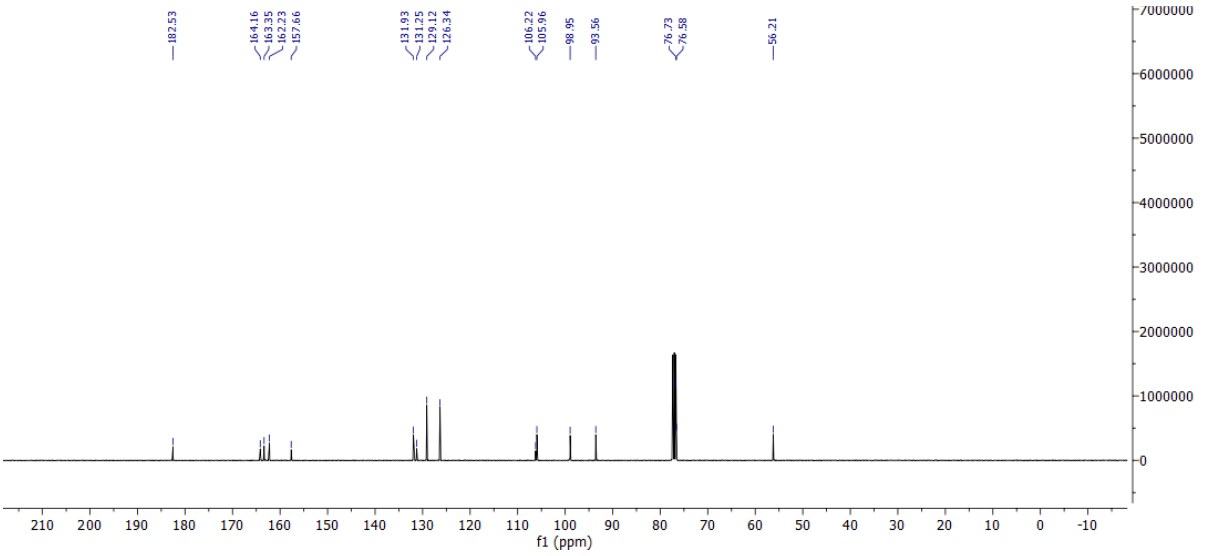

APPENDIX-50. ^{13}C NMR Spectrum of Compound 14 (101 MHz, $CDCl_3$)

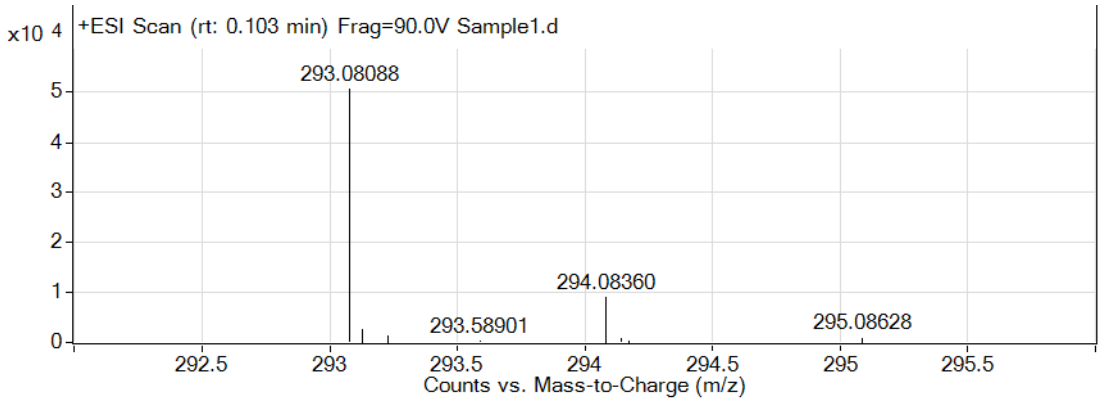

APPENDIX-51. QTOF-LC/MS Spectra of Compound 14

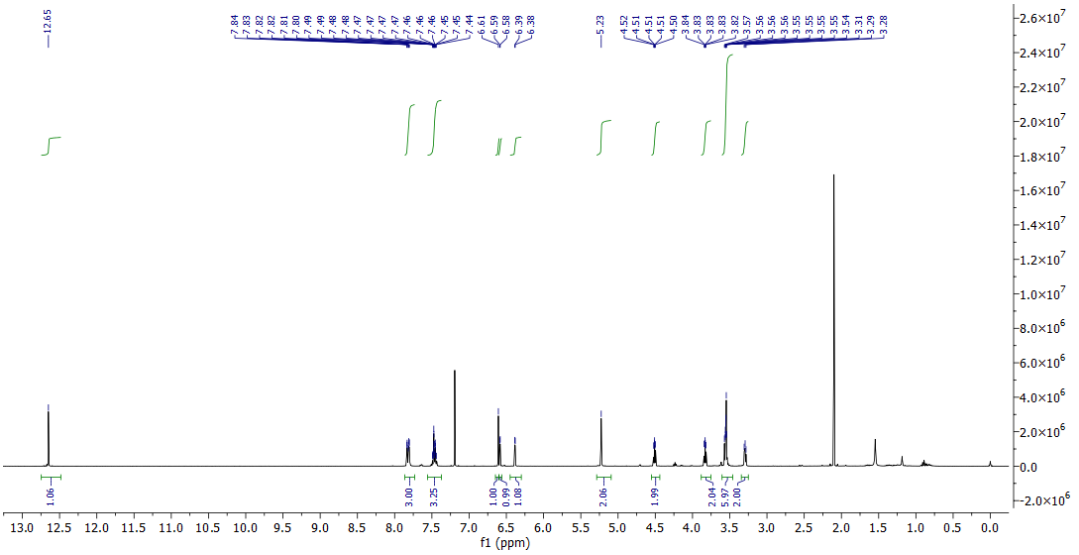

APPENDIX-52. ^{1}H NMR Spectrum of Compound 15 **(**400 MHz, $CDCl_3$)

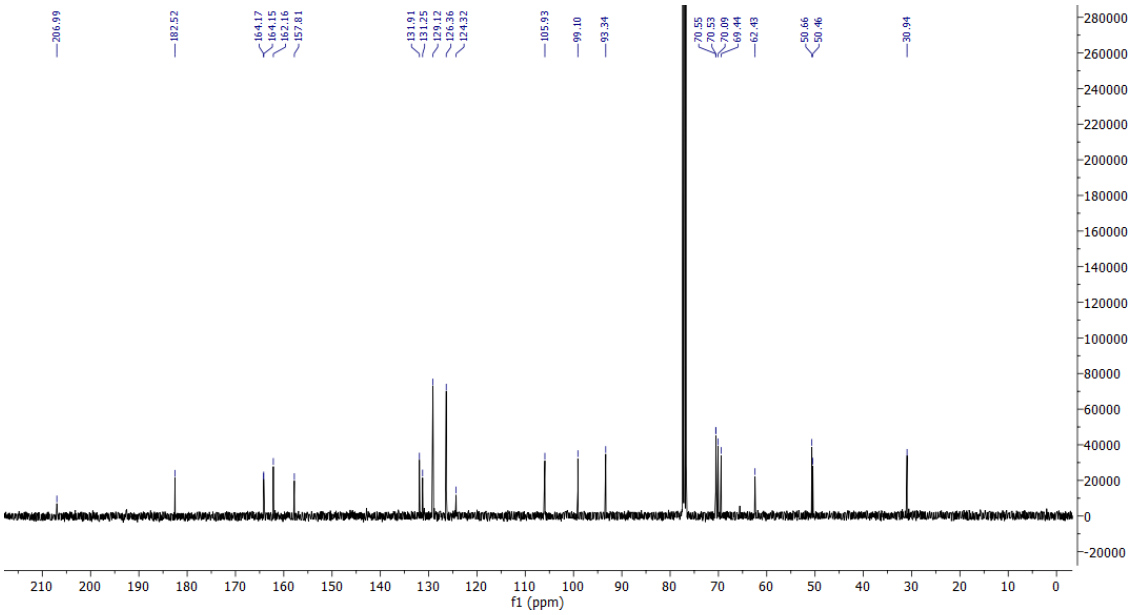

APPENDIX-53. ^{13}C NMR Spectrum of Compound 15 (101 MHz, $CDCl_3$)

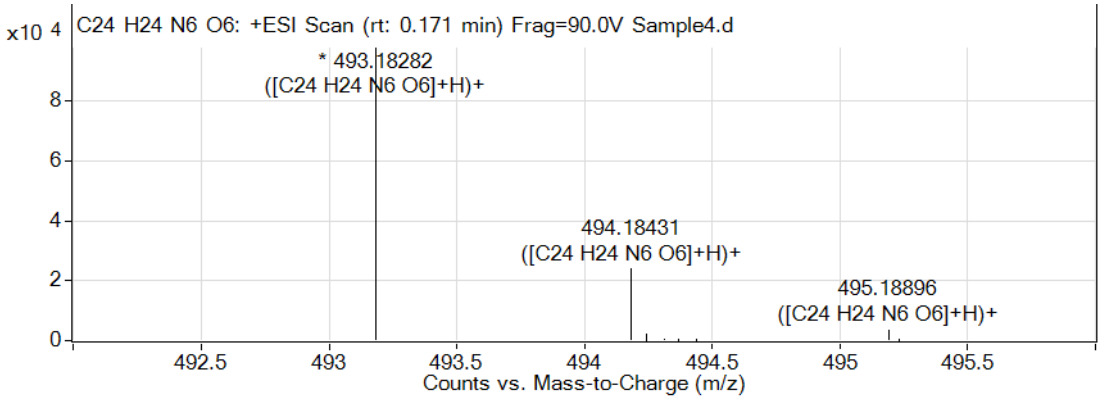

APPENDIX-54. QTOF-LC/MS Spectra of Compound 15

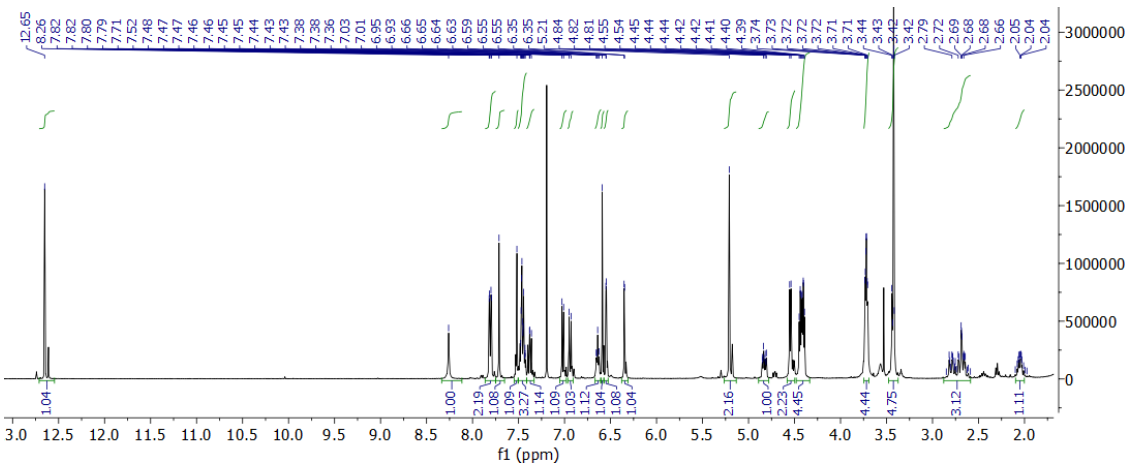

APPENDIX-55. ^{1}H NMR Spectrum of Compound **B2 (**400 MHz, $CDCl_3$)

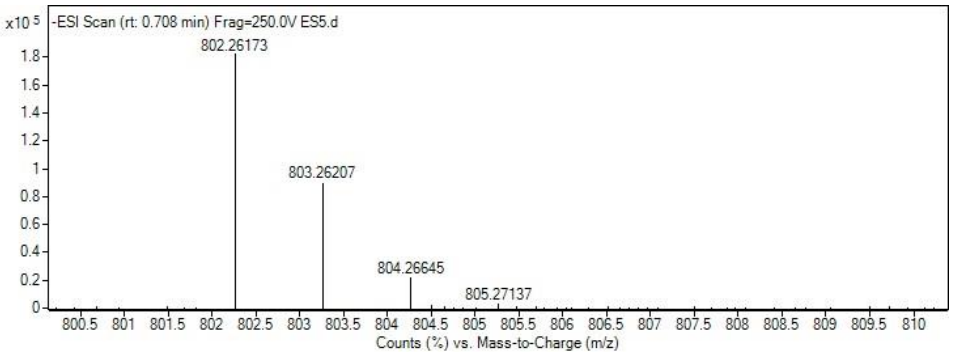

APPENDIX-56. QTOF-LC/MS Spectra of Compound **B2**

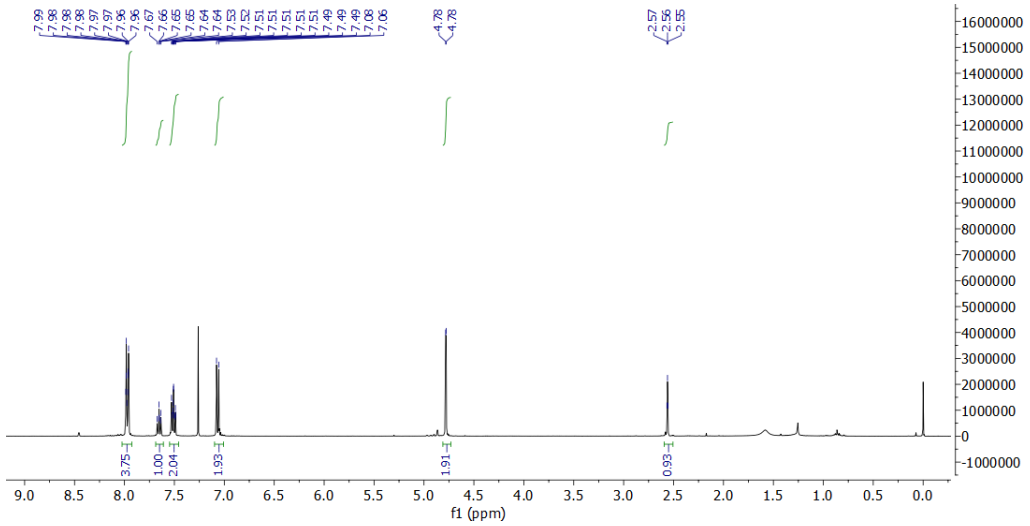

APPENDIX-57. ^{1}H NMR Spectrum of Compound 17 (400 MHz, $CDCl_3$)

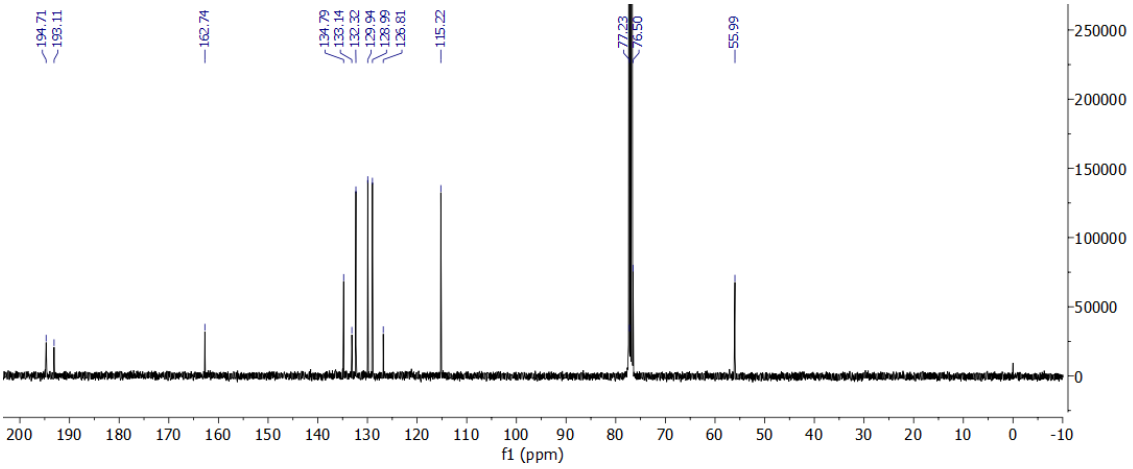

APPENDIX-58. ^{13}C NMR Spectrum of Compound 17 (101 MHz, $CDCl_3$)

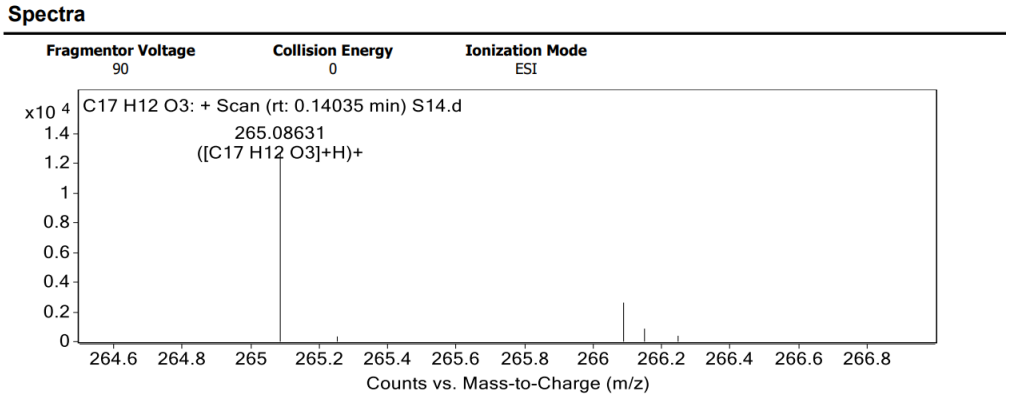

APPENDIX-59. QTOF-LC/MS Spectra of Compound 17

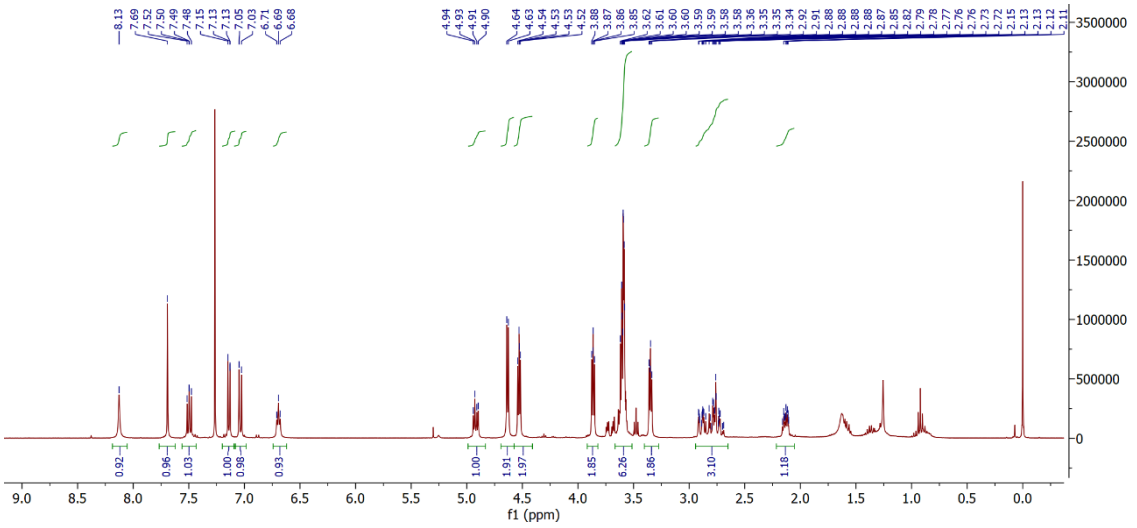

APPENDIX-60. ^{1}H NMR Spectrum of Compound 18 (400 MHz, $CDCl_3$)

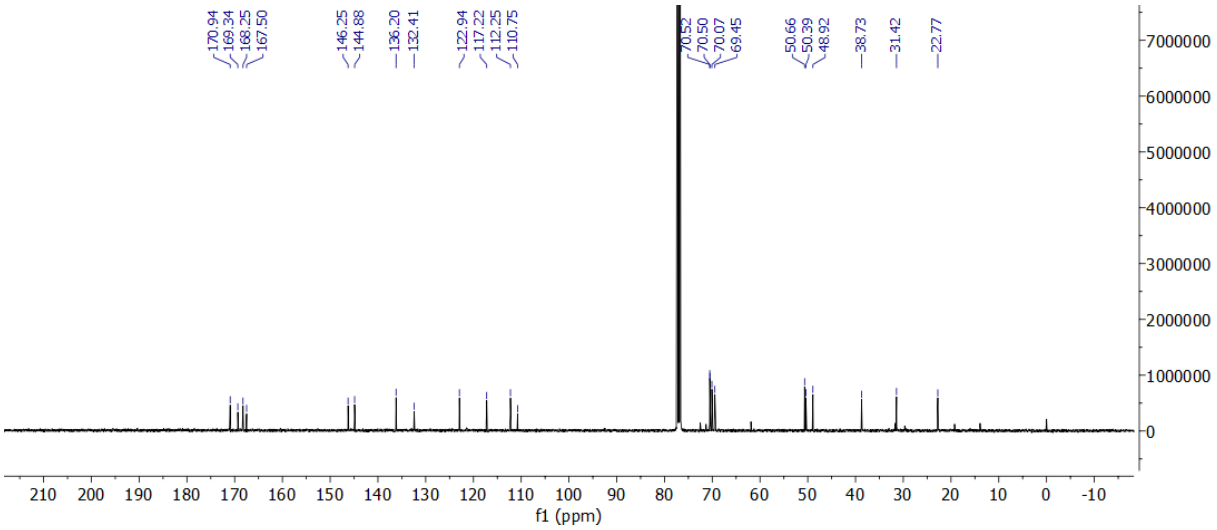

APPENDIX-61. ^{13}C NMR Spectrum of Compound 18 (101 MHz, $CDCl_3$)

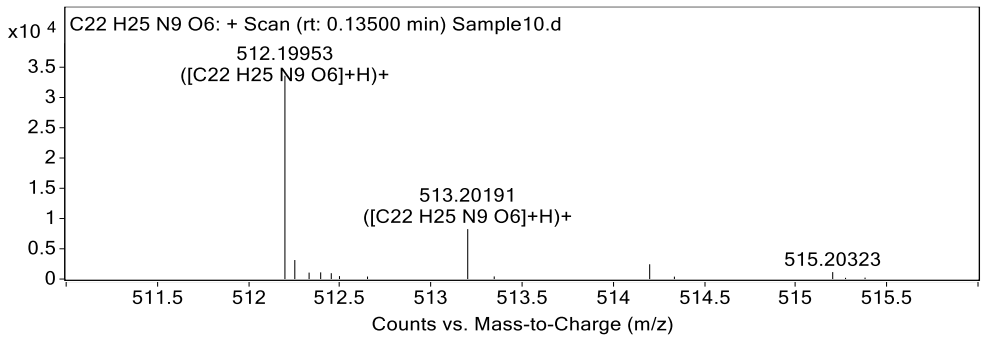

APPENDIX-62. QTOF-LC/MS Spectra of Compound 18

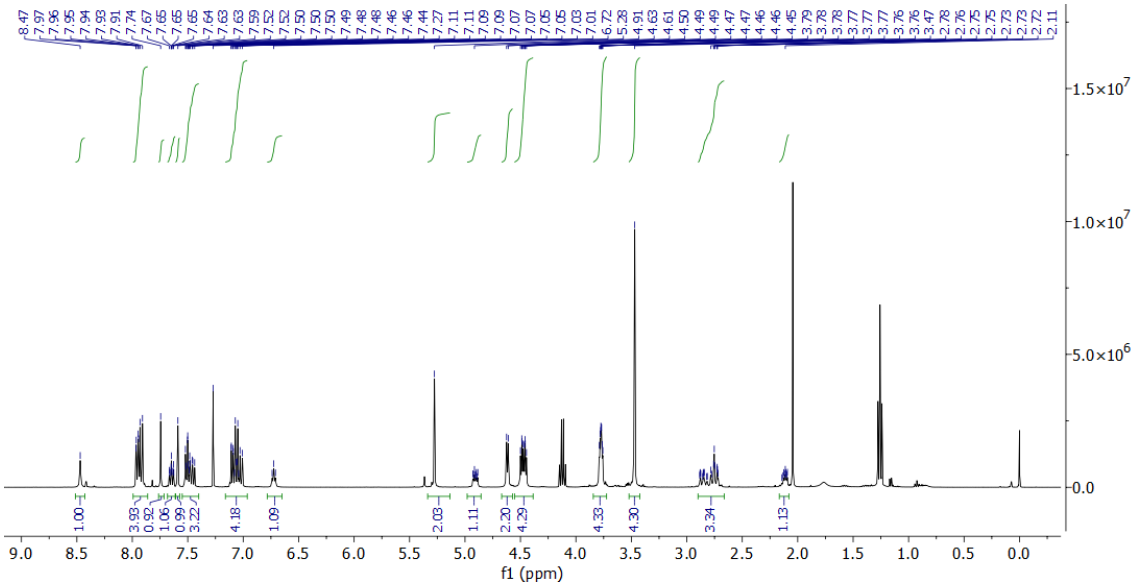

APPENDIX-63. ^{1}H NMR Spectrum of Compound **B3** (400 MHz, $CDCl_3$)

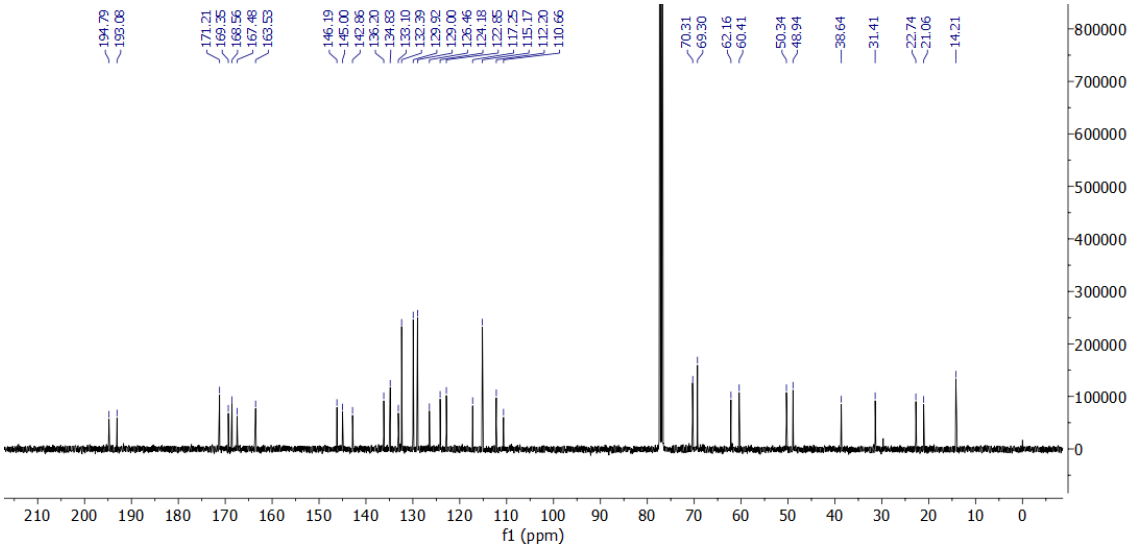

APPENDIX-64. ^{13}C NMR Spectrum of Compound **B3** (101 MHz, $CDCl_3$)

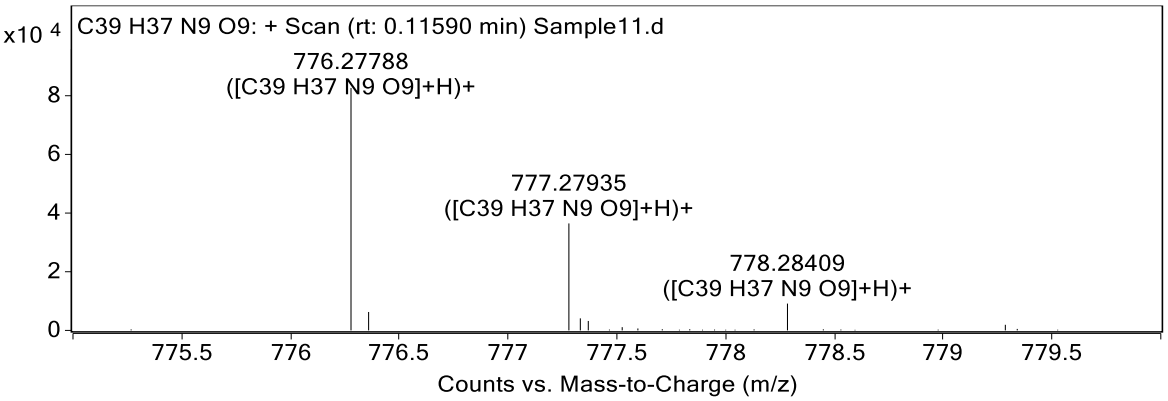

APPENDIX-65. QTOF-LC/MS Spectra of Compound **B3**